

TRACKING SAND DUNE MOVEMENTS USING MULTI- TEMPORAL REMOTE SENSING IMAGERY: A CASE STUDY OF THE CENTRAL SAHARA (LIBYAN FAZZĀN / UBĀRĪ SAND SEA)



ANJA ELS

454829

A dissertation submitted to the Faculty of Science, University of the Witwatersrand, in fulfilment of the requirements for the Degree of Master of Science

Supervisors: Prof. Jasper Knight and Dr. Stefania Merlo

Declaration

I declare that this Dissertation is my own, unaided work unless where specific acknowledgment has been made. It is being submitted for the degree of Master of Science within the School of Geography, Archaeology and Environmental Science at the University of the Witwatersrand, Johannesburg under the supervision of Prof. Jasper Knight and Dr. Stefania Merlo. It has not been submitted before for any degree or examination at any other University.



2017/01/20

Signed by Anja Els

Date

454 829

Abstract

Sand dune movements can be effectively monitored through the comparison of multi-temporal satellite images. However, not all remote sensing platforms are suitable to study sand dunes. This study compares coarse (Landsat 7 and 8) and fine (Worldview 2) resolution platforms, specifically focussing on sand dunes within the Ubārī Sand Sea (Libya), and identified the average migration rate and direction for the linear dunes within a section of the Ubārī sand sea for the time period from 2002-2015 with the use of Landsat imagery.

Two band combinations were compared with the use of two supervised classifications. The best combination was found to be red, green, blue and near-infrared band combination and the maximum likelihood classifier.

The dune features, namely the crest, slope and interdunal areas were successfully classified based on both the coarse and fine resolution imagery, but the accuracy with which it can be classified are different between the two resolutions. The classifications based on the Worldview 2 imagery had overall accuracies ranging from 55.43 - 60.83% with kappa values of 0.3486 – 0.4225 compared to the overall accuracies and kappa values of the classifications based on the Landsat 8 imagery ranging from 52.11 – 64.67% and 0.3878 – 0.4927 respectively. An average migration rate of 8.64 (\pm 4.65) m/yr in a generally north western direction was calculated based on the analysis of remote sensing data with some variations in this rate and the size and shape of the dunes.

It was found that although Worldview 2 imagery provides more accurate and precise mensuration data, and smaller dunes identified from Worldview data were not delineated clearly on the Landsat imagery. Landsat imagery is sufficient for the studying of dunes at a regional scale. This means that for studies concerned with the dune patterns and movements within sand seas, Landsat is sufficient. In studies where the specific dynamics of specific dunes are to be selected, a finer resolution is required; platforms such as Worldview are needed in order to gain more detailed insight and to link the past and present day climate and environmental change.

Acknowledgements

I would like to thank the following organizations and individuals for their assistance and support:

- Digital Globe Foundation - for the high resolution Worldview data of the study area
- Prof. Jasper Knight and Dr. Stefania Merlo - for their ongoing guidance and support, and the revision of the dissertation
- WITS University, Faculty of Science and GAES for the opportunity of pursuing my Master Degree
- GeoAgro Africa and its personnel for their support, “sound boarding” and understanding throughout the past two years

A special thank you to Donna Koch, Dr. Cheryl Chamberlain and Dr. Danny Simatele for their motivational talks and always being available for a “chat”...

A very special thank you to my family and friends for the understanding and support throughout the last couple of years, without you it would have been a dull couple of years.

Finally I would like to thank God for the love, talents, gifts and opportunities that He has bestowed upon me, without Him I would be nothing.

Table of Contents

Declaration	i
Abstract	ii
Acknowledgements.....	iii
List of Figures	vii
List of Tables	x
1. Chapter 1: Introduction.....	1
1.1 Introduction	1
1.2 Aims	5
1.3 Objectives	5
1.4 Study Area.....	6
1.4.1 Introduction	6
1.4.2 Location	7
1.4.3 Geology.....	8
1.4.4 Quaternary Climate	11
1.4.5 Present Climate.....	13
1.4.6 Sand Dunes of the Central Sahara	14
2. Chapter 2: Literature review	17
2.1 Introduction	17
2.2 Sand dunes and dune migration in arid environments	17
2.2.1 Sand dunes in arid environments.....	17
2.2.2 Dune Morphology.....	19
2.2.3 Sand seas	25
2.2.4 Sand dune migration in arid environments.....	26
2.2.5 Studying sand dunes and sand dune migration.....	30
2.3 Remote sensing and GIS in relation to sand dunes and sand dune migration.....	30
2.3.1 Introduction	30
2.3.2 The use of remote sensing and GIS in the study of sand dunes and dune migration in arid environments.....	32
2.3.3 Limitations associated with the use of remote sensing and GIS in sand dune and sand dune migration studies.....	33
2.4 Previous Research.....	34
2.4.1 Coarse spatial resolution imagery studies.....	34
2.4.2 Fine spatial resolution imagery studies	37

2.5	Remote Sensing Analysis Methods.....	40
2.5.1	Pre-Processing of Satellite Imagery	40
2.5.2	Radiometric and Atmospheric Corrections.....	40
2.5.3	Panchromatic Sharpening.....	41
2.5.4	Co-Registration/Geometric Correction.....	41
2.5.5	Image Classification (Feature Extraction), using a Supervised Classification	42
	<i>Accuracy Assessment</i>	43
2.6	Conclusions	44
3.	Chapter 3: Materials and Methods	46
3.1	Introduction	46
3.2	Imagery Acquisition and Scenes Used	47
3.3	Pre-Processing of Satellite Imagery	51
3.3.1	Radiometric and Atmospheric Corrections.....	51
3.3.2	Panchromatic Sharpening.....	52
3.3.3	Co-Registration/Geometric Correction.....	53
3.3.4	Mosaicing.....	53
3.4	Image Classification (Feature Extraction)	53
3.4.1	Auto Feature Extraction / Image Classification	53
	<i>Accuracy Assessment</i>	58
3.4.2	Pixel Resizing.....	59
3.5	Comparison of Coarse and Fine Resolution Imagery / Post-Classification Change Analysis	59
3.6	Time Series Analysis (Dune Migration)	60
4.	Chapter 4: Results	65
4.1	Introduction	65
4.1.1	Unsupervised Classification	66
4.1.2	Supervised Classification.....	72
4.1.3	Accuracy Assessment.....	75
4.1.4	Comparison of Mapped Dunes Based on the Spatial Resolution of Imagery	88
4.2	Dune Migration.....	94
4.2.1	Supervised Classification.....	94
4.2.2	Change Analysis	98
4.2.3	Changes in Dune Morphology (Shape, Size, Length, Width)	101
4.2.4	Changes in Location	103
4.3	Key Findings	108

5.	Chapter 5: Discussion	109
5.1	Introduction	109
5.2	Phase 1: The Comparison of Two Spatial Resolutions (Worldview 2 and Landsat 8 Images).....	110
5.2.1	Band Combinations & Classification Module.....	110
5.2.2	Spatial Resolution Comparison: Landsat 8 vs Worldview 2.....	111
5.3	Phase 2: Dune Migration within the Ubārī Sand Sea.....	113
5.3.1	Morphology	114
5.3.2	Location	114
5.4	Limitations	119
6.	Chapter 6: Conclusions.....	120
7.	References.....	122

List of Figures

Figure 1.1: Location map of the Ubārī, Murzuq and Uan Kasa Sand Seas, the locations of the towns Sabhā and Ubārī and the Al Qarqaf Arch, Messak Plateau and Acacus Tadrart (the “subset” is the area which was zoomed in on in this study).	7
Figure 1.2: Geological map of Libya, showing the Ubārī (outlined: red dashed line) and Murzuq (outlined: green dashed line) sand seas (Adapted from: Hallett, 2002).	9
Figure 1.3: Topographic map of Libya, with the subsets for phase 1 (boxed in red) and phase 2 (boxed in green).	9
Figure 1.4: (A) The stratigraphic sequences and the lithology within the Murzuq Basin (Goudarzi, 1980: Figure 9, pp 889).	10
Figure 1.4: (B) N-S schematic cross-section, western Libya (Tawardos, 2001).	11
Figure 1.5: Mosaic image of six Landsat 8 tiles covering the Ubārī Sand Sea (October 2015), depicting the following types of dunes: (A) star dunes (three individual star dunes are circled in yellow), (B) linear dunes (three individual linear dunes are circled in red)	16
Figure 2.1: (a) Sketch of a cross section of a sand dune, showing the windward slope, crest and slipface, (b) Satellite image of a section of the Rub’Al-Khali sand sea showing the dune morphology from above and (c) a cross section of the same section within the dune field showing the dune and interdune areas, dune wavelength and spacing (Al-Masrahy & Mountney, 2013: their Figure 4, p. 161).	18
Figure 2.2: Sand dune types and their dominant wind direction (show with black arrows) (McKee, 1979: his Figures 3-5, 11, pp. 11 & 13)	19
Figure 2.3: Dune types in relation to the variability of wind direction and sand supply (Huggett, 2007: his Figure 12.4, p. 303).	20
Figure 2.4: (a) Google Earth image of a Mega Barchan dune in Morocco (du Pont, 2015: his Figure 3d, p. 126); (b) satellite image of mega-barchan dunes in the north eastern section of the Rub’ Al-Khali sand sea (Saudi Arabia); (c) satellite image of complex barchans dunes with superimposed dunes on the northern section of Rub’ Al-Khali sand sea (Saudi Arabia) (Al-Masrahy & Mountney, 2013: their Figures 6a and b, p. 163); and (d) Photo of a Barchan dune in the vicinity of Tarfaya (Morocco) (du Pont, 2015: his Figure 3a, p. 126).	21
Figure 2.5: Google Earth images of transverse dunes in (a) Morocco and (b) Mocamedes desert (Angola) (du Pont, 2015: his Figures 4a and b, p. 128).	22
Figure 2.6: Google Earth images of (a) Seif dunes in Niger (b) Linear dune fields (top) and superimposed dunes (bottom) in the Rub’Al-Khali sand sea (Saudi Arabia); and (c) dunes in the Mu Us Desert (China) (du Pont, 2015: his Figures 5b, c and e, p. 130); and (d) a satellite image of compound linear ridges from the southern section of the Rub’ Al-Khali sand sea (Al-Masrahy & Mountney, 2013: their Figure 6c, p. 163).	23
Figure 2.7: (a) Photo of a star dune in the Rub Al-Khali sand sea, (b & c) Google Earth images of star dunes in Algeria (du Pont, 2015: his Figures 6a, b and c, p.132); and (d) satellite image of star dunes in the central section of the Rub’ Al-Khali sand sea (Al-Masrahy & Mountney, 2013: their Figure 6d, p. 163).	24

Figure 2.8: Sand Seas of the Sahara, 1. Grand Erg Occidental; 2. Grand Erg Oriental; 3. Ubārī; 4. Murzuk; 5. Calanscio; 6. Great Sand Sea; 7. Selima; 8. Fachi-Bilma & Te’ne’re’; 9. Majabat al Koubra; 10. Aouker; 11. Akchar; 12. Iguidi; 13. Chech (from Badescu <i>et al.</i> , 2008: their Figure 1, p. 2).	26
Figure 2.9: The downwind progress of a transverse dune (Adapted from Huggett, 2007: his Figure 12.3, p.303).	27
Figure 2.10: A schematic representation of the different modes of transport of sand grains (Adapted from Masselink <i>et al.</i> , 2011).	27
Figure 3.1: Flow diagram of the methods used for the image processing and change analysis.	46
Figure 3.2a: Location map of the Ubārī Sand Sea with the study area for phase 1 (the comparison of spatial resolutions) boxed in solid red.	50
Figure 3.2b: Location map of the Ubārī Sand Sea and the study area for phase 2 (time series analysis) boxed in solid red.....	51
Figure 3.3: Linear Dunes (39 dune bases outlined in black) used for the analysis of dune migration	61
Figure 3.4: Google Earth image of a linear dune within the Ubārī Sand Sea showing the morphology of a dune as (a) a cross section and (b) view from above.....	62
Figure 3.5: (a) The transect lines (purple lines) used in the measurements of the width of the dunes (outlined in black); (b) Crest lines (red) used in the measurement of the length of the dunes (outlined in black).	63
Figure 3.6: Migration measurement transect lines (red lines) at 300 m intervals perpendicular to the orientation of the dune.....	64
Figure 4.1: Atmospherically corrected images for Phase 1 (the comparison of the spatial resolutions and classification methods): Landsat 8 (a1), Worldview 2 (a2), and Phase 2 (the time series analysis): Landsat 7 (b1) and Landsat 8 (b2), with the study areas boxed in red.	66
Figure 4.2: The resulting images from the unsupervised classification module (K-Means) for Landsat 8 (for band combinations: (a1): R+NIR; (a2): RGB+NIR) and Worldview 2 (for band combinations: (b1): R+NIR; (b2): RGB+NIR).	68
Figure 4.3: The resulting change maps of the comparison of the two band combinations used in the unsupervised classification module (K-Means) for (a) Landsat 8 and (b) Worldview 2.	69
Figure 4.4: Minimum Distance Supervised Classification Images: Landsat 8 (A1: R+NIR; A2: RGB+NIR) and Worldview 2 (A3: R+NIR; A4: RGB+NIR).....	73
Figure 4.5: Maximum Likelihood Supervised Classification Images: Landsat 8: (A1: R+NIR; A2: RGB+NIR); Worldview 2 (A3: R+NIR; A4: RGB+NIR).....	74
Figure 4.6: Change detection map indicating the areas of difference between the Worldview 2 and Landsat 8 Maximum Likelihood classifications; zoomed in section on the edges of the sand sea – showing the smaller amount of change that occurred.....	90
Figure 4.7: Flow diagrams of the changes that occurred in the dune feature classes from the Worldview 2 image to the Landsat 8 Image.....	90

Figure 4.8: The dune outlines and crest lines for (a) 2002 (dune outline: solid and crest: dashed red lines); (b) 2015 (dune outline: solid and crest: dashed blue lines) and (c) the crest lines from 2002 overlaid over those from 2015..... 91

Figure 4.9: The resulting maximum likelihood classified images for A: 2002 (Landsat 7) and B: 2015 (Landsat 8) (zoomed in on study area - right)..... 95

Figure 4.10: A change detection map superimposed on the atmospherically corrected image from 2015 – indicating the areas where change occurred and finally the subsection (boxed) that was used in the analyses (where no change occurred there is no colour - it is transparent). 98

Figure 4.11: The isolated dune classes extracted from the maximum likelihood classification images for A: 2002 and B: 2015. 101

Figure 4.12: The isolated dune classes extracted from the maximum likelihood classification images for A: 2002 and B: 2015 with the overlay of the digitized dunes (outlined in red (A) and blue (B))..... 102

Figure 4.13: Digitized dunes from 2002 (blue) superimposed on top of the digitized dunes from 2015 (red); A: the 39 dunes that were used for the migration analysis and B: zoomed in section 102

Figure 4.14: Sand dune movement map - resulting areas of change (green polygons) from the subtraction of the digitized dunes of 2015 from the digitized dunes of 2002; A: the dunes used in the analysis of the dune migration and B: zoomed in section 103

Figure 5.1: Zoomed in area (boxed in red) of the (a) Worldview 2 image showing the better visibility of the superimposed dunes compared to the same zoomed in area of the (b) Landsat 8 image. On the Worldview 2 image (left) ripples on top of the dune can be seen as well as better defined urban structures (top centre) which are not identifiable as urban structures on the Landsat 8 image (right).. 113

Figure 5.2: The average migration rate (m/yr) in relation to the dune width (m) with a trend line (dashed blue line) 116

Figure 5.3: Zoomed in image on dune 30 showing the oasis (circled in red) on its windward side. 117

List of Tables

Table 1.1: Commonly used satellite remote sensing platforms, their resolutions and average revisit times.	4
Table 1.2: Quaternary period climatic timeline of the Saharan region, and indicative references	12
Table 2.1: Dune migration rates per dune type from the literature.	29
Table 2.2: Examples of remote sensing data that have been used for sand dune characterization from the literature	32
Table 2.3: Algorithms used in ENVI for the different classification modules (Canty, 2010).....	43
Table 3.1a: Detailed information (criteria) on the imagery that were chosen for the spatial resolution comparison section (phase 1) of this research.	48
Table 3.1b: Detailed information (criteria) on the imagery that were chosen for the time series analysis section (phase 2) of this research.	48
Table 3.1c: The band numbers, designations, wavelengths and resolutions for the three platforms that were used in this research.	49
Table 3.2: FLAASH Atmospheric Correction Model Parameters used in the correction of Landsat imagery.52	
Table 3.3: Training classes, their feature descriptions and number of Regions of Interest	55
Table 3.4: Matrix of the J-M Distance values comparing the ROIs, resulting from the ROI separability test.	57
Table 3.5: Percentage change ranges shown on the change detection area map.	60
Table 4.1: The classes resulting from the unsupervised K-Means classification were assigned to predefined features as follows:	67
Table 4.2: The change in area (km ²) per class from the (R+NIR) band combination to the (RGB+NIR) band combination – of the K-Means (unsupervised classification) images for Landsat 8 and Worldview 2, respectively.	70
Table 4.3: The error matrix for the Minimum Distance and Maximum Likelihood classifications across the two spatial resolutions (Landsat & Worldview) and band combinations (red & near infrared; and red, green, blue & near infrared)	77
Table 4.4: The Kappa Coefficient Statistic values for the minimum distance and maximum likelihood classifications of the two platforms and two sets of band combinations, resulting from the Confusion (Error) Matrix.	85
Table 4.5: The error matrix for the Minimum Distance and Maximum Likelihood classifications across the two spatial resolutions (Landsat & Worldview) and band combinations (red & near infrared; and red, green, blue & near infrared), based only on the three dune feature classes that were identified (i.e. crest, slope and interdune).	85
Table 4.6: The Kappa Coefficient Statistic resulting from the Confusion (Error) Matrix module, based on only the three dune feature classes (crest, slope and interdune).	88
Table 4.7a: The change in area (km ²) per class from the Wordlview 2 to Landsat 8 Maximum Likelihood Classification Images	92

Table 4.7b: The percentage change per class from the Wordlview 2 to Landsat 8 Maximum Likelihood Classification Images.....	93
Table 4.8: Error Matrix for the Maximum Likelihood Classification for; (a) Landsat 7 (2002) and (b) Landsat 8 (2015) imagery.....	96
Table 4.9a: The overall change in area (km ²) per class for the time period of 2002-2015.....	99
Table 4.9b: The overall percentage change per class for the time period of 2002-2015.....	100
Table 4.10: Changes in dune crest length, dune width and area from 2002-2015.	104
Table 4.11: The average distance each of the sample dunes migrated (m) for the time series (13 years), as well as the average migration rate per dune per year (m/yr) and the overall migration distance (m) and migration rate (m/yr) for the dunes in question	106

Chapter 1: Introduction

1.1 Introduction

Sand dunes (and *draa* or mega dunes) are one of the most significant features created by wind driven deposition (Blumberg, 2006). For sand dunes to form, a delicate balance between the sediment supply, microtopology and boundary layer climate is needed (Tsoar, 2001). Usually sand dune formation requires an ample supply of loose sand, little or no vegetation cover, strong winds (of which the velocity has to be above the threshold velocity of the grain size) as well as unidirectional and long duration winds; and topography that is of such a nature that it favours the sedimentation process (deposition of the grains) (Tsoar, 2001; du Pont, 2015; Telfer *et al.*, 2015).

When considering the global context, inland dunes are concentrated within the mid-latitudes, two “rings” of aridity form at around 30° north and south of the equator, and are often found in structural basins where the sand accumulate (du Pont, 2015). This can be mainly attributed to the descending arid air associated with the descending arm of the Hadley Cell (of the global air circulation pattern) (du Pont, 2015), precipitation in these areas is rare contributing to the aridity of the area. This aridity in combination with the high temperatures that occur there has led to a decrease in vegetation cover which in turn also contributes to the high temperatures and overall aridity of the area (rocks and bare soil lose moisture more readily and also experience faster changes in temperature than vegetation) (Hermas *et al.*, 2012).

Inland dunes are often concentrated within larger areas called sand seas (also known as ergs) (Blumberg, 2006). Dune areas are of a dynamic nature, as dunes change location by migration, can extend or grow (in length and height), or can change form depending on the wind direction and strength (Levin *et al.*, 2004; Blumberg, 2006; Howari *et al.*, 2007).

Dune patterns can be identified within dune fields/sand seas (Blumberg, 2006; Al-Masrahy & Mountney, 2013). In some cases the dunes have a spatial regularity or one or more defining attributes and may change gradually in a specific direction or may be controlled by the climate, topography and geology of the area in combination (Al-Masrahy & Mountney, 2013).

In hot desert areas (e.g. Egypt, Libya) sand dune movement is a hazardous phenomenon and can pose a major threat to modern anthropogenic activities, developmental plans as well as existing land use and land cover, and to the survival of archaeological sites and ancient places (Hermas *et al.*, 2012; El-Magd *et al.*, 2013; Sparavinga, 2013). Determining the rates of sand dune movements and their spatial variations can be useful in order to protect both anthropogenic and natural resources (Hermas *et al.*, 2012; El-Magd *et al.*, 2013).

In order to enable mitigation and/or prevention of this damage, dune migration rates and direction need to be studied (Sparavinga, 2013). This is not an easy task as dunes often cover large areas and are located in remote and/or inaccessible areas (Paisley *et al.*, 1991; Howari *et al.*, 2007; El-Magd *et al.*, 2013). Previous research focussing on the measuring and detection of sand dune movements in desert areas has utilized conventional ground based techniques (steel and iron rods, sand traps, fluorescent dye, and geomorphological mapping) (e.g. Paisley *et al.*, 1991; Levin *et al.*, 2004; Hermas *et al.*, 2012; El-Magd *et al.*, 2013). These methods may be more accurate than remote sensing methods at the mesoscale but lack the ability to cover large areas easily (they provide measurements at smaller temporal and spatial scales), and are expensive and time consuming (Hermas *et al.*, 2012; Mohamed & Verstraeten, 2012; El-Magd *et al.*, 2013). Due to the difficulties and expense that accompany extensive field surveys of dunes, these studies cannot be repeated often enough to capture the dynamics that potentially occur within dune fields (Yao *et al.*, 2007; Hermas *et al.*, 2012; El-Magd *et al.*, 2013).

Remote sensing has been suggested as a possible solution to this problem (Yao *et al.*, 2007; Hermas *et al.*, 2012), as it can cover large and remote areas (Hermas, *et al.*, 2012; El-Magd *et al.*, 2013) and today remote sensing data are available for most of the world's land surfaces.

Sand dune movements can be effectively monitored through multi-temporal satellite images (Hermas *et al.*, 2012; El-Magd *et al.*, 2013). Remotely sensed data show regular/multi-temporal and wide/large area coverage for analysis and measurements at relatively low costs, unlike field measurements (Hermas *et al.*, 2012; El-Magd *et al.*, 2013).

Several studies have used remote sensing to study the morphology and migration of single dunes (White *et al.*, 1997; Al-Dabi *et al.*, 1998; Levin *et al.*, 2004) and some research studied parts or entire dune fields (composed of several dunes) (Janke, 2002; Levin *et al.*, 2006; Mohamed & Verstraeten, 2012). However, Hermas *et al.* (2012) and El-Magd *et al.* (2013) stated that individual sand dune boundary classification is highly affected by satellite geometry, sensor parameters and illumination conditions, which require complex pre-processing of imagery, these boundaries are sometimes even difficult to map in the field.

There are several different satellite remote sensing platforms available that have different spatial and spectral resolutions as well as different revisit times (temporal resolution, number of days before the sensor captures the same area) (see Table 1.1 for a few examples). Not all remote sensing platforms are suitable to study sand dunes and their movement. Spatial scale and spectral resolution play an important role, and are also connected to the expense concerned with acquiring remotely sensed data (the higher the resolution, the more expensive the data becomes). Spatial resolution of a platform refers to the pixel size and influences the smallest feature that can be detected. The spectral resolution is the number of bands and the wavelengths of these bands that the sensor can record, per pixel (Aldossary, 2012). A coarse resolution can also be described as a low resolution and a fine resolution as a high resolution. “Coarse and Fine” resolution and “Low and High” resolution are used interchangeably (respectively) within this research.

If the same patterns can be detected at a coarser spatial resolution as at a finer spatial resolution, future studies may avoid unneeded high costs associated with high spatial resolution data, unless very detailed data are needed (for example when small, and/or superimposed dunes are the focus of the research). Similarly, high spectral resolution imagery (e.g. hyperspectral imagery) may be required in studies concerned with the composition of the sediment on the surface of the dunes/ area in question (Minu *et al.*, 2016).

Table 1.1: Commonly used satellite remote sensing platforms, their resolutions and average revisit times.

Platform	Typical Spatial Resolution*	Temporal Resolution (Average Revisit Time)*	Active period
Landsat	30 – 120 m	16 – 18 days	1972 – present
IKONOS	0.8 – 4 m	3 days	1999 – present
SPOT (5-7)	2.2 – 20 m	1 – 5 days	2002 – present
Quickbird	0.6 – 2.4 m	1 – 3.5 days	2001 – present
Worldview 2	0.46 – 2.4 m	1.1 – 3.7 days	2009 – present
Corona	1.22 – 12.19 m	Unknown	1960 – 1972
ASTER	30 - 90 m	16 days	1999 – present
SRTM	90 m	Unknown	2000

*These may vary per mission

Al-Dabi *et al.* (1998) and Yao *et al.* (2007) concluded that Landsat imagery is a useful tool in the tracking of dune migration and pattern identification. This conclusion was made based not only on the results from their own analyses but also on the successes of previous studies that used Landsat imagery for the study of sand dunes and desertification. These studies were able to monitor desertification and study dune migration rates among other things in San Luis, Argentina (Collado *et al.*, 2002), classify dunes as active or inactive (Mojave Desert, California) based on spectral brightness (inactive sands were found to be darker than finer than active sands) (Paisley *et al.*, 1991); to monitor spatial and temporal changes in dune patterns (Kuwait) as well as identifying rates of dune movement and development (Al-Dabi *et al.*, 1997); characterizing the distribution of minerals in sand seas and the identification of sediment transport pathways (from Oman's Wahiba Sand Sea); to distinguish between different geomorphic regions in a dune field and deduce the origins of some of the deposited sediments to just name a few (Pease *et al.*, 1999) (more examples can be seen in Al-Dabi *et al.* (1998) and Yao *et al.* (2007)). More recent research includes (but is not limited to); the comparison of dune dynamics within five dune fields (Mohamed & Verstraeten, 2012); tracking dune encroachment in California (Lam *et al.*, 2011); quantifying sand dune movement in Egypt (El-Magd *et al.*, 2013); and

quantifying the spatial relationship between dune and interdune areas in the Rub' Al-Khali (Al-Masrahay & Mountney, 2013).

The Ubārī Sand Sea (Libya) has gone relatively unnoticed by these studies, but due to its location and climate it is ideal for remote sensing studies. In this research, coarse and fine spatial resolution imagery are compared with relation to their usability in the identification of desert dunes and dune patterns as well as studying dune migration in the aforementioned area. Landsat and Worldview imagery and a digital elevation model (DEM) derived from Shuttle Radar Topography Mission (SRTM) data were used to study a section within the Ubārī Sand Sea (Libya).

1.2 Aims

The main aim of this study was to determine if similar dune spatial patterns can be detected at different spatial resolutions, and to ultimately study dune migration within a section of the Ubārī Sand Sea to determine if this is a suitable alternative to the traditional field-based measurement of dune migration. The following research questions were identified to guide the study: (1) Can similar dune patterns be detected at different spatial resolutions? And (2) what is the net direction and rate of dune movement within a section in the Ubārī Sand Sea (over a time period of 13 years from 2002 to 2015, calculated with the use of Landsat imagery)?

1.3 Objectives

The objectives of this study were as follow:

1. Produce maps of sand dunes within the study area at a coarse/ low (Landsat 8) and fine/ high resolution (Worldview 2) (Images from September 2014).
 - Identify, describe and map the spatial patterns of the dunes within the subsection at a coarse resolution (Landsat 8, SRTM), with the use of unsupervised and supervised classifications and imagery from September 2014.
 - Identify, describe and map the spatial patterns and geomorphic attributes of the dunes within the same subsection at a fine resolution (Worldview 2),

- with the use of unsupervised and supervised classifications and imagery from September 2014.
2. Compare the spatial patterns of the dunes at a coarse/ low (Landsat 8) and fine/ high (Worldview 2) spatial resolution (Images from September 2014).
 - Use the sand dune maps (produced in objectives 1) to compare the spatial patterns from the coarse resolution to those from the fine resolution, with the use of visual interpretation, classification, accuracy assessment and image differencing
 3. Evaluate the dune “migration” (rate and direction/ changes in shape and size) within a section of the Ubārī Sand Sea, from 2002 to 2015 with the use of Landsat 7 and Landsat 8 imagery.
 - Temporal changes: Identify the net rate and direction of dune movement within a section of the Ubārī Sand Sea, for the time period of 2002-2015.
 - Spatial changes: Determine the changes in the dune location, size and shape over time, for the time period of 2002-2015.
 - Objective 3 was achieved by comparing multi-temporal Landsat images (for the time period 2002-2015) with the use of change detection modules (Envi v5.1), on-screen digitizing and vector subtraction (ArcGIS v10.3).

1.4 Study Area

1.4.1 Introduction

The region considered for this study is the Ubārī Sand Sea (Fig. 1.1) located in the Libyan Fazzān in Southwestern Libya (Central Sahara). It covers an area of approximately 61 000 km² and is located north of the Murzuq Sand Sea. Limited studies of the Ubārī Sand Sea have been conducted but due to its location and climate, it is ideal to study via remote sensing methods.

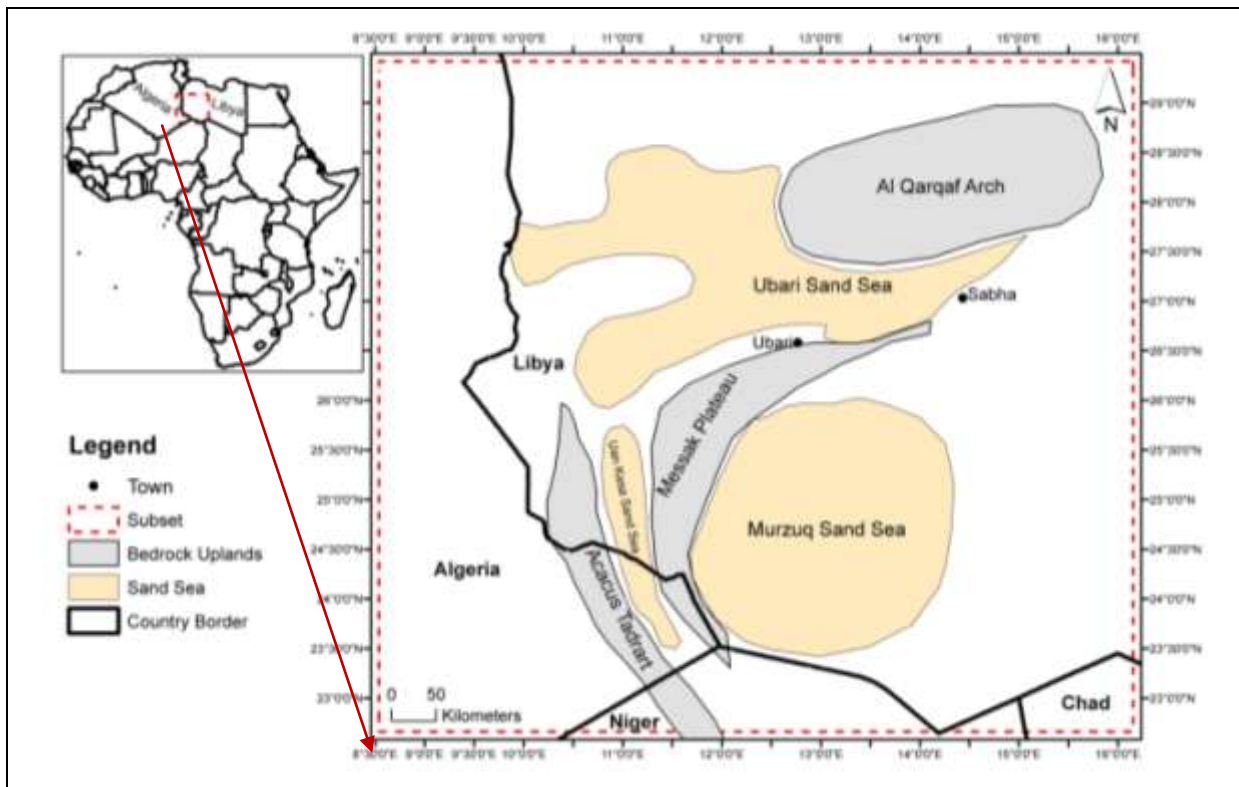


Figure 1.1: Location map of the Ubārī, Murzuq and Uan Kasa Sand Seas, the locations of the towns Sabhā and Ubārī and the Al Qarqaf Arch, Messak Plateau and Acacus Tadrart (the “subset” is the area which was zoomed in on in this study).

1.4.2 Location

The Ubārī Sand Sea (from here on referred to as “the sand sea”) can be found by between the Wādī ash-Shātī and Wādī al-Ajāl and forms part of the Murzuq Basin (Tawardos, 2001). The Basin is bordered by the Tibesti (south-east) and Hoggar (south-west) Massifs, by the Al Qarqaf Arch to the north and by the Tadrart Akākūs range to the east, and is separated from its western extension, the Illizii basin (Algeria), by the Tihemboka anticline (a late Caledonian and Middle Devonian uplift) (Goudarzi, 1980; Lorenz, 1980; Tawardos, 2001; Hallett, 2002) (Figures 1.1 & 1.2).

The sand sea has predominantly linear dune ridges orientated southwest to northeast (Goudarzi, 1970; White *et al.*, 2006) that can exceed 200 m in height, often with barchan-like dunes on the surface (McKee, 1979); star-dunes can be seen in the central part of the sand sea (McKee, 1979). Seasonal and perennial lakes can be seen in some interdune corridors (indicating the high seasonal water table in those areas), and several oases can also be found in the southern section of the sand sea

(Goudarzi, 1970; White *et al.*, 2006). Duricrust deposits (consisting of calcium carbonate, silica and gypsum with abundant root casts) can also be found on the slopes and interdune areas. Lithic artefacts are often associated with duricrust outcrops, suggesting that these areas have been important at some stages of human occupation of these landscapes (White *et al.*, 2006). The sand sea is bordered to the northeast by the Al Qarqaf Arch (aka Gargaf Arch), that reaches a height of approximately 700 m asl, and by the Massak Escarpment (also known as Āl-Hamāda Murzuq or Massak Plateau, consisting of Nubian sandstone) to the south, that also reaches a height of approximately 700 m asl and separates the Ubārī and Murzuq sand seas that are approximately 400 and 650 m asl respectively (Lorenz, 1980) (Figure 1.3 & 1.4).

1.4.3 Geology

Limited subsurface data are available for the Murzuq Basin area; however, close to the centre of the basin the Precambrian basement is about 3000 m bsl (Goudarzi, 1980). At the base of the Mesozoic rocks a rise can be seen from 1500 m bsl, at the centre of the basin, to over 280 m asl at the basin rim (Goudarzi, 1980).

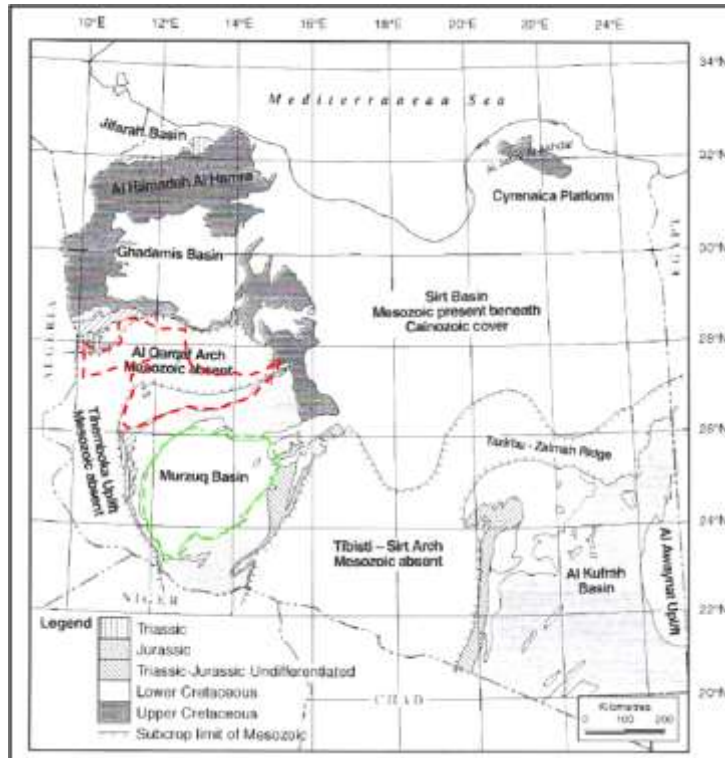


Figure 1.2: Geological map of Libya, showing the Ubārī (outlined: red dashed line) and Murzuq (outlined: green dashed line) sand seas (Adapted from: Hallett, 2002).

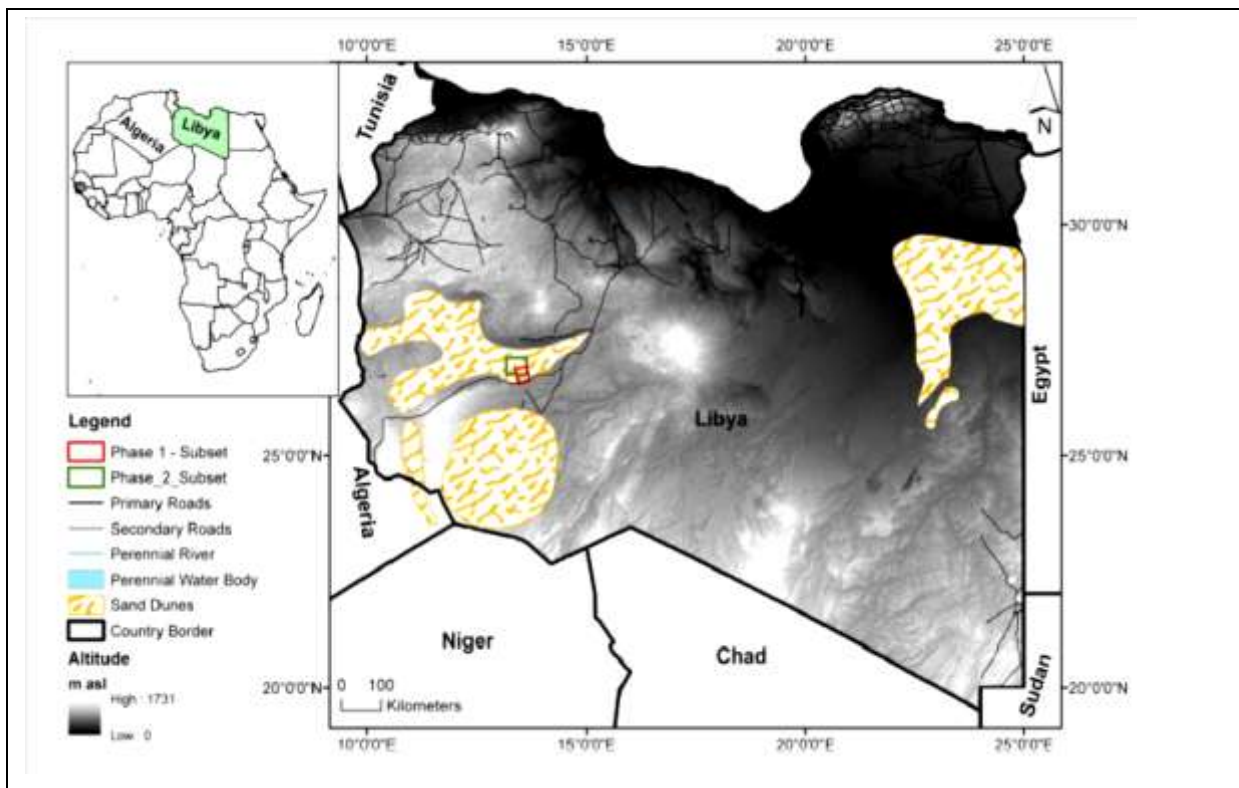


Figure 1.3: Topographic map of Libya, with the subsets for phase 1 (boxed in red) and phase 2 (boxed in green).

The Murzuq basin (from here on referred to as the basin) consists primarily of Paleozoic to Mesozoic sandstones and shale (Cremaschi & Zerboni, 2009). The base of the basin is mainly composed of continental sandstones (Cambrian and Ordovician age) and is overlain by Paleozoic rocks (mostly sandstones). These are in turn overlain by shallow-water and/or continental sediments of Jurassic and Lower Cretaceous age (see Figure 1.4). A large part of the area is covered in recent windblown sand separated by isolated bedrock hills (Sinha & Pandey, 1980).

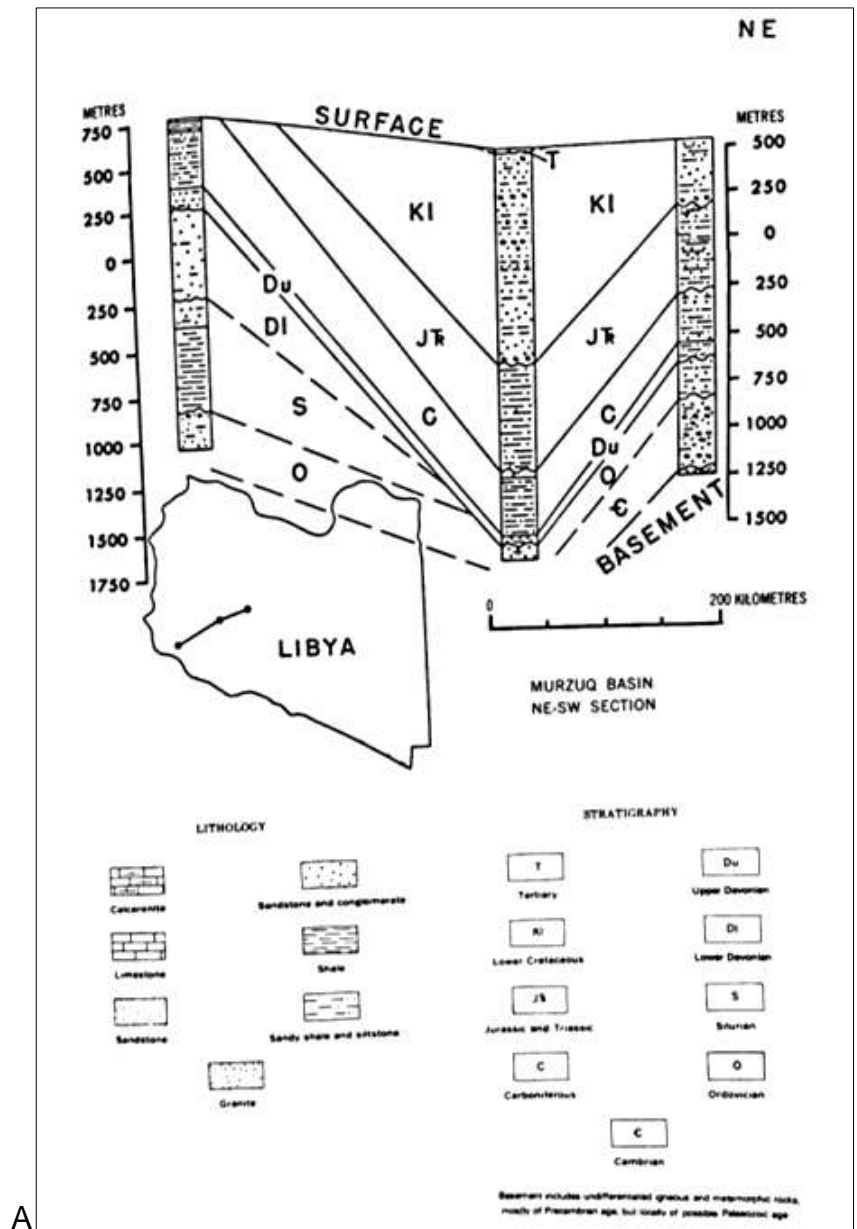


Figure 1.4: (A) The stratigraphic sequences and the lithology within the Murzuq Basin (Goudarzi, 1980: Figure 9, pp 889).

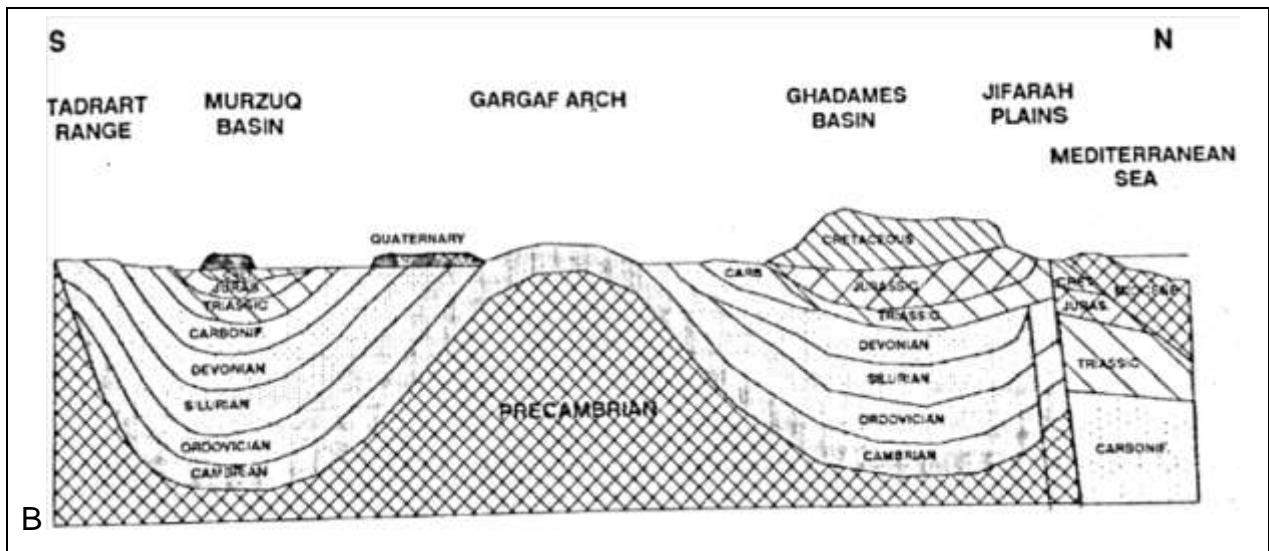


Figure 1.4: (B) N-S schematic cross-section, western Libya (Tawardos, 2001).

Sediments of the basin's south and east margins consist of conglomerate alluvial-fan type deposits. Only the coarser fraction of the deposited sediments was retained in the basin due to the differing rates of uplift and subsidence of the Tibetsi Massif and Al Qarqaf arch respectively (Bellini & Massa, 1980). Of this coarse sediment only a portion was permanently deposited in the basin, the rest was deposited as the Kikla and Cabao Formation of Tripolotania (Bellini & Massa, 1980).

The Sahara was glaciated during the late Ordovician period which left striations, tillites and erratics as evidence (Grove, 1980). Marine transgressions followed in the Silurian and Mesozoic, interspersed with periods of continental erosion and basin filling (Goudarzi, 1980; Thomas, 1997; Tawardos, 2001). The Al Qarqaf Arch (also known as the Gargaf Arch) was also formed during the Paleozoic. Subaerial weathering and erosion marked the Cenozoic (in North Africa, particularly the southern Sahara), and led to the development of silicate karst landscapes (Thomas, 1997). During this time the escarpment to the east (Fig. 2.4) formed and continental brackish water sediments filled the depressions (Goudarzi, 1980; Tawardos, 2001). This was followed by a dry period that persists to the present (Goudarzi, 1980; Tawardos, 2001)

1.4.4 Quaternary Climate

The Quaternary period was characterised by successive humid and arid phases in the Sahara region (Edmunds and Wright, 1979; White *et al.*, 2006; Biagetti and Di Lernia, 2013) (Table 1.2). During this period there have been variations in climate especially

in the mean annual temperature and the precipitation amount and intensity. Several shorter humid phases separated by arid intervals have occurred since the end of the Pleistocene period (11 700 years BP). A general rise in temperature (increasing aridity) starting approximately 14 000 years BP is supported by several lines of evidence including radiocarbon dating of lacustrine carbonates and shells, mammal remains and soil pedestal wood samples. Two short humid phases can be distinguished during the Holocene (a rainfall maxima approximately 8500 and 5500 years BP) with one arid phase interval that occurred around 7000 years BP. An increase in aridity has been noted since 4800 years BP, no significant humid phase has occurred since 3500 years BP (Edmunds and Wright, 1979; White *et al.*, 2006).

Table 1.2: Quaternary period climatic timeline of the Saharan region, and indicative references

Date	Arid/Humid	Evidence/ Other Information
35-13 ka BP	Humid	Uninterrupted cold wet period with average mean annual temperature of 16°C during cold period (5°C increase in Holocene) (Giraudi <i>et al.</i> , 2012)
13 – 11 ka BP	Arid	Enhanced aeolian transport; sporadic fluvial floods resulting in increased transport of coarse material (Swezey, 2001; Giraudi, 2005)
10.5 – 8.7 ka BP	Humid	Aquifers risen, fluctuation of ecological conditions from fresh to eusaline water (increase in salinity due to increased evaporation from continental water); stratigraphic record – indicating high water table position and sea level, and pollen analyses (Fontes & Gasse, 1991; Swezey, 2001, 2009; Giraudi <i>et al.</i> , 2012)
9 - 6 ka BP	Arid	Based on data from lake levels (Fontes & Gasse, 1991)
6 - 4.8 ka BP	Humid	Increased rainfall (Edmunds & Wright, 1979) (mean annual rainfall approximately 300-400 mm/yr - enough to sustain savannah vegetation) based on radiocarbon dating and pollen analyses (Swezey, 2001)
4 – 3 ka BP	Arid	Arid conditions re-established – resulting in changes in human occupation and habits in the area (based on archaeological evidence from excavations in the area) (Biagetti & di Lernia, 2013), and fluctuations in lake levels (Fontes & Gasse, 1991)
3 ka BP - Present day	Extremely Arid	Based on analysis of soil pedestal wood samples, terrestrial dust concentrations, lacustrine data sets and climatic modelling (Cremaschi <i>et al.</i> , 2006)

1.4.5 Present Climate

The present climate of the area is arid (Biagetti and di Lernia, 2013) and characterised by the *harmattan* (north eastern trade winds) that prevails across the Sahara; these winds extend to the Inter Tropical Convergence Zone (ITCZ) at the surface and carry dust (Laity, 2008). The desert climates in the Sahara can mainly be attributed to the Subtropical high pressure cell that covers a large area of the African continent (Thomas, 1997; Mamtimin *et al.*, 2011). The Central Sahara has been described as being the most arid sector within the Sahara, however occasionally moisture enters this area and the mountains in the area orographically enhance rainfall (White *et al.*, 2006).

Cremašchi and Zerboni (2009) stated that the climate of the south western Fazzān is hyper arid, with a mean annual temperature of 30 °C and mean annual precipitation of 0-20 mm. These precipitation values correspond with a study by Mercuri (2008) who found mean annual precipitations of approximately 10 (19) mm and mean annual temperatures of 23.4 (26.6) °C with mean maximum temperatures ranging from 30.6 (34.0) °C in June and mean minimum temperatures of 12.8 (13) °C in January from weather stations in the towns Sabhā and (Ghat). In a more recent study by Mamtimin *et al.* (2011) mean annual temperatures of 23.3, 22.4 and 23.4 °C and mean annual rainfall totals of 1.8, 7.13 and 8.08 mm were recorded at three weather stations representative of the hot desert type in Libya.

The average summer (winter) temperature and precipitation (2005-2014) within Sabhā and Ubārī (two of the towns) located at the edges of the Ubārī Sand Sea are 31 (15) °C, with an average rainfall of 1.7 (1.9) mm in Ubārī (26°34'59" N; 12°45'59" E; 463 m a.s.l.; Fig. 1.1). Similarly Sabhā (27°02'19" N; 14°25'35" E; 432 m a.s.l.; Fig. 2.1) has average summer (winter) temperatures of 31 (14) °C but no precipitation was recorded for a ten year period within this time series. The average wind speed for these two areas ranges between 6.5-8.3 km/h (winter and summer respectively) in a dominantly Easterly direction (Ubārī) and 15.7-20.1 km/h (winter and summer respectively) in a dominantly East to North-East direction (Sabhā) (WeatherOnline, 2014a; 2014b; Weatherbase, 2015a; 2015b).

1.4.6 Sand Dunes of the Central Sahara

Within Saharan sand seas the most common dune type is linear dunes (with no sand in the interdunal areas). These dunes have a well-defined wavelength and are arranged in parallel ridges (this is true mostly for the large dunes; smaller linear dunes generally do not have a well-defined wave length). These dunes are up to 200 m in height and several hundred kilometres in length (along the crest), and are often superimposed by transverse and/ or barchans dunes. It can be inferred that a change occurred in the wind regime based on the variation in dune scale and orientation that appear to coexist. The huge linear dunes then serve as the erodible bed from which the instability develops (du Pont, 2015).

Within the Central Sahara desert there are several sand seas, including the Ubārī, Murzuq and Uan Kasa sand seas (Figure 1.1).

Sand seas typically consist of complex dune patterns, in which two or more dune types have joined together or are superimposed (du Pont, 2015). A complex dune pattern usually forms over several generations of formation in which the larger, slower dunes are surpassed by smaller, faster moving dunes (du Pont, 2015). Holocene dunes are typically superimposed on Pleistocene linear megadunes (draa) (Bubenzer & Bolten, 2008; Mercuri, 2008). The linear megadunes were most likely formed during the hyper-arid Last Glacial Maximum (more than 20 ka cal BP), as a result of the increase in the wind velocity (due to the enhanced pressure gradient between the larger cold polar region and the tropics (Bubenzer & Bolten, 2008; Mercuri, 2008).

Due to the limited amount of studies conducted in the Ubārī Sand Sea little information is available on the dunes in the area. Therefore the dune patterns and origins of the Great Sand Sea of Egypt and the Uan Kasa Sand Sea will be briefly discussed. Both sand seas occur within the wider Central Sahara desert (Bubenzer & Bolten, 2008; Cremaschi & Zerboni, 2009).

Within the Great Sand Sea of Egypt the linear megadunes were formed by strong trade winds during the last glacial maximum (Bubenzer & Bolten, 2008). Strong, dry westerlies deposited sand further south on the eastern slopes of the megadunes at the end of the Pleistocene. The upper parts of the megadunes were reactivated approximately 7 ka cal BP (with the onset of the modern hyper aridity), due to the decrease in the velocity of the wind the bodies of the megadunes remained stable –

resulting in active dunes that reach heights of 5 – 30 m superimposed on the stable linear megadunes that reach heights of 50 m (Bubenzer & Bolten, 2008).

The Uan Kasa sand sea (Figure 1.1) is north-south orientated and 200 km in length. It is made up of linear dunes that are parallel aligned, exceeding 100 m in height, with interdune corridors that are wide and flat. The hydromorphic conditions of the area resulted in accumulation of saprolite (friable weathered sand stone) and etiolated sand (bleached and mottled sand) at the base of the dunes. A rise in the water table and the storage of rain water in the intergranular pore spaces of the sand due to enhanced water supply resulted in an increase in the water availability. This water availability led to an increase in weathering of the dune slopes and resulted in the formation of deep soils. Small, shallow lakes and ponds formed in areas with suitable geomorphologic conditions and outcrop aquifers – a phenomenon that can also occur in the Murzuq sand sea (coinciding with 8000 years BP dry event) (Cremaschi & Zerboni, 2009).

The general dune type within most parts of the Central Sahara is linear dunes. From the Landsat satellite image (Figure 1.5) it can be seen that the dominant dune type within the Ubārī Sand Sea is also linear dunes. These dunes have been described as having heights of approximately 100 m and lengths of 100 km and covered by barchan dunes on the surface (McKee, 1979). These superimposed barchans are believed to be a result of modern aeolian activity, whereas the large primary dunes were most likely formed by aeolian activities of the past (McKee, 1979). In the northern and western part of the sand sea some star dunes can also be seen, as described by McKee (1979) the linear ridges combine forming a star dune field in the centre of the sand sea (Figure 1.5).

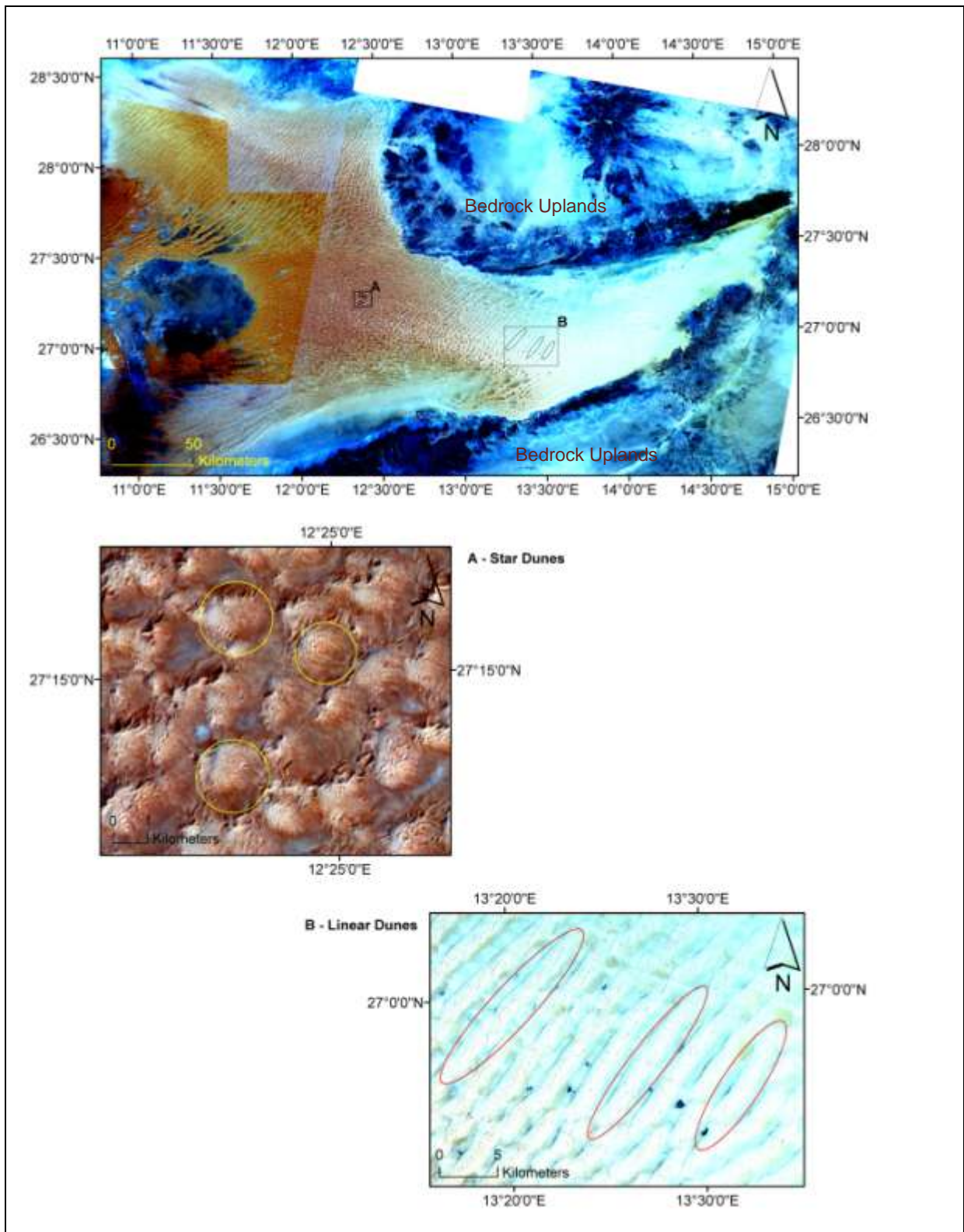


Figure 1.5: Mosaic image of six Landsat 8 tiles covering the Ubārī Sand Sea (October 2015), depicting the following types of dunes: (A) star dunes (three individual star dunes are circled in yellow), (B) linear dunes (three individual linear dunes are circled in red)

Chapter 2: Literature review

2.1 Introduction

Sand dunes (both coastal and inland) cover approximately 10% of the land area between 30° north and south latitudes (Levin *et al.*, 2004) and 14.2% of the land surface of Earth (Badescu *et al.*, 2008). Dune heights generally range from 30 cm to over 300 m, but their extent is usually more accurately known than the height (Levin *et al.*, 2004).

Dune movement or migration occurs when individual grains are transported by the wind. This movement (stability of the sand dune) is influenced by the wind strength, duration and direction; erosion (extent and rate), distance from the source, grain size, topography and the texture of the surface, it is also influenced by vegetation cover and surface moisture (El-Baz, 2000; Badescu *et al.*, 2008; Flagg *et al.*, 2014).

This chapter will explore the formation and migration of sand dunes specifically within arid environments as well as the possibilities of using remotely sensed satellite imagery (specifically multispectral imagery) in combination with a GIS to study these dunes and their movement.

2.2 Sand dunes and dune migration in arid environments

2.2.1 Sand dunes in arid environments

Sand dunes are “heaps of sand” that are formed by the transport and deposition of sand grains, in arid environments dunes are usually seen in sand sea systems (or Ergs) (du Pont, 2015).

These grains are deposited (where they then accumulate) either when faced by an obstruction/ obstacle (rock, tree, etc) or if the wind velocity no longer exceeds the grain size threshold velocity (thus the wind is not strong enough to carry the grains) (Goudarzi, 1970; du Pont, 2015). Sand dunes usually consist of a windward slope, a crest and a lee- / slipface (avalanche face). The crest is the break of slope between the windward slope and slipface. The windward slope is usually characterised as longer with gradual gradient whilst the slipface usually has a steep gradient and

regularly has a concave shape (Fig. 2.1). The heavier grains are deposited on the windward slope and the smaller/ lighter grains are transported further up the slope, as it passes the crest due to gravity and decreased wind speed the deposition rate increases and grain flow results from overloading at the brink point.

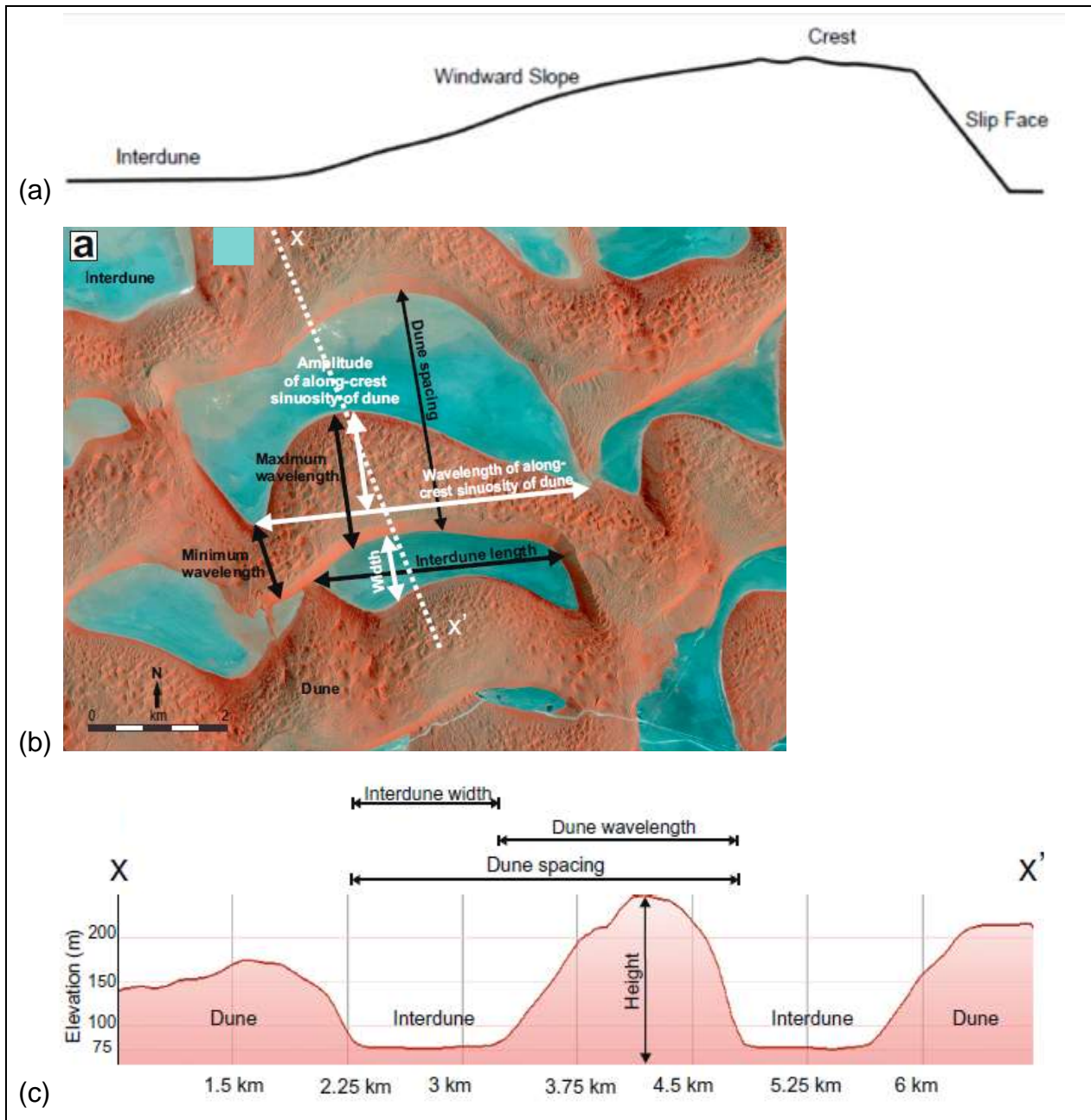


Figure 2.1: (a) Sketch of a cross section of a sand dune, showing the windward slope, crest and slipface, (b) Satellite image of a section of the Rub'Al-Khali sand sea showing the dune morphology from above and (c) a cross section of the same section within the dune field showing the dune and interdune areas, dune wavelength and spacing (Al-Masrahy & Mounney, 2013: their Figure 4, p. 161).

2.2.2 Dune Morphology

There are several different types of dunes: Barchan dunes, transverse dunes, linear dunes, star dunes and parabolic dunes. Based on the wind directionality, sediment supply (Mainguet & El-Baz, 1986; du Pont *et al.*, 2014) and topography of the area (Goudarzi, 1970; du Pont, 2015), dunes can be classified into three groups (those that form in a monodirectional, bidirectional and multidirectional wind regime) and six types based on the shape and orientation of the resulting dune crest (Barchan, Transverse, Star, Linear and Parabolic dunes, see Figures 2.2 and 2.3) (Mainguet & El-Baz, 1986; du Pont *et al.*, 2014; du Pont, 2015). In areas with a larger supply of sand combined with a unimodal wind regime, transverse or barchans dunes are usually the results. Similarly, in areas with smaller sand supply and accompanied by a multidirectional or complex wind regime star dunes usually occur (Huggett, 2007) (Figure 2.3).

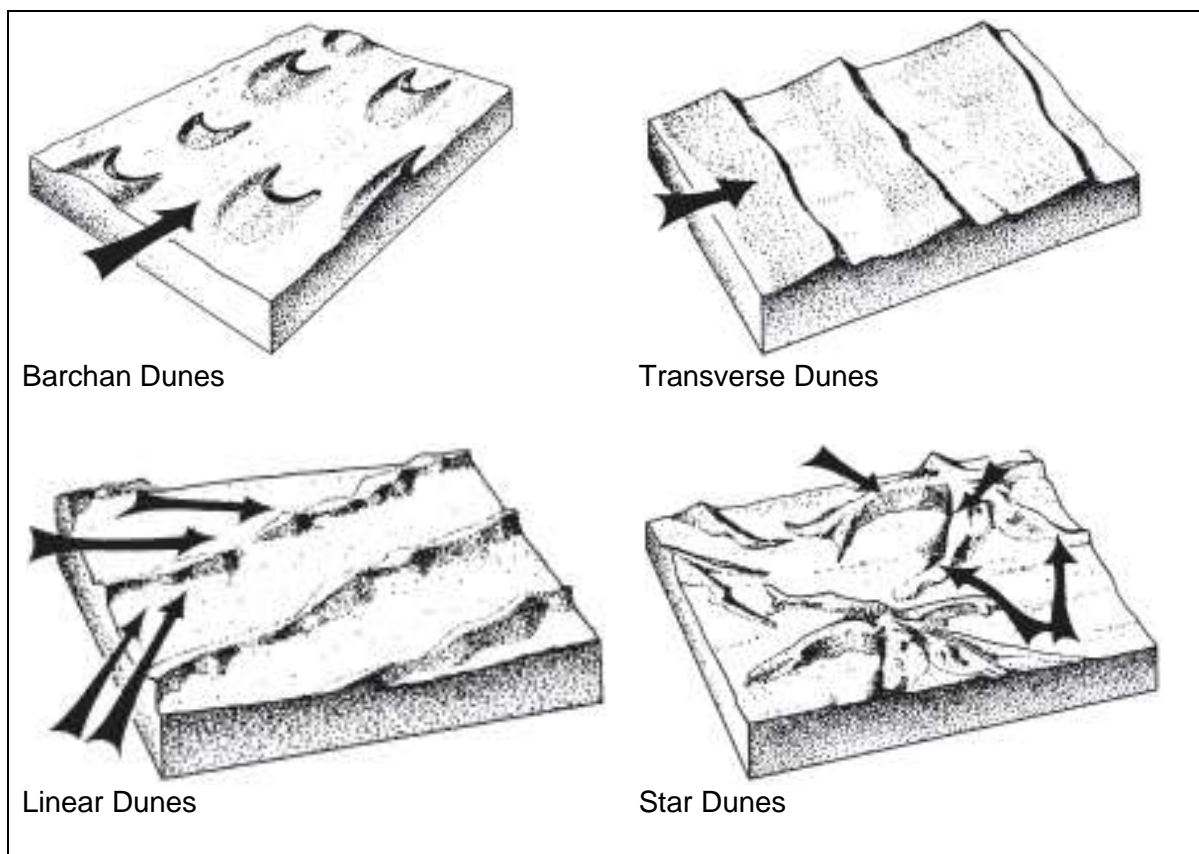


Figure 2.2: Sand dune types and their dominant wind direction (show with black arrows) (McKee, 1979: his Figures 3-5, 11, pp. 11 & 13)

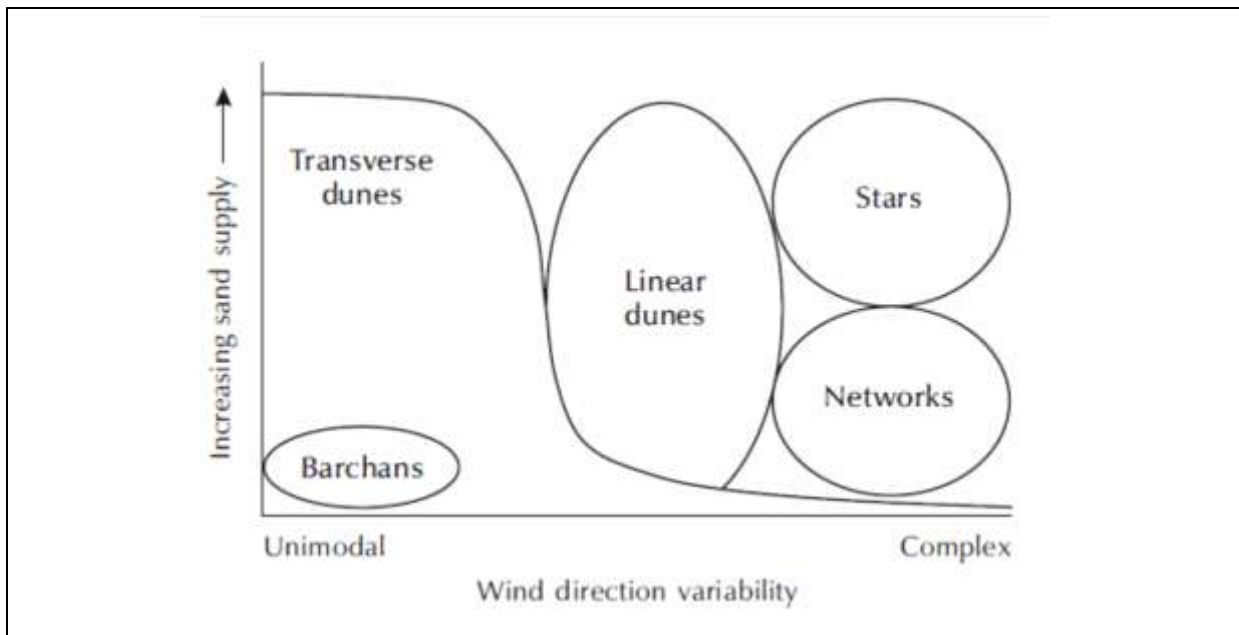


Figure 2.3: Dune types in relation to the variability of wind direction and sand supply (Huggett, 2007: his Figure 12.4, p. 303).

Uni-directional wind regimes results in dunes with crest orientations that are perpendicular to the wind direction. Bi- and multi-directional wind regimes result in an “averaged” crest orientation maximizing the normal transport of sand to the dune crest as winds from different directions and strengths each contributes to the dune’s development over time (du Pont, 2015).

3.2.2.1 Uni-directional wind regime:

a. Barchan dunes

Barchan dunes are thought to be the “elementary dune form” and forms in areas with moderate sediment supply and wind velocity. This dune type most commonly occurs in isolation on a non-erodible surface. When viewed from above the dunes have a crescent shape with two arms extending in the downwind direction (Fig. 2.4). The crescent shape of the dune develops under a uniform wind approaching the dune but due to the increased height of the centre (compared to the sides) of the barchans the grains in the centre have to be transported higher (and further) than those at the sides. This results in faster transport of grains along the sides/arms than the centre of the dune resulting in the crescent shape of barchans (du Pont, 2015). The slipface of

barchan dunes are on the concave side of the dune (Mainguet & El-Baz, 1986; Livingstone, *et al.*, 2007; du Pont *et al.*, 2014; du Pont, 2015) (Fig. 2.2 and 2.4). Barchan dunes range in height from 1 to 50 m and between 10 to 500 m range in length and width. These dunes typically migrate fast at a rate ranging from 1 to 70 m/year (depending on wind strength and dune size) (du Pont, 2015).

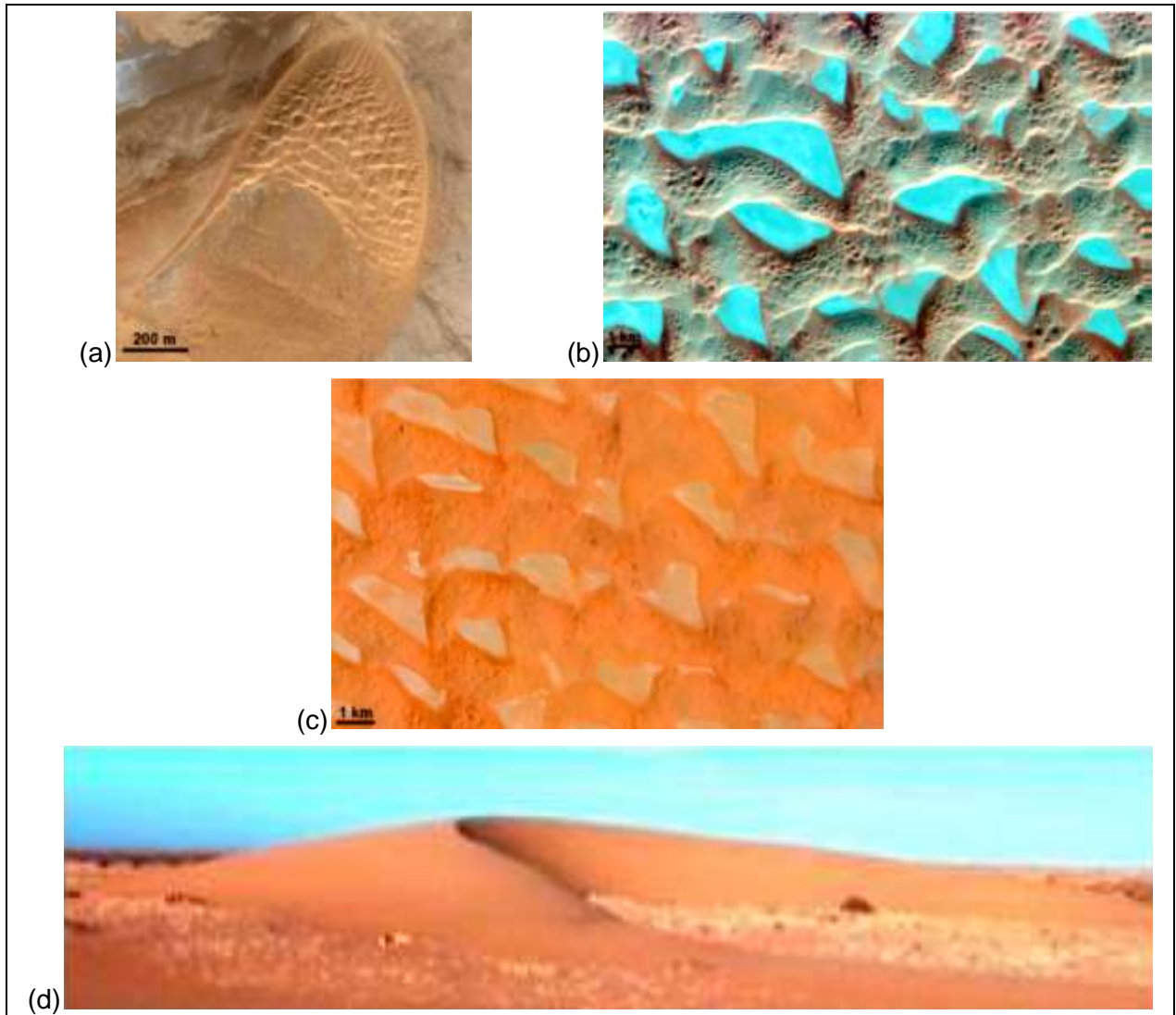


Figure 2.4: (a) Google Earth image of a Mega Barchan dune in Morocco (du Pont, 2015: his Figure 3d, p. 126); (b) satellite image of mega-barchan dunes in the north eastern section of the Rub' Al-Khali sand sea (Saudi Arabia); (c) satellite image of complex barchans dunes with superimposed dunes on the northern section of Rub' Al-Khali sand sea (Saudi Arabia) (Al-Masrahy & Moutney, 2013: their Figures 6a and b, p. 163); and (d) Photo of a Barchan dune in the vicinity of Tarfaya (Morocco) (du Pont, 2015: his Figure 3a, p. 126).

b. Transverse dunes

Transverse dunes are found in arid areas with a unidirectional wind regime on a erodible surface (du Pont, 2015). Transverse ridges can also form when the sand supply increases to such an extent that migrating barchan dunes link into barchanoid ridges and then form transverse ridges (dunes). These dune crests form perpendicular to the dominant wind direction and are usually long linear dunes (Figure 3.2 and 3.5). This type of dune is commonly found in dune fields with a well-defined wavelength (Livingstone, *et al.*, 2007; du Pont, 2015). Transverse dunes are also commonly found superimposed upon larger dunes or draa (du Pont, 2015).

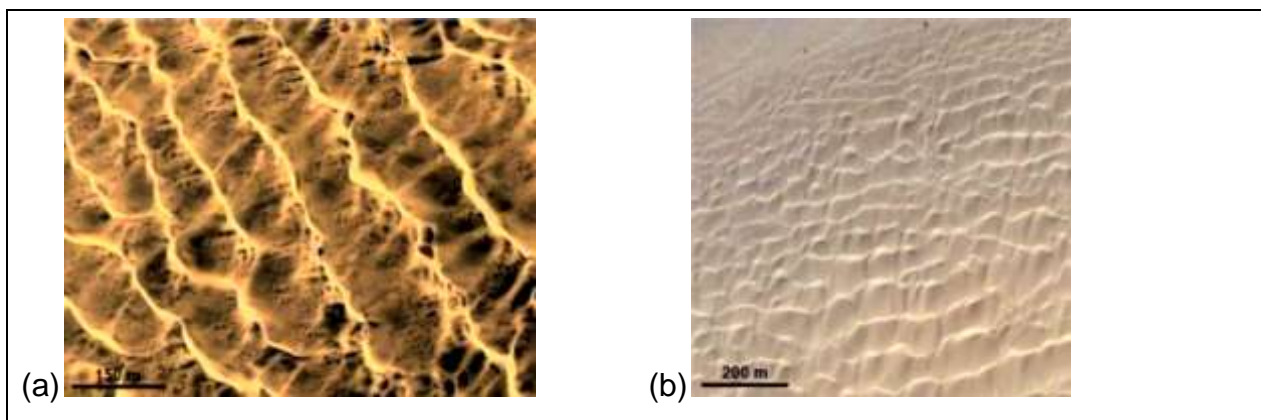


Figure 2.5: Google Earth images of transverse dunes in (a) Morocco and (b) Mocamedes desert (Angola) (du Pont, 2015: his Figures 4a and b, p. 128).

3.2.2.2 Bidirectional wind regime

a. Linear (seif) dunes

Linear dunes can be identified as straight dunes, parallel to the dominant wind regime, and are usually smaller in width than length (Fitzsimmons *et al.*, 2007; Telfer *et al.*, 2015) (Figures 2.2 and 2.6). These dunes occur in regions with a bimodal wind regime (with an obtuse angle between the two wind directions) (Livingstone *et al.*, 2007; du Pont *et al.*, 2014; Telfer *et al.*, 2015). The bimodal wind regime is not necessarily symmetrical resulting in an asymmetrical development of the dune (Livingstone *et al.*, 2007).

The crests of simple linear dunes are sharp and the orientation of the slipface may change (as a result of the bidirectional winds) but the crests can also be broad with

superimposed dunes (Livingstone *et al.*, 2007; du Pont *et al.*, 2014; Telfer *et al.*, 2015) and in some areas linear dunes may have more than one crest line (e.g. Great Sandy Desert in Australia). Although individual dunes are sometime only ~10 m high and ~100 m wide, they can range in length from ~10-100 km (Telfer *et al.*, 2015). Linear dunes are usually evenly spaced resulting in highly organized linear dune fields (major dune fields contain thousands of dunes) (Telfer *et al.*, 2015). Patterning in the dunefield can occur as the dunes coalesce and bifurcate resulting in an irregular spread of dunes and interdunes. This patterning is subjective to the interactions of the individual dunes based on the area and or site specific boundary conditions (Telfer *et al.*, 2015).

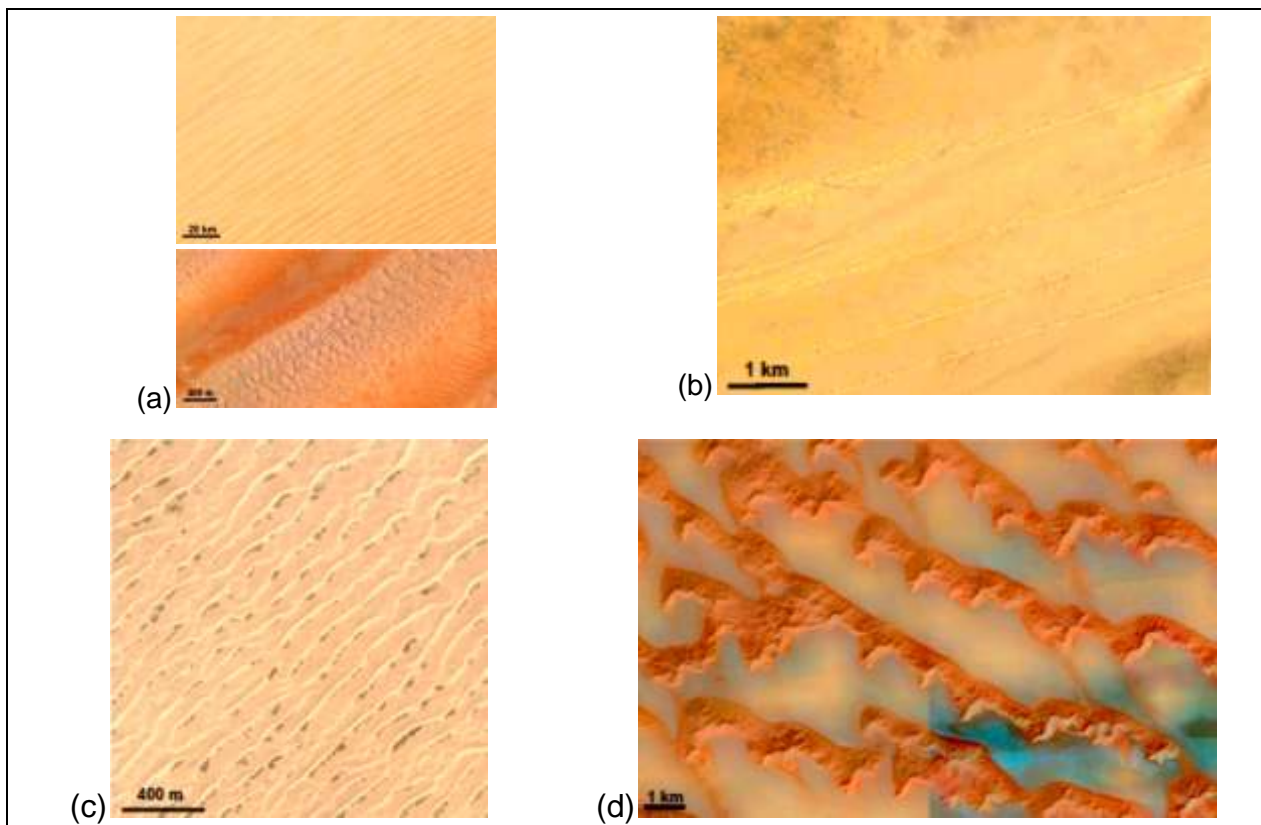


Figure 2.6: Google Earth images of (a) Seif dunes in Niger (b) Linear dune fields (top) and superimposed dunes (bottom) in the Rub'Al-Khali sand sea (Saudi Arabia); and (c) dunes in the Mu Us Desert (China) (du Pont, 2015: his Figures 5b, c and e, p. 130); and (d) a satellite image of compound linear ridges from the southern section of the Rub' Al-Khali sand sea (Al-Masrahy & Mountney, 2013: their Figure 6c, p. 163).

3.2.2.3 Multidirectional wind regime

a. Star dunes

Star dunes can be identified by their multiple radiating arms from the massive pyramidal centre (Figures 2.2 and 2.7) and are formed under multidirectional wind regimes (resulting in a small overall sand flux) (Mainguet & El-Baz, 1986; du Pont *et al.*, 2014; du Pont, 2015). These dunes can usually be found at the boundaries of sand seas especially close to topographic boundaries and are most commonly seen at high pressure belt latitudes (du Pont, 2015). Initially the dune grows by sand accumulating at the centre of the dune pile, only when a maximum height and length has been reached does the radiating arms start to grow. These dunes are relatively large (as a result of the small overall sand flux) and can be approximately 1 km wide and 100 m high. These dunes appear to interact with their radiating arms forming a regular network (du Pont, 2015).

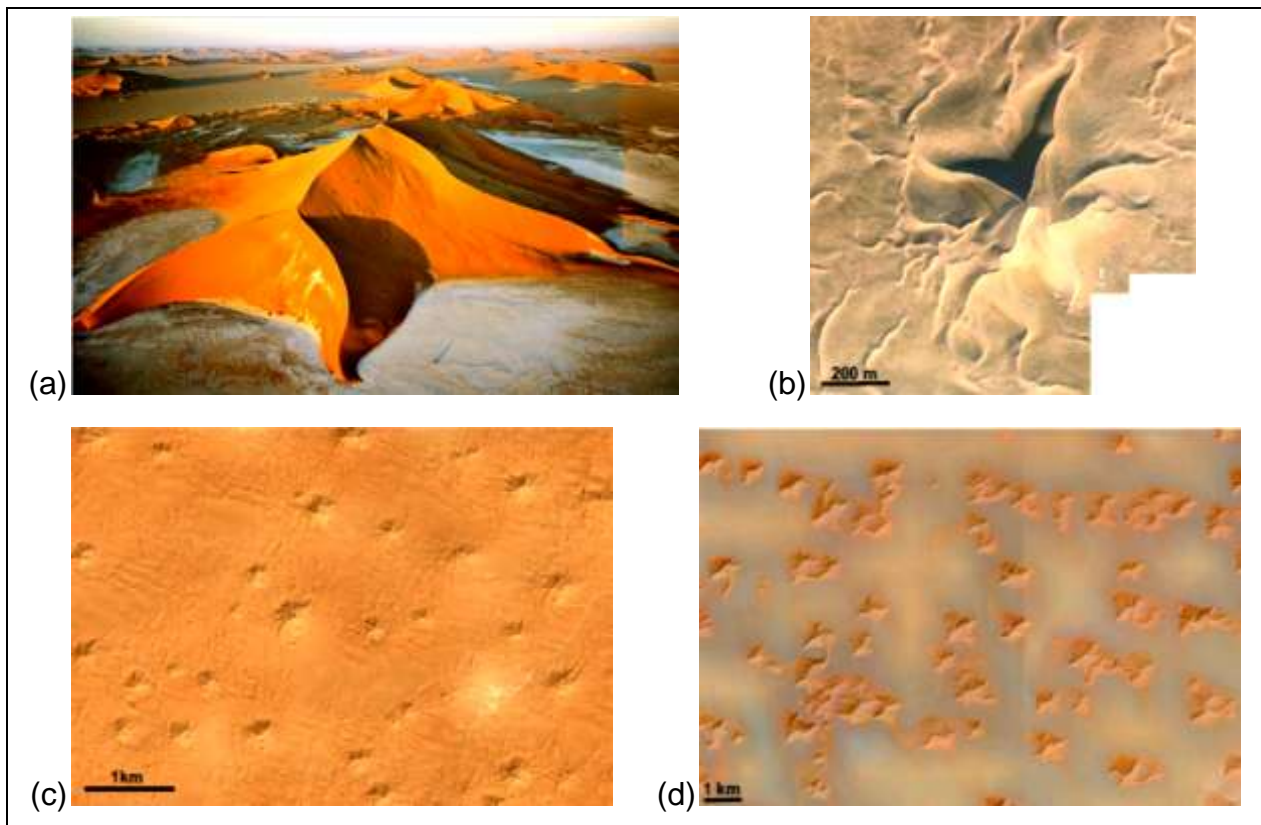


Figure 2.7: (a) Photo of a star dune in the Rub Al-Khali sand sea, (b & c) Google Earth images of star dunes in Algeria (du Pont, 2015: his Figures 6a, b and c, p.132); and (d) satellite image of star dunes in the central section of the Rub' Al-Khali sand sea (Al-Masrahy & Mountney, 2013: their Figure 6d, p. 163).

2.2.3 Sand seas

Some desert dunes can be found in seclusion but are more often clustered together in groups (in some cases thousands of dunes), these dune groups are referred to as sand seas (dune-fields or ergs) (Al-Masrahy & Mountney, 2013; du Pont, 2015; Telfer *et al.*, 2015). Within these sand seas both systematic patterns and a certain degree of spatial uniformity can be found (Al-Masrahy & Mountney, 2013; Telfer *et al.*, 2015). The dunes present within these sand seas may merge or split apart forming new patterns. This patterning is a result of self-organizing systems with complex interactions with the regional atmospheric boundary layer and sediment source (Al-Masrahy & Mountney, 2013; Telfer *et al.*, 2015). Du Pont *et al.* (2014) stated that sand seas exhibit a great variety of dune shapes, sizes and orientations as a result of the wide variety of wind directionality and velocities (in relation to seasonality and long term climate changes) that are experienced within most of the sand seas.

Sand seas are not completely covered in active sand dunes, other morphological bodies (interdunes, soil cover, sand sheets, fluvial systems and lacustrine systems) may also be present (Al-Masrahy & Mountney, 2013). The formation of sand seas and the spatial variations therein are influenced by several factors including: sediment supply and availability and wind strength, these factors influence the time and place where growth may occur (Al-Masrahy & Mountney, 2013; du Pont, 2015).

Because dunes only migrate in the presence of wind, if there is no wind there is no movement and therefore dunes represents the wind regime over long periods and not just the present wind regimes, thus superimposed patterns are formed with a range of shapes and sizes. This information is used to predict climatic conditions on other planetary bodies where similar dune patterns are found (du Pont, 2015). Large dunes represent the different wind regimes of its past and shows this hierarchy of superimposed dunes starting from its elementary length (~20 to 30 m) (du Pont, 2015). It has been found that primary linear dune trends do not always correspond to the modern wind regime (the orientation of the superimposed dunes that are younger than the primary dunes do match the modern wind regime). This can be attributed to the age of the primary dunes (the wind regimes may have changed since the formation of the primary dunes) (Mainguet & El-Baz, 1986; Fitzsimmons *et al.*, 2007; du Pont *et al.*, 2014; du Pont, 2015). Fitzsimmons *et al.* (2007) stated that fully

stabilised dune field are considered to preserve periods of past aridity and desert expansion more effectively than semi-active dunes in the arid core.

Several sand seas occur within the Sahara (see Figure 2.8).

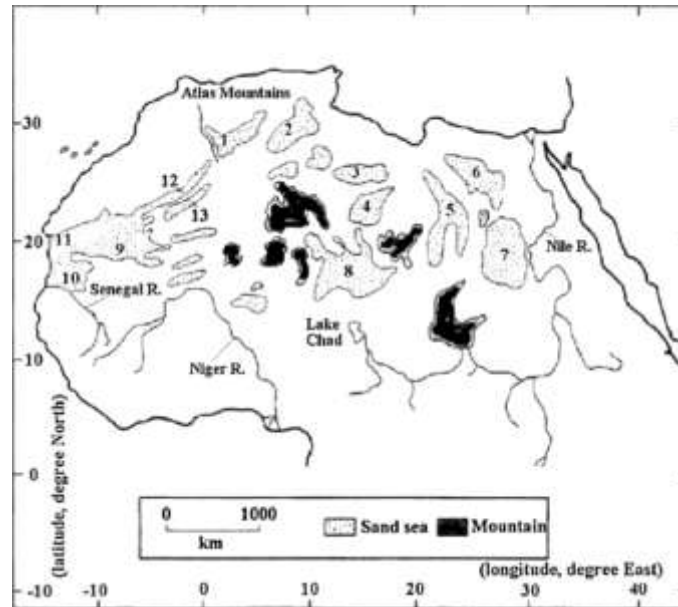


Figure 2.8: Sand Seas of the Sahara, 1. Grand Erg Occidental; 2. Grand Erg Oriental; 3. Ubārī; 4. Murzuk; 5. Calanscio; 6. Great Sand Sea; 7. Selima; 8. Fachi-Bilma & Te'ne're'; 9. Majabat al Koubra; 10. Aouker; 11. Akchar; 12. Iguidi; 13. Chech (from Badescu *et al.*, 2008: their Figure 1, p. 2).

2.2.4 Sand dune migration in arid environments

Sand dune migration is the process where the sand particles are transported (usually includes grains eroded from the windward slope) by the wind across the dune where it falls down the slip face and settles. The next set of grains is also transported across the dune and settles on top of the previously transported grains. This process continues as long as there is wind and so the dune migrates grain by grain in the direction of the wind transport (see Figure 2.9).

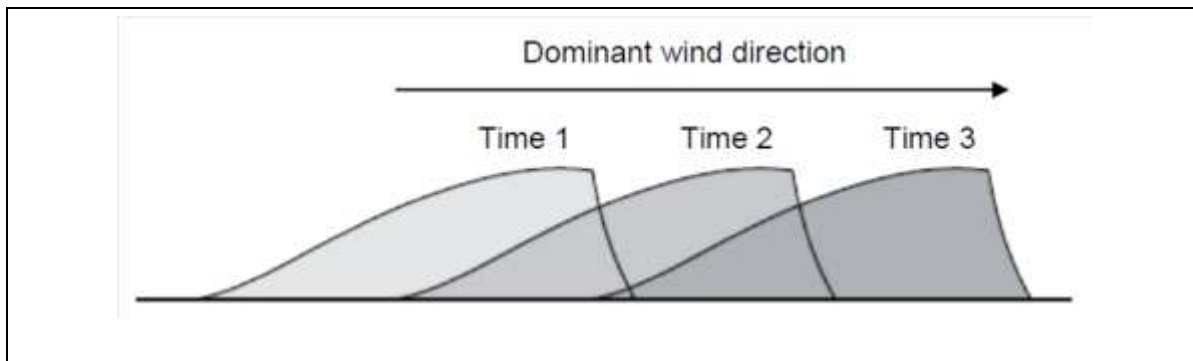


Figure 2.9: The downwind progress of a transverse dune (Adapted from Huggett, 2007: his Figure 12.3, p.303).

The transportation of sand grains can be divided into three groups: 1. Saltation, 2. Creep, and 3. Suspension (du Pont, 2015; See Figure 2.10). Saltation is characterised by “jumping” grains, creep by rolling grains (that are often dislodged by saltating grains), and suspended grains are those that are “air borne” and can be transported over long distances. Only saltation and creep modes of transport are relevant to dune dynamics (Masselink *et al.*, 2011; du Pont, 2015).

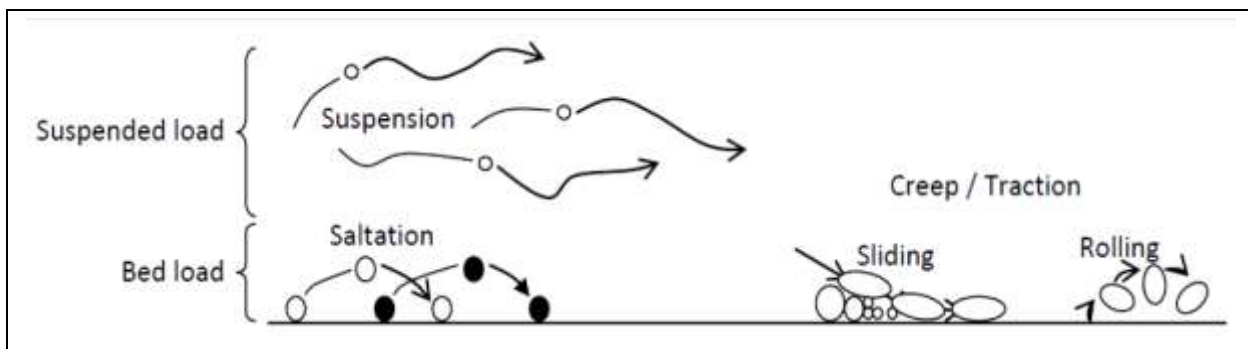


Figure 2.10: A schematic representation of the different modes of transport of sand grains (Adapted from Masselink *et al.*, 2011).

Different dune types have different characteristics that influence their rate and direction of migration. Tsoar *et al.* (2004) and El-Magd *et al.* (2013) classified dunes into three distinct groups: net migrating (transverse and barchan dunes), net elongating (linear dunes), and net accumulating (star dunes) dunes, based on the wind regime and topography (Mainguet & El-Baz, 1986; Tsoar *et al.*, 2004; du Pont *et al.*, 2014). In the case where the entire body of the dune moves with little/no change in the shape and dimensions of the dune it is known as a migrating dune (Tsoar *et al.*, 2004; El-Magd *et al.*, 2013). Migrating dunes are the most active group of dunes and can pose a threat to infrastructure and land cover/use, e.g. covering fertile soil with

sand (Ghadiry *et al.*, 2012; El-Magd *et al.*, 2013). Elongating dunes are dunes that experience an increase in length (as the migration occurs parallel to the wind direction) over time. Accumulating dunes (e.g. star dunes) may grow in height not necessarily in width or displacement (Mainguet & El-Baz, 1986; Tsoar *et al.*, 2004; El-Magd *et al.*, 2013). Transverse dunes typically migrate perpendicular to the orientation of the dune crest in the direction of the dominant wind regime, whilst linear dunes extends (migrating parallel with the crest orientation in the direction the direction of the dominant wind regime) and oblique dunes (barchans) both migrate and extend (du Pont, 2015).

Due to the dynamic nature of dunes, the different types of dunes change and/ or migrate at different rates, for example barchan dunes (reaching heights of 50 m or more) from Ceara, Brazil, move at an average rate of 17.5 m/year (Levin *et al.*, 2004) whereas the seif dunes from the Negev Desert migrated laterally at an average rate of 0.3 m/year over a 26 year period (1973-1999) (Rubin *et al.*, 2008) (these values are averages over several years, the annual migration rates varies from year to year). Refer to Table 2.1 for more examples.

Table 2.1: Dune migration rates per dune type from the literature.

Dune Type	Location	Migration Rate (m/yr)	Method	Source
Linear	Qaidam Pendi, NW China	1.3	Aerial photography	Livingstone <i>et al.</i> , 2007
Linear	NW Sinai (Bir El Abd & Wadi El Gady)	0.7 & 2 (lateral)	Field Study	Phillip <i>et al.</i> , 2004
Linear	NW Sinai (Bir El Abd & Wadi El Gady)	2.25 & 13 (elongation)	Field Study	Phillip <i>et al.</i> , 2004
Barchan	Toshka Depression	1.3-19.3	OSD* (Landsat)	El-Magd <i>et al.</i> , 2012
Barchan	NW Sinai (Wadi El Massaged)	3.5	Field Study	Phillip <i>et al.</i> , 2004
Barchan	Daklha Oasis, Egypt	3-9	SPOT	Ghadiry <i>et al.</i> , 2012
Combination (Linear, Barchan, Transverse)	Great kobuk Sand Dunes	0.5-3.8	SPOT & ASTER	Necsoiu <i>et al.</i> , 2009

*OSD – on screen digitization

Sediment mobility is usually related to precipitation and surface moisture (sand mobility is decreased with increased moisture content), evaporation, wind magnitude, sediment supply, grain size properties and vegetation cover (increased vegetation cover inhibits sediment movement) (Walsh *et al.*, 1988; Levin *et al.*, 2004, 2006). Several wind parameters need to be considered including wind velocity and direction, these parameters can be influenced by the topography, vegetation cover, biogenic crust, surface moisture content, water table position and deposition of fine particles (Walsh *et al.*, 1988; Levin *et al.*, 2004, 2006, 2012). Dune mobility indices are usually based on climatic variables such as temperature, evapotranspiration, wind energy, rainfall and sediment supply (Levin *et al.*, 2012).

Ramsey *et al.* (1999) stated that sediment weathering, transport and erosion are ongoing processes within active sediment transport pathways in arid environments. They also stated that the analysis of dune-fields (composition and movement) is a critical component for interpreting past climatic conditions, local geology, and future desertification potential.

2.2.5 Studying sand dunes and sand dune migration

In order to develop models with which the principal controls on the distribution of desert dunes can be explained, it is important to understand the morphology and distribution of dune deposits and interdune areas (Al-Masrahy & Mountney, 2013). Establishing spatial trends in dune morphology and understanding the morphological complexity of modern systems can also assist in the reconstruction of palaeoenvironments and predictions of subsurface strata successions (Al-Masrahy & Mountney, 2013) and wind patterns (Varma *et al.*, 2014). It has become important to be able to accurately map and monitor deserts and desert environments in order to employ the correct management actions (e.g. if the dunes are migrating in the direction of populated or agricultural areas, it would be necessary to take immediate steps) (Varma *et al.*, 2014).

Various challenges and problems (including dune formation, desertification, land-degradation, climate change, water shortages, urbanization and management concerns regarding waste, land and vegetation shortages) are faced by urban areas, engineering practices and humans in desert cities (Badescu *et al.*, 2008; Aldossary, 2012). Within Mauritania, good examples of urban areas affected by dune migration can be found, where in the ancient city Chinguetti, several of the homes on the edge of the city were abandoned due to the invasion of desert sands (Badescu *et al.*, 2008).

2.3 Remote sensing and GIS in relation to sand dunes and sand dune migration

2.3.1 Introduction

Satellites acquire images of the earth's surface by measuring the energy (reflected from the earth's surface) in different spectral bands. The physical and chemical

properties of materials absorb, reflect and emit electromagnetic energy in different parts of the Electromagnetic (EM) spectrum. The amounts of energy measured can be used to deduce information about the object being observed (Kennedy *et al.*, 2009).

Mohamed & Verstraeten (2012) state that several factors influence the electromagnetic spectrum (EMS) of dunes and should be taken into account when using satellite remote sensing to analyze dunes. Vegetation cover, biogenic-soil crust, moisture content, dune texture, morphological parameters and dune sand mineralogical composition are some of the relevant factors (Ramsey *et al.*, 1999; Howari *et al.*, 2007; Mohamed & Verstraeten, 2012).

Several remote sensing platforms have been used to study different aspects of sand dunes/seas (See Table 2.2). The most common platform used is Landsat (Pease *et al.*, 1999; Mohamed & Verstraeten, 2012; Al-Masrahy & Mountney, 2013), DEMs derived from ASTER and SRTM (Warren & Allison, 1998; Levin *et al.*, 2004; Necsoiu *et al.*, 2009) and some high resolution platforms such as SPOT (Ayad, 2005; Necsoiu *et al.*, 2009; Ghadiry *et al.*, 2012) and Quickbird (Hesse, 2009; Levin *et al.*, 2012).

Several types of geomorphological analyses (including area change, elevation change maps, elevation profiles, volumetric change calculations, identification of areas of net erosion and deposition, geomorphological mapping) can be done with the use of a Digital Elevation Model (DEM). In conclusion, using satellite imagery can enhance our understanding of dune processes and enable analysis of larger areas (Levin *et al.*, 2004; El-Magd *et al.*, 2013).

Table 2.2: Examples of remote sensing data that have been used for sand dune characterization from the literature

Remote Sensing Platform	Studied	Reference
ASTER Global Digital Elevation Model (GDEM)	Dune Morphometric Analysis	Bullard <i>et al.</i> , 2011 Mohammed &
Landsat	Dune Dynamics at the Dune Field Scale	Verstraeten, 2012 Al-Masrahy &
Landsat & SRTM	Spatial Variability of Dune and Interdune	Mountney, 2013
Landsat TM	Mapping Sand Dune Patterns Mineralogical Characterization &	Al-Dabi <i>et al.</i> , 1998
Landsat TM	Transport Pathways of Sand Dunes Dune Size and its relation to to the	Pease <i>et al.</i> , 1999 Warren & Allison,
Landsat TM	environment	1998
Landsat TM & ETM+	Dune Characterization	Levin <i>et al.</i> , 2004
Quickbird	Determining Dune Age Linear Dune Identification &	Hesse, 2009
SAR	Characterization	Qong, 2000
SAR (Polametric Synthetic Aperture Data)	Dune type identification Land use change in relation to dune	Blumberg, 1998
SPOT	migration	Ayad, 2005
SPOT	Sand dune encroachment	Ghadiry <i>et al.</i> , 2012 Necsoiu <i>et al.</i> ,
SPOT & ASTER GDEM	Monitoring Migration of Dunes	2009
SRTM	Dune Field Characterization	Bishop, 2010

2.3.2 The use of remote sensing and GIS in the study of sand dunes and dune migration in arid environments

The availability of high resolution satellite imagery has resulted in significant advances being made in the understanding of the spatial arrangement of dune patterns (Al-Masrahy & Mountney, 2013). Satellite remote sensing in combination with a geographic information system (GIS) can be used for the examination of spatial relationships at different scales that would be difficult to do with the use of only fieldwork or traditional aerial photography. Traditional methods are limited spatially

and is time consuming and very expensive for a small amount of data. Satellite remote sensing can cover larger areas in less time, is less expensive and several different processing techniques can be applied to the data to differentiate the multitemporal information (Paisley *et al.*, 1991; Levin *et al.*, 2004; Aldossary, 2012; El-Magd *et al.*, 2013). Remotely sensed data of any point on earth are collected every time from the same reference point and through the same sensors (Collado *et al.*, 2002). Remotely sensed data can also be used to explore spatial distributions and temporal trends of the earth's surface (Collado *et al.*, 2002; Aldossary, 2012).

Satellite remote sensing has been used over the past several decades to study desertification and sand dune morphology (Ramsey *et al.*, 1999; Collado *et al.*, 2002). Desert dunes have been termed an “ideal target” for monitoring (due to their remoteness and general lack of data; low cloud cover; uniform surfaces and low vegetation and urban cover) with the use of satellite remote sensing (Ramsey *et al.*, 1999). In some cases, actual sand dune migration rates can be measured from satellite imagery (Ramsey *et al.*, 1999; Ghadiriy *et al.*, 2012; Mohamed & Verstraeten, 2012; El-Magd *et al.*, 2013). This can give geologists a summarized view of large aeolian systems and their sediment sources (Ramsey *et al.*, 1999). Satellite imagery has also enabled a the study of the Toshka Depression (Egypt) on a wider scale and the determination of dune migration rates (El-Magd *et al.*, 2013), identifying and characterizing sand dunes and their dynamic nature (Collado *et al.*, 2002). Collado *et al.* (2002) made the observation that in order to discriminate sand bodies most authors rely on analysing the visible reflectance (0.4 – 0.7 μm), because it has been found that bare soil effectively reflect the visible bands (Collado *et al.*, 2002).

2.3.3 Limitations associated with the use of remote sensing and GIS in sand dune and sand dune migration studies

The main limitation associated with the study of sand dunes (especially in desert areas) with the use of multispectral remotely sensed data is the difficulty to discern the different parts of the dunes based on the spectral response alone, as the different parts of a dune (that are mainly made up of the same substance = sand) may have similar spectral signatures (Varma *et al.*, 2014). However, Mohamed & Verstraten (2012) noted that there may be different brightness patterns in the different parts of the dunes. This limitation may be overcome by combining multispectral and elevation data in order to assist in defining training data. Another possible solution to this is the

use of high spectral resolution data and/ or high resolution elevation data from active sensors, however, the costs related to this kind of data may outweigh the advantages associated with it.

2.4 Previous Research

Within this section previous research concerned with multi-spectral data will be reviewed with the focus placed on the influence of spatial resolution specifically on the analysis of dunes in arid regions.

2.4.1 Coarse spatial resolution imagery studies

In this study a coarse spatial resolution will be considered as a pixel size of 30 x 30 m or larger. Landsat is one of the most common forms of coarse resolution satellite imagery that has previously been used in sand dune studies (Paisley *et al.*, 1991; Al-Dabi *et al.*, 1998; Pease *et al.*, 1999; Ramsey *et al.*, 1999; Lam *et al.*, 2011; Mohamed & Verstraeten, 2012; Al-Masrahy & Mountney, 2013; Telfer *et al.*, 2015). This can be attributed to it often being public and freely available, has a wide temporal coverage and has a reasonable ground resolution for detecting dune system changes as well as limited radiometric and geometric problems (Mohamed & Verstraeten, 2012). The images are taken at Nadir and the sand cover can be identified through the spectral reflectance, it can easily be used for mapping dune patterns and therefore the movement of dunes (Al-Dabi *et al.*, 1998; Ramsey *et al.*, 1999).

Previous research using Landsat have been concerned with (1) determining sediment pathways (Pease *et al.*, 1999), (2) dune migration and migration rates (monitoring spatial and temporal changes in dune patterns) (Al-Dabi *et al.*, 1998; Mohamed & Verstraeten, 2012), (3) tracking desertification and dune encroachment processes (Lam *et al.*, 2011), (4) documenting the spatial variability of dune and interdune morphology in dune systems (Al-Masrahy & Mountney, 2013; Telfer *et al.*, 2015), (5) discriminating between different sand size populations (Paisley *et al.*, 1991; Lam *et al.*, 2011), and (6) monitoring desertification and dune encroachment (Paisley *et al.*, 1991). These studies have been conducted on the Wahiba Sand Sea (Pease *et al.*, 1999), South-Rayon Dune Field, Namib Sand Sea, White Sand Dune Field, Gran Desierto Sand Sea, Rub' Al-Khali, Great Linear Dunes (Mohamed & Verstraeten, 2012), Kelso Dunes (Mojave Desert) (Paisley *et al.*, 1991; Lam *et al.*, 2011), northwest

Kuwait (Al-Dabi *et al.*, 1998), Rub' Al-Khali (Al-Masrahy & Mountney, 2012) and the Great Sandy Desert, the Kalahari, Simpson Desert and Strzelecki (Telfer, *et al.*, 2015).

Pease *et al.* (1999) used Landsat TM data to propose sediment transport pathways in the Wahiba Sand Sea based on mineralogy spatial patterns. They found that Landsat TM data were valuable in the geomorphic interpretation of the desert, to discriminate different minerals found in the Wahiba area. They used different band combinations to discriminate between the different minerals (quartz, mafic- and carbonate minerals with the use of bands 6 and 4 (thermal infrared and infrared respectively) for example, the minerals were discriminated based on the variation in temperatures (the temperature variations were caused by the variation in the absorption and emission of energy by the different minerals).

Another study by Mohamed & Verstraeten (2012) stated that the crest of the dune appears brighter than the rest of the dune (due to its higher reflectance) in the Thematic Mapper's Near-Infrared (TM-NIR) images. They made use of this to develop a quick method of examining dune migration for large areas based on dune-crest/slipface migration (identified as a "spectrally-stable and easy-to-detect feature"). A combination of Bi-Temporal Layer stacking and RGB-Clustering was used to produce a preliminary, fast understanding of the dune dynamics without any preceding fieldwork or knowledge. It was concluded that this approach could be used as an initial step to detect areas where migration/change is occurring, in order to provide a starting point for further analysis (Mohamed & Verstraeten, 2012), in this case assessing the rate of crest migration.

Paisley *et al.* (1991) and Lam *et al.* (2011) also found that dunes are characteristically unique with regards to their spectral brightness, and this could be used to differentiate between different sand populations (based on spectral brightness). They stated that inactive dune sands reflect less electromagnetic radiation than active dunes; active dunes thus appear brighter than inactive dunes. This was attributed to the higher albedo of active sand surfaces (Lam *et al.*, 2011) due to the presence of a higher amount of quartz sand-size grains than darker inactive sands (Paisley *et al.*, 1991). Based on this albedo difference, active sand surfaces were successfully traced on Landsat TM data to track the desertification/ dune encroachment process of the Kelso

dunes (Lam *et al.*, 2011). The discrimination of active and inactive sands can help to assess sand transport and to interpret regional geologic history (Paisley *et al.*, 1991).

Al-Dabi *et al.* (1998) used multi-date Landsat TM images to monitor the temporal and spatial changes in the sand dune patterns in northwest Kuwait. They were able to detect migration of the dunes as well as changes in the overall shape of the dune field. They used Landsat band 2 (green), 4 (NIR) and 7 (short wave infra-red) – these were selected because they show high reflectance variability of the desert surface. The images were processed and enhanced with several different methods after which the dunes were mapped with a technique called on-screen-digitizing to create dune density maps. They excluded dunes that were smaller than the pixel resolution (30 m), hidden by topographic shadows or next to a major road.

Al-Masrahy & Mountney (2013) attempted to quantitatively document the spatial variability of dune forms and interdune morphology from the centres of the aeolian dune-field systems to their margins (Rub' Al-Khali, Saudi Arabia). They used multi-spectral Landsat data (spatial resolution of 15 m per pixel derived from 15-30 m resolution Landsat MSS pansharpened with panchromatic Landsat image processing software; and Landsat 7 near-infrared band) and derived elevation data from SRTM data (absolute vertical accuracy of 16 m and relative vertical accuracy of 10 m). The resultant net direction of sediment transport was identified from the analysis of dune bedform type and slipface orientation and through reference to the Resultant Drift Direction calculations.

ASTER and SRTM images have been used to construct global DEMs (Blumberg, 2006; Bullard *et al.*, 2011). From these DEMs, elevation and sand volume data can be extracted (Blumberg, 2006; Hesse, 2009; Al-Masrahy & Mountney, 2013). Al-Masrahy & Mountney (2013) derived elevation data from SRTM data (absolute vertical and horizontal accuracy of 16 m and relative vertical accuracy of 10 m). Blumberg (2006) attempted to use SRTM DEM data (C-band and X-band) to characterize and map the spacing and height of dunes within large sand seas. It was found that only larger dune forms could be mapped reliably and that the dune height and spacing extracted from the SRTM DEMs were generally similar to those reported in the literature (Blumberg, 2006). A comparison of the C- and X-band data led Blumberg to conclude that X-band

data showed the dune height better and is more sensitive to smaller scale undulations on large dunes with smaller superimposed dunes.

Limitations of coarse resolution imagery and derived products (DEMs)

The most pronounced limitation of a coarse spatial resolution (especially in change analysis) is that it is not useful where the amount of change is smaller than the pixel size. Another limitation of coarse spatial resolution data is that geo-rectification errors are greater and may result in a lower geometric accuracy than higher spatial resolution data.

Landsat has a relatively coarse spatial resolution (between 15 and 120 m, depending on the mission) (Levin *et al.*, 2004) and steep topography can result in specular reflectance areas (Birnie *et al.*, 1989).

ASTER DEMs are unsuitable for quantitative analysis of dune morphometry where dune heights are less than 20-30 m, but may be applicable where dunes are spatially larger (due to the low resolution of the DEM) (Hugenholtz & Barchyn, 2010; Bullard *et al.*, 2011). It has limited value for differentiating small, simple dune forms and small-scale superimposed dunes and the Global DEM is not suitable for small or closely spaced dunes (Bullard *et al.*, 2011). The same is true for SRTM data (Bullard *et al.*, 2011).

SRTM DEMs are only suitable for the detection of large dunes (heights of 50 m or more and spacing of 1.5 km) due to its low horizontal resolution and vertical accuracy (Bullard *et al.*, 2011).

2.4.2 Fine spatial resolution imagery studies

Fine spatial resolution in terms of this study will be considered as an image pixel size smaller than 30 x 30 m (for example Spot, Ikonos, Worldview and RapidEye). Very few studies (Ghadiry *et al.*, 2012) utilized fine resolution data only. This could possibly be attributed to the small areal and temporal coverage that is currently available for high resolution data. The measurement of slow migration rates (e.g. glacier flow, mass movements, dune migration and other local processes) have been made possible with the use of fine resolution imagery accompanied by the appropriate analytical methods (e.g. COSI-Corr technique) (Necsoiu *et al.*, 2009).

Several studies on sand dunes (in particular) have used a combination of coarse (especially DEMs) and fine spatial resolution imagery (e.g. SPOT, IKONOS and Quickbird) (Hesse, 2009; Necsoiu *et al.*, 2009; Effat *et al.*, 2012; El-Magd *et al.*, 2013). These studies mostly used combinations of fine resolution imagery (e.g. SPOT, IKONOS, Quickbird) and coarser resolution digital elevation models (DEMs) (ASTER & SRTM) to (1) identify and estimate sand dune migration rates and age based on terminal sand volume and sand flux (Hesse, 2009; Necsoiu *et al.*, 2009), and (2) assess the potential risk associated with the movement of the dunes (by tracing dune morphology and determining the position of the crests on succeeding images) (Effat *et al.*, 2012; El-Magd *et al.*, 2013). These studies were focused on the Great Kobuk Sand Dunes (Necsoiu *et al.*, 2009), Peruvian-Chilean coastal desert (Hesse, 2009), Sinai Peninsula (Effat *et al.*, 2012) and the Toshka Depression, Egypt (El-Magd *et al.*, 2013).

Ghadiry *et al.* (2012) used two SPOT images to study dune encroachment in the Dakhla Oases (Egypt), and to develop a user friendly tool (integrating both remote sensing and GIS) for automated feature extraction that enables the quantification of dune migration rates. The results showed that the dune migration rate in the area ranged between 3-9 m per year. The majority of sand dunes had a migration rate between 0-6 m/year and very few dunes had a migration rate of more than 6 m/year.

Necsoiu *et al.* (2009) stated that the COSI-Corr technique has proven to be a reliable technique for measuring dune migration rates. A combination of ASTER Visible and Near Infrared (VNIR) and SPOT Panchromatic images was used to estimate unbiased velocity magnitudes of the Great Kobuk Sand Dunes (Necsoiu *et al.*, 2009). It was estimated that these dunes migration rates vary from 0.5 m to 1.5 m/year with peak velocities up to 3.8 m/year (with an uncertainty of approximately 0.16 m/year) (Necsoiu *et al.*, 2009).

Hesse (2009) made use of DEMs derived from both SRTM and ASTER satellite imagery as well as Landsat and Quickbird imagery to determine dune migration rates and age based on the terminal sand volume of the dunes and the sand flux associated with those dunes in the Peruvian-Chilean coastal desert, Dunas Pampa Blanca. The migration rate of the transverse dunes calculated by Hesse (2009) was lower than the migration rate Gay (1999) calculated for the barchans dunes of the Pampa de Jaguay (approximately 90 km away from the Dunas Pampa Blanca of Hesse (2009)). These

differences were attributed to the number of independent factors (e.g. dune type, different sediment supplies and wind regimes) (Hesse, 2009).

El-Magd *et al.* (2013) made use of Landsat TM and SPOT imagery to determine the sand dune movements and trace dune morphology to provide a baseline for the operational system to assess the hazard associated with sand dunes in the study area (Toshka depression, southwestern Desert of Egypt). It was stated that such a tool is needed to enable wide coverage in order to assist decision makers and planners to reduce the risk associated with this natural hazard (dune migration). Satellite imagery enabled a wider understanding of the dune system of the Toshka Depression area and determination of dune migration rates and thus potential hazard threats.

Sand dune encroachment threatens the development of countries in arid zones (Effat *et al.*, 2012). Effat *et al.* (2012) modelled the potential risk of the movement of sand dunes in the Sinai Peninsula, Egypt. SPOT 4 imagery was used along with SRTM data and wind direction and speed data to identify the dune bodies from the Sinai desert. There data was used to create a sand dune migration risk map for the area.

Limitations of Fine Resolution Imagery

Fine resolution imagery is expensive and usually associated with a time lag due to the processing time of imagery orders. It also has a limited historical temporal coverage (mostly only the past decade) as the earliest high resolution sensor was only launched in the late 1990's compared to Landsat (for example) that was launched in the 1970's, this is a limitation for time series studies and not necessarily other studies concerned with the present day only. However, the small temporal scale may not be as big a limitation for time series analyses – since the higher spatial resolution may allow for time series analysis on a shorter time scale than was previously possible. Another limitation that has to be considered is the amount of disk space it requires not only for storing the raw data but also for the analyses of the data – since the resolution (whether considering spatial and/ or spectral resolution) the higher the resolution the higher the disk space and processing capabilities that are required.

2.5 Remote Sensing Analysis Methods

2.5.1 Pre-Processing of Satellite Imagery

Pre-processing of imagery is necessary to avoid or minimize the effects related to the different platforms and/or sensors and different atmospheric conditions during the acquisition date and time of the images. When comparing multispectral images from different sensors and/or different times, it is advisable to perform corrections (regarding illumination, sensor calibration and atmospheric conditions) and geometric registration of the images as much as possible in order to prevent or limit false differences (Canty, 2010) due to pixel misalignment (for example), especially if the analyses are performed on a pixel-by-pixel basis.

2.5.2 Radiometric and Atmospheric Corrections

The main aim of the radiometric calibration is to minimize the scene-to-scene radiometric variability and to decrease the effect of shadow as it corrects for different sun zenith angles due to different acquisition times (Mohamed & Verstraeten, 2012).

The reflectance result as received on the sensor is dependent upon (1) the dune surface characteristics; (2) the relative angles between the sensor, sun and surface; and (3) attenuation produced by the atmosphere (Ramsey *et al.*, 1999).

Radiometric and atmospheric correction is the process of converting digital numbers to radiance or surface reflectance, to enable the quantitative analyses of multi-temporal images. Without these corrections, variations may be detected due to differences in lighting conditions such as change in solar angle or changes in cloud, haze and atmospheric conditions (including aerosols and moisture content) (Collado *et al.*, 2002; Kennedy *et al.*, 2009; Aldossary, 2012).

Radiometric calibration is the process of removing radiometric differences (not related to the surface) that are a result of images that were acquired at two different times or by two different sensors (Kennedy *et al.*, 2009; Aldossary, 2012). Thus the purpose of radiometric calibration is to let the images appear as though they were acquired at the same time with the same sensor, same illumination and same atmospheric conditions. This will ensure that the changes in pixel value that are detected are the actual changes that occurred on the surface (it also improves the accuracy of the analysis) (Kennedy *et al.*, 2009; Aldossary, 2012). Several different techniques to correct for

atmospheric and radiometric conditions have been developed and include relative calibration and dark object subtraction (Kennedy *et al.*, 2009; Aldossary, 2012).

The Bidirectional Reflectance Distribution Function (BRDF) also need to be taken into account, as this influences the reflectance of sand and plays an important role at solar zenith angles greater than 30° (Ramsey *et al.*, 1999). These BRDF effects are characterized by two specific areas of minimum and maximum reflectance and are governed by the sun-object geometry. A “hotspot” effect occurs when the scattering angle is zero, thus the area appears brighter than the rest of the image and a dark area is found at large scattering angles (Ramsey *et al.*, 1999).

Imagery collected by satellites is subject to modification or changes in solar radiation reflected by the earth’s surface due to scattering and absorption of the radiation by particles in the atmosphere. The aim of atmospheric correction is to eliminate the effect of the atmosphere and recover the true surface reflectance values (characterizing the physical parameters of the surface of the earth) (Hadjimitsis *et al.*, 2010). Radiometric calibration and atmospheric correction consist of the conversion of radiance values into top-of-atmosphere reflectance values, after which the effects of the atmosphere are removed from the image with an atmospheric correction algorithm.

2.5.3 Panchromatic Sharpening

Several of the satellite platforms are accompanied by a co-registered panchromatic image. These panchromatic images have higher spatial resolution than the multispectral bands (an increase in spatial resolution results in a decrease in the spectral resolution of images, and vice versa). Panchromatic sharpening (Pan-Sharp) can be used to combine the panchromatic image with the multispectral image in order to increase the spatial resolution of the multispectral image (a downside to this method is the resulting decrease in spectral resolution of the multispectral data) (Canty, 2010).

2.5.4 Co-Registration/Geometric Correction

An essential undertaking in remote sensing data processing is the process of image registration or co-registration, especially if two images from different platforms are

compared or multi temporal or time-series analysis are done, and is necessary for georeferencing. Image registration can be done from one image to a map or to another image (Canty, 2010; Asha *et al.*, 2013). The process of aligning two or more images geometrically is also known as image co-registration, this is done to integrate or fuse corresponding pixels representing the same features. This is necessary to minimize the detection of false change/difference between the two images due to pixels that were misaligned (Canty, 2010; Asha *et al.*, 2013).

2.5.5 Image Classification (Feature Extraction), **using a Supervised Classification**

A supervised classification is a classification based on predefined training areas or areas of interest, and clusters pixels into classes (Devi & Baboo, 2011).

Minimum Distance and Maximum Likelihood Classification

The minimum distance classification calculates the spectral distance between the measurement vector for the candidate pixel and the average vector for each sample (Pernuman & Bhaskaran, 2010; Devi & Baboo, 2011). The algorithm is based on a Euclidian distance equation. The pixels in question are assigned to the class that has the minimum spectral distance (Pernuman & Bhaskaran, 2010; Devi & Baboo, 2011).

The maximum likelihood classification algorithm is one of the most widely used classifications in remote sensing (Pernuman & Bhaskaran, 2010; Devi & Baboo, 2011). The algorithm is based on the Bayesian probability theory, and the assumption that each pixel fits in a specific class (Pernuman & Bhaskaran, 2010; Devi & Baboo, 2011). This algorithm classifies a pixel based on the probability that it fits within a specified class (Devi & Baboo, 2011). The algorithms used within the ENVI v5.1 environment can be found in Table 2.3.

Table 2.3: Algorithms used in ENVI for the different classification modules (Canty, 2010).

Classification module	Algorithm (ENVI)
Minimum Distance	$d(x, y) = \sqrt{\sum_{i=1}^n (x_i - y_i)^2}$ <p> x = spectral signature vector of pixel y = spectral signature vector of training area n = number of image bands </p>
Maximum Likelihood	$d_k(g) = \log(\text{Pr}(k)) - \frac{1}{2} \log \Sigma_k - \frac{1}{2} (g - \mu_k)^T \Sigma_k^{-1} (g - \mu_k)$ <p> d_k = land cover class k x = spectral signature vector of pixel $(\text{Pr}(k))$ = probability that correct class is d_k Σ_k = determinant of the covariance matrix Σ_k^{-1} = inverse of covariance matrix μ_k = spectral signature vector of class k </p>

Accuracy Assessment

Accuracy assessments are used to show how closely the classified image represents what is actually found in the field (Foody, 2002). The confusion (error) matrix gives information on the overall accuracy, producer's accuracy, user's accuracy, and a Kappa coefficient. Accuracy assessments are crucial to the evaluation of the results and then ultimately using these results in further analysis and/or management strategies (Aldossary, 2012). The producer accuracy gives an indication of how well the training samples are classified and the user accuracy gives an indication of the probability that a pixel belongs to the class it was assigned (represents that class in reality). The kappa value is used to determine if there is a significant difference

between two confusion matrices (Congalton & Green, 2009; Peruman & Bhaskaran, 2010; de Souza *et al.*, 2013).

2.6 Conclusions

Based on the previous research the different attributes of dunes and their migration would be better analyzed with different platforms. For example if the interest of the research is on the composition of the sediment that make up the dunes it would be best to use hyperspectral data, and the analyses of the height and changes in the volume of the dunes a DEM would be best. A platform with a high temporal resolution and wide temporal coverage is required for time series analysis, especially in dune migration analysis (which occurs over long time periods).

Ideally a combination of high spatial and spectral resolution data with a long temporal scale (of at least 10-15 years or more) accompanied by high resolution digital elevation models with extensive ground truthing would result in the highest accuracy of both dune morphology mapping and migration rate calculations – especially since some dunes have a very low migration rate – which may often be missed on low spatial resolution data.

A combination of different bands will have to be tested – no definite consensus was found in the literature – however the most common band combinations that were used included the visible (red, green and blue) and near infrared bands and in some instances the thermal band was found to be useful.

A low spatial resolution may result in the overestimation of dune size, length and width as well as the overestimation and/ or underestimation of the dune migration rate.

A higher spectral resolution may assist in better defining (and identifying) the different dune features more easily and more accurately as well as the determination of the composition of the dune sands.

A fully automated, self-learning algorithm may decrease the processing time – especially compared to on-screen digitization.

Based on what is currently freely available and easy to come by a combination of a moderate spatial resolution (like Landsat) and DEMs would have to suffice until the

high resolution imagery (both spatial and spectral) are more freely available and have been around for a longer time period (in the case of time-series analysis). For current time dune morphology studies high spatial resolution data is recommended.

Chapter 3: Materials and Methods

3.1 Introduction

The main aim of this study is to identify the most suitable spatial resolution at which to study sand dunes (with heights of 100 m or more) in the arid areas of the Ubārī Sand Sea, Central Sahara (Libya), in order to determine the net direction and rate of dune movement. Unfortunately no ground truthing could be done as this area is currently inaccessible due to safety concerns.

This chapter outlines the methods used for this study, including the process of acquiring suitable satellite imagery, the pre-processing of this imagery, the comparison of imagery with two different spatial resolutions, and finally a time series change analysis to determine dune movement. A workflow of the methods used in this study can be seen in Figure 3.1, this workflow gives an overall idea of the sequence and type of analyses that was used in this research.

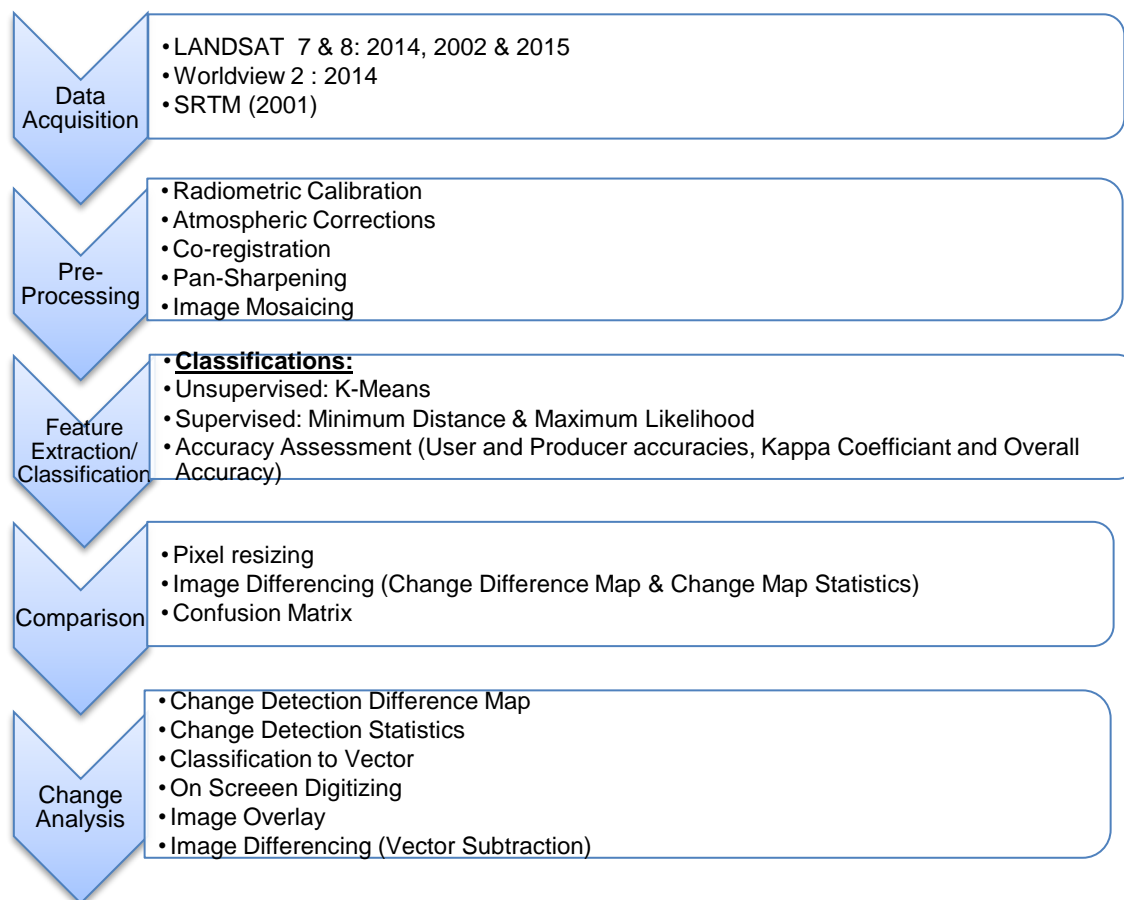


Figure 3.1: Flow diagram of the methods used for the image processing and change analysis.

3.2 Imagery Acquisition and Scenes Used

In this study, images from two satellite imaging platforms, one of high resolution and the other of medium resolution, were used, these being Worldview 2 and Landsat (7 and 8) respectively. The Landsat images were acquired from the USGS Earth Explorer website and the Worldview images were acquired courtesy of a Digital Globe Foundation Imagery Grant. The characteristics of the chosen images are found in Tables 3.1a, b & c.

Table 3.1a: Detailed information (criteria) on the imagery that were chosen for the spatial resolution comparison section (phase 1) of this research.

Phase 1: Comparison Analysis

Platform	Source	Imagery Dates	Spatial Resolution	Spectral Resolution	Cloud Cover (%)	Scenes Acquired (Path Row according to WRS-2)
Landsat 8	US Geological Survey	20 September 2014	30 m	11 Bands	< 5	187 041; 187 042
Worldview 2	Digital (Imagery Grant)	Globe 20 September 2014	2 m	8 Bands	< 5	P001 - P003
SRTM DEM	US Geological Survey	2000	90 m	-	< 5	-

Table 3.1b: Detailed information (criteria) on the imagery that were chosen for the time series analysis section (phase 2) of this research.

Phase 2: Time Series Analysis

Platform	Source	Imagery Dates	Spatial Resolution	Cloud Cover (%)	Spectral Resolution	Scenes Acquired (Path Row according to WRS-2)
Landsat 7 - ETM	US Geological Survey	September 2002	30 m	< 5	8 bands	187, 041; 187, 042
Landsat 8 - OLI	US Geological Survey	September 2015	30 m	< 5	11 bands	187, 041; 187, 042

Table 3.1c: The band numbers, designations, wavelengths and resolutions for the three platforms that were used in this research.

Platform	Band Number (Designation)	Wavelength (μm)	Resolution (m)
Landsat 7 - ETM +	1 (blue)	0.45 – 0.52	30
	2 (green)	0.52 – 0.60	30
	3 (red)	0.63 – 0.69	30
	4 (near infrared)	0.77 – 0.90	30
	5 (short wave infrared)	1.55 – 1.75	30
	6 (thermal infrared)	10.40 – 12.50	60 (30*)
	7 (short wave infrared)	2.09 – 2.35	30
	8 (panchromatic)	0.52 – 0.90	15
Landsat 8 - OLI	1 (coastal aerosol)	0.43 – 0.45	30
	2 (blue)	0.45 – 0.51	30
	3 (green)	0.53 – 0.59	30
	4 (red)	0.64 – 0.67	30
	5 (near infrared)	0.85 – 0.88	30
	6 (short wave infrared - 1)	1.57 – 1.65	30
	7 (short wave infrared - 2)	2.11 – 2.29	30
	8 (panchromatic)	0.50 – 0.68	15
	9 (cirrus)	1.36 – 1.38	30
	10 (thermal infrared - 1)	10.60 – 11.19	100 (30*)
	11 (thermal infrared - 2)	11.50 – 12.51	100 (30*)
Worldview 2	1 (coastal)	0.40 – 0.45	1.85 – 2.07
	2 (blue)	0.45 – 0.51	1.85 – 2.07
	3 (green)	0.51 – 0.58	1.85 – 2.07
	4 (yellow)	0.58 – 0.62	1.85 – 2.07
	5 (red)	0.63 – 0.69	1.85 – 2.07
	6 (red edge)	0.70 – 0.74	1.85 – 2.07
	7 (near infrared - 1)	0.77 – 0.79	1.85 – 2.07
	8 (near infrared - 2)	0.86 – 1.04	1.85 – 2.07
	Panchromatic	0.45 – 0.80	0.45 – 0.52

*after 25 February 2010 the resolution of these bands improved to the values stated in brackets.

The study was carried out in two phases: 1. the comparison of the spatial resolution of Worldview and Landsat in sand dune morphology analysis, and 2. a time series analysis of the net dune movement and direction within the Ubārī Sand Sea.

For the section on the comparison of two spatial resolutions, Landsat 8 and Worldview 2 imagery covering a subset of the Ubārī Sand Sea was used (Figure 3.2a), both sets of imagery were acquired for September 2014 and the SRTM DEM data were acquired for 2001. Only a subset of the Ubārī Sand Sea was covered in this section of the study due to the area restriction associated with the Worldview imagery grant, and the cost related to acquiring additional high resolution imagery.

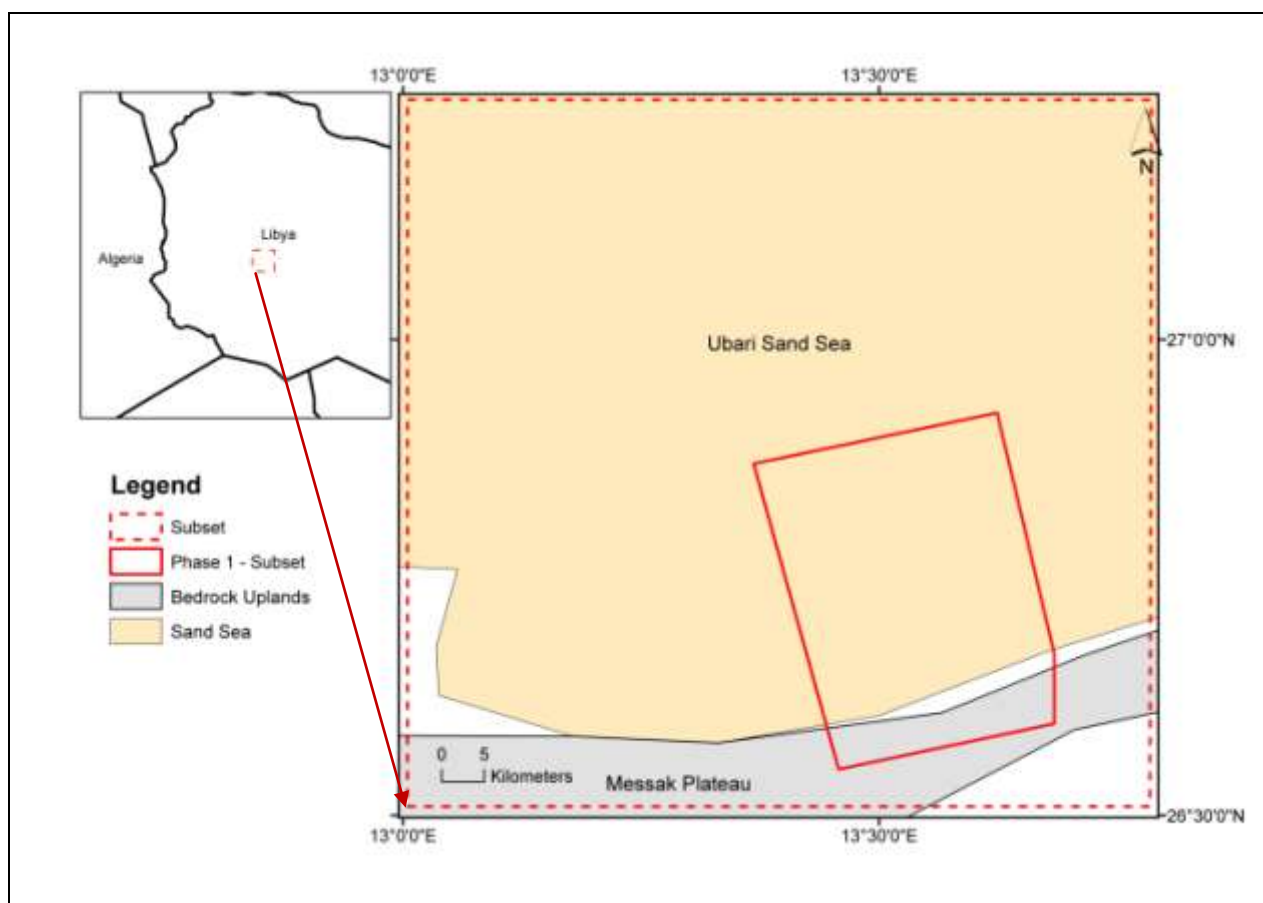


Figure 3.2a: Location map of the Ubārī Sand Sea with the study area for phase 1 (the comparison of spatial resolutions) boxed in solid red.

Following the development of phase one (the comparison of the two spatial resolutions), which proved that the coarse spatial resolution imagery yields reliable sand dune morphology results (See Section 4.2), Landsat 7 and 8 imagery were used for the time-series comparison (Table 3.1) covering a larger subset of the sand sea

(Figure 3.2b). There were no restrictions in terms of financing for the Landsat imagery as it is freely available but in order to minimize the processing time required due to the time constraints associated with a Masters project, a subset of the Ubārī Sand Sea was used for phase 2 (Figure 3.2b).

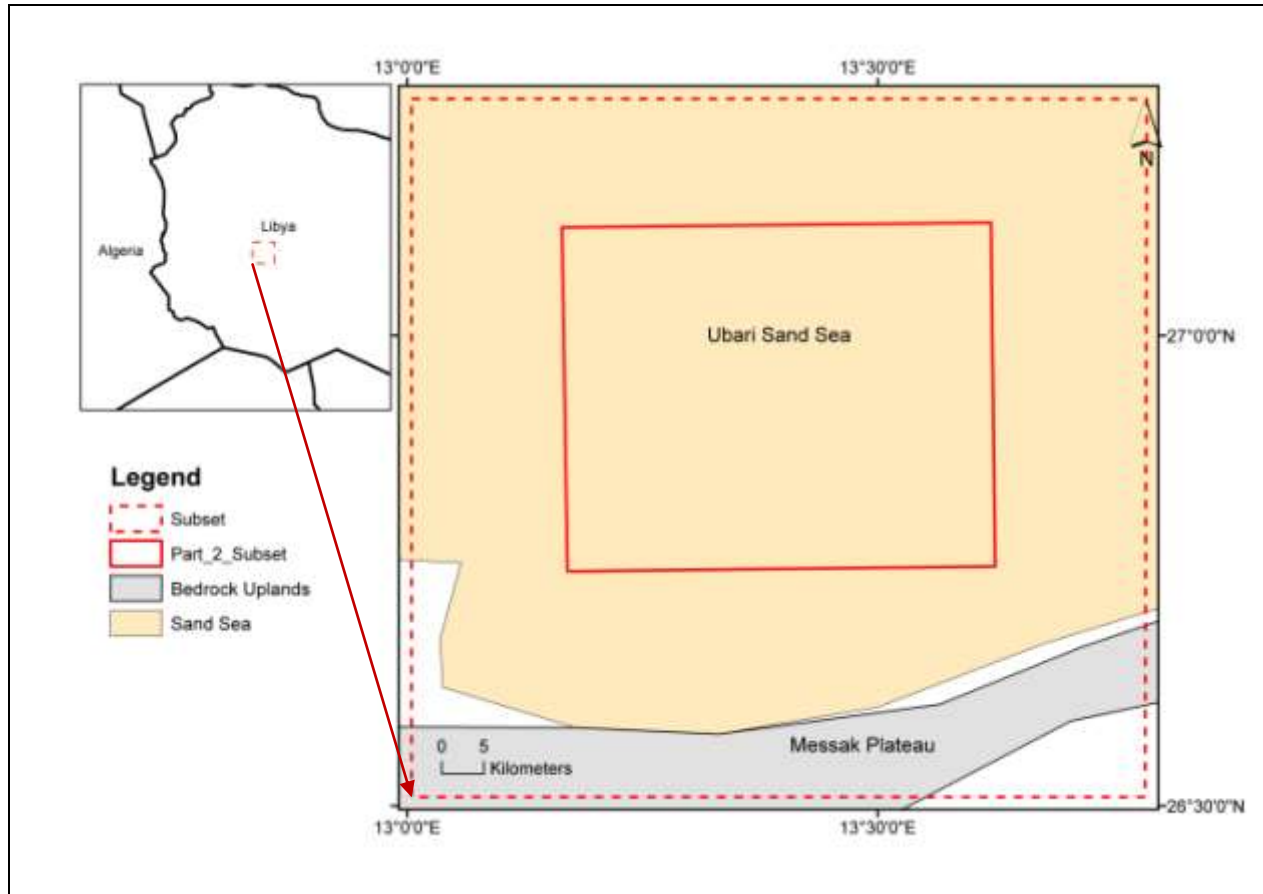


Figure 3.2b: Location map of the Ubārī Sand Sea and the study area for phase 2 (time series analysis) boxed in solid red.

3.3 Pre-Processing of Satellite Imagery

Pre-processing of imagery is necessary to avoid or minimize the effects related to the different platforms and/or sensors and different atmospheric conditions during the acquisition date and time of the images.

3.3.1 Radiometric and Atmospheric Corrections

The main aim of the radiometric calibration was to minimize the scene-to-scene radiometric variability and to decrease the effect of shadow as it corrects for different sun zenith angles due to different acquisition times (Mohamed & Verstraeten, 2012).

Within this study each tile's (both Landsat and Worldview) digital number values were converted into radiance-at-sensor and then into reflectance values with the use of the Radiometric Calibration function in ENVI v5.1. The tiles were then atmospherically corrected with the use of the Fast Light-of-Sight Atmospheric Analysis of Hypercubes (FLAASH) algorithm as described in the Atmospheric Correction Model within ENVI v5.1 (based on MODTRAN 4 code). The parameters reported in Table 3.2. were used (these parameters were optimized based on the environment and location of the study area). FLAASH is a physics based algorithm used for atmospheric corrections of the visible to infrared spectrum.

Table 3.2: FLAASH Atmospheric Correction Model Parameters used in the correction of Landsat imagery.

Parameter	Used
Ground Elevation	500 m a.s.l.
Atmospheric Model	Tropical
Aerosol Model	Rural
Aerosol Retrieval	2-Band (K-T)
Water Column Multiplier	1
Initial Visibility	40 km
Multispectral Settings	Kaufmann-Tanre Aerosol
Retrieval	Over-Land Retrieval Standard (660-2100 nm)

3.3.2 Panchromatic Sharpening

There are several different methods by which panchromatic sharpening can be done, in this study the "SPEAR Pan-Sharpen" method (available in ENVI v5.1) was used. The pan-sharpening process was only applied to the Worldview 2 imagery, in order to make the identification of the different features in the area easier when creating the training samples. The resulting pan-sharpened images were used exclusively for the

identification of training samples, no further analyses or classifications were conducted on these.

3.3.3 Co-Registration/Geometric Correction

Both sets of imagery (for the comparison of the different platforms as well as for the time series change analysis) were co-registered with the “Geometric Correction” – “Registration” tool within ENVI v5.1. This tool uses area-based matching to identify tie-points automatically.

3.3.4 Mosaicing

Mosaicing is the process in which two or more images are combined into one composite image. The Seamless Mosaic function (with a nearest neighbour re-sampling method) within ENVI v5.1 was used to mosaic the atmospherically corrected images of both the Landsat tiles (of corresponding dates) and Worldview strips, respectively, to form one image of the area in question. These mosaic images were the input images for the subsequent classifications.

3.4 Image Classification (Feature Extraction)

3.4.1 Auto Feature Extraction / Image Classification

A range of classification modules (available in ENVI v5.1) were explored as described herein. An unsupervised classification module (K-Means clustering) was used to determine if the different dune features (especially the dune crest and interdune area) can be identified based on spectral information only. After this procedure, two supervised classifications (maximum likelihood and minimum distance) were performed in order to verify and/or assess the reliability of the classifications from the unsupervised module.

Band Combinations

All the classification modules were performed on both the Landsat and Worldview imagery. The classifications were performed on the bands of the visible range (red green and blue) and near infrared (NIR) (see Table 3.1c). These bands were chosen as they are present in both the Landsat and Worldview images and were the most common bands used in previous research (Al-Dabi *et al.*, 1998; Collado *et al.*, 2002; Necsoiu *et al.*, 2009; Al-Masrahay & Mountney, 2013; Telfer *et al.*, 2015).

The focus of this study was to determine what influence the spatial resolution of different platforms has on the identification and study of desert dunes, therefore the same spectral resolution had to be used for both sets of imagery. This resulted in the exclusion of the thermal and short-wave infrared bands of the Landsat 8 imagery as these bands are not present in the Worldview 2 imagery (refer to Table 3.1c for a review of the bands and their properties).

4.4.1.1 Unsupervised Classification

The K-Means unsupervised classification module was performed on both the Landsat and Worldview mosaiced images, to test if the different dune features are identifiable based on the spectral signatures alone. A 5% change threshold, which is the “point” at which the iterative process is stopped when the pixels in a class changes by less than the threshold, was used. Two band combinations were used in this classification, these band combinations were: 1. red and near-infrared and 2. red, green, blue and near-infrared. Nine classes were used in order to allow for the identification of both dune features as well as other features present in the area (e.g. settlements, vegetation, water, etc.). These features were identified with the visual inspection of the RGB images to identify what features are present in the study area. This allows for the exclusion of the features not associated with the dunes.

4.4.1.2 Supervised Classification

A supervised classification is a classification based on predefined training areas or areas of interest, and clusters pixels into classes (Devi & Baboo, 2011). Two supervised classifications (Minimum Distance and Maximum Likelihood) were performed on the red, green, blue and infrared bands of both the Landsat and Worldview mosaiced images. Training samples for the supervised classification were developed (with the use of the Regions of Interest tool available in ENVI v5.1) based on the pan-sharpened higher spatial resolution Worldview mosaiced image overlain onto a SRTM DEM of the area. The Worldview image was overlain over the SRTM DEM in order to help identify the crest of the dunes and the interdunes (highest and lowest areas). A total of 9 training classes (or Regions of Interests) was identified (Table 3.3).

A mixed classification of the surface features and their morphology (which is assumed affects the reflectance characteristics) was used. The training classes represent mixed feature classes, some classes depict surface features (i.e., vegetation and rocky outcrops) and other classes depict the morphology (i.e. dune crest and slope). The dune feature was separated into three separate classes based on the morphology of the dune: crest, slope and interdune. These classes consist of the same material but the assumption is made that due to the dune morphology they have different reflectance characteristics. Surface features were also used as means of excluding these features later on.

Table 3.3: Training classes, their feature descriptions and number of Regions of Interest

Class	Feature Description	Number of Regions of Interest (Reference Data Polygons)		
		Training Set (70 %)	Data Test (30 %)	Data Set Total
1	Water (lakes)	95	41	136
2	Gypsum Deposits	180	80	260
3	Urban	132	60	192
4	Vegetation	123	55	178
5	Rocky Outcrops	140	60	200
6	Soil (non dune)	182	79	261
7	Inter-dune	105	45	150
8	Dune Crest	113	49	162
9	Dune Slope	110	48	158

Regions of Interest – ENVI Procedure

Regions of interest (ROIs) were created with the Regions of Interest Tool in ENVI v5.1. In order to limit the number of vertices that have to be specified, square

ROIs were created at a size of 64 x 64 pixels (corresponds to 128 m x 128 m or 16 384 m²). These ROIs must be uniform and homogeneous and representative of the class/category under investigation. A minimum of one hundred regions of interest were created per class (Table 3.3).

The “uniqueness” of each class (separability between classes) was tested with the use of the “ROI separability” function in ENVI v5.1. This test gives an indication of the uniqueness and homogeneity of the classes – a high separability value indicates that the classes have unique spectral signatures thus easing the classification process.

The resulting Jeffries-Matusita Distance (JM Distance) values (range 0-2) can be seen in Table 3.4. It can be seen that there is less separability between the three classes that are representative of the dunes (the crest, slope and interdune classes – with JM Distance values close to 0) indicating that there is less difference between these three classes. There is however a higher separability (JM Distance values close to 2) between the three dune classes and the other identified classes – thus having unique spectral signatures leading to the conclusion that the classification modules would most likely successfully separate the dune features from the other features that were identified.

Table 3.4: Matrix of the J-M Distance values comparing the ROIs, resulting from the ROI separability test.

	Crest	Gypsum	Interdune	Rocky Outcrop	Slope	Soil	Urban	Vegetation	Water
Water	-	-	-	-	-	-	-	-	-
Vegetation	-	-	-	-	-	-	-	-	2.0000
Urban	-	-	-	-	-	-	-	1.9575	1.9440
Soil	-	-	-	-	-	-	1.5137	1.9977	1.6941
Slope	-	-	-	-	-	1.9977	1.9747	2.0000	1.9989
Rocky Outcrop	-	-	-	-	2.0000	1.9821	1.8295	1.9520	1.9995
Interdune	-	-	-	2.0000	0.5960	1.9961	1.9615	2.0000	1.9959
Gypsum	-	-	1.6119	2.0000	1.5463	1.7535	1.8453	2.0000	1.9324
Crest	-	1.6944	0.7389	2.0000	0.1395	1.9995	1.9844	2.0000	1.9998

A very low separability between the three dune feature classes (crest, slope and interdune) was found. This would result in a lower accuracy in terms of the classification of the different dune features. However, compared to the other six classes a high separability value was found, thus the accuracy of classifications of the other classes should be high and should be relatively well defined – allowing the exclusion of these classes – thus the overall dune should be clearly defined.

The ROIs were separated into “test ROIs” and “training ROIs”. Of the total amount of samples; 20% of the samples from each class were assigned as “test ROIs” (for use in the accuracy assessment) and the remaining 80% were assigned as the “training ROIs” (used in the supervised classifications).

Minimum Distance and Maximum Likelihood Classification

The “training ROIs” were used in the minimum distance and maximum likelihood classifications of both the Worldview and Landsat images. The Minimum Distance and Maximum Likelihood Classification modules in ENVI v5.1 were used.

The following processes were applied on both the Landsat and Worldview images: The minimum distance module was activated with the pre-processed Worldview-2 image as the input. The regions of interest that were previously identified were loaded and the classification was executed. A similar process was used for the Minimum distance classification of the Landsat 8 Images and the Maximum Likelihood classifications of both the Worldview-2 and Landsat 8 images. The algorithms used within the ENVI v5.1 environment can be found in Table 2.3.

Accuracy Assessment

The accuracy of the supervised classifications was assessed with the use of the test data set (30% of the total dataset). The confusion matrix module within ENVI v5.1. was used to construct a confusion matrix in order to calculate the overall accuracy, overall accuracy, producer’s accuracy, user’s accuracy, and a Kappa coefficient. The producer accuracy gives an indication of how well the training samples are classified and the user accuracy gives an indication of the probability that a pixel belongs to the class it was assigned (represents that class in reality). The kappa value is used to

determine if there is a significant difference between two confusion matrices (Congalton & Green, 2009; Peruman & Bhaskaran, 2010; de Souza *et al.*, 2013).

3.4.2 Pixel Resizing

In both phase one and two of the study change detection analyses were performed. Within phase 1 imagery from different sensors (Landsat 8 and Worldview 2) were compared. Due to the difference in the pixel size between these two sets of imagery, pixel-resizing was required in order to allow for the comparison of these images. The change detection analysis is performed on a pixel-by-pixel basis (Ghadiry *et al.*, 2012), thus pixel resizing was applied to the classified Landsat 8 image (with a nearest neighbour resampling) to reduce the pixel size from 30 m to 2 m to match the pixel size of the classified Worldview 2 image using the “resize data” tool available in ENVI v5.1.

3.5 Comparison of Coarse and Fine Resolution Imagery / Post-Classification Change Analysis

Based on the outcome of the previous section – the comparison of classification methods across the two platforms – the most accurate classification (Maximum Likelihood in this case) was used to compare the two platforms.

A simple comparison of the classified Worldview and the re-sampled classified Landsat images was made on a subset of the study area with the Change Detection Difference Map and the Change Detection Statistics models in ENVI v5.1.

The change detection area map results in a difference map that allows for visualisation of the location and amount of difference/change between the two platforms. This map shows changes in ranges or brackets of percentage change (see Table 3.5). The change detection statistics model compares the area classified as specific features between the two images (based on paired samples specified by the user). The results show a statistical comparison of the differences between the platforms in the form of percentage and squared kilometre change in the total area of the specified features. The following features were compared: dune slope, interdune area, lake area, vegetation, and settlements not located within the sand sea.

Table 3.5: Percentage change ranges shown on the change detection area map.

Label	Percentage change
Change (+3)	$x > 67$
Change (+2)	$33 < x \leq 67$
Change (+1)	$0 < x \leq 33$
No Change	$x = 0$
Change (-1)	$0 > x \geq - 33$
Change (-2)	$-33 > x \geq - 67$
Change (-3)	$x < - 67$

3.6 Time Series Analysis (Dune Migration)

The maximum likelihood classification as described in section 3.4 was applied to Landsat tiles 187041 and 188041 for October 2002 and 2015 respectively (see Table 4.1b). The accuracy of the two time series classifications were assessed with the confusion matrix as described in section 3.4.

Due to the size of the Ubārī sand sea and the time needed to process the amount of data associated with such an area, a subset was used (see Figure 3.2b). The subset was chosen because change analysis or migration rates analysis are best done on dunes that are linear which are moving in a single direction. Star dunes' "migration" occurs in more than one direction and more commonly as changes in height and volume, not location. The analysis of migration in star dunes would be better analysed with the use of DEM data.

To determine the general locations where change in the position and orientation of the dunes within the sand sea occurred, the two sets of classified Landsat images (Landsat 7: 2002 and Landsat 8: 2015) were used as input images in the Change Detection Difference Map, Thematic Change Workflow and Change Detection Statistics module of ENVI v5.1. The resulting images were used to identify areas where change occurred and to quantify the change in the shape, area, width and location of 39 dunes (figure 3.3) identified within the subsection of the Ubārī and Sea

(those dunes that were not entirely within the boundaries of the subsection were excluded).

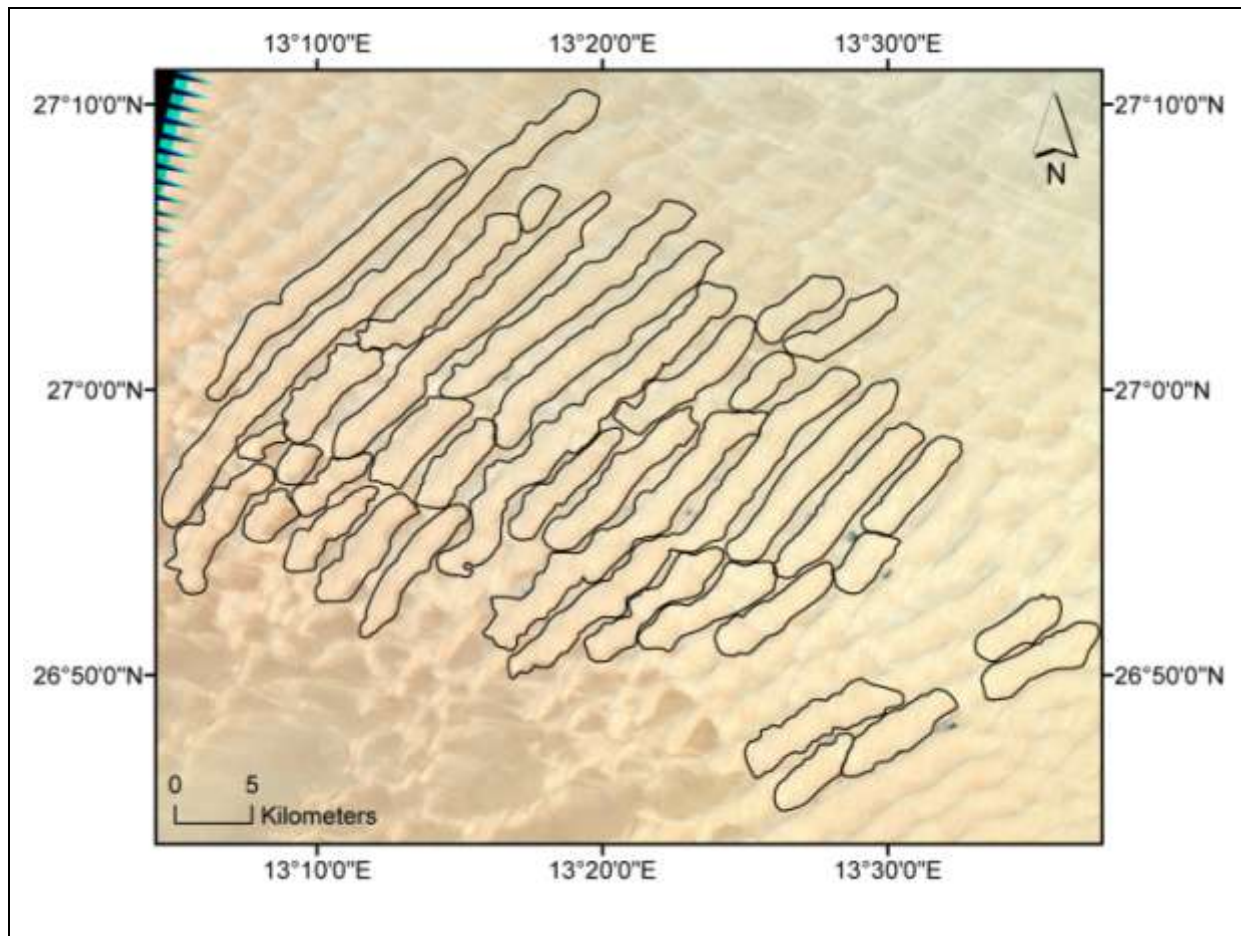


Figure 3.3: Linear Dunes (39 dune bases outlined in black) used for the analysis of dune migration

Dune Digitizing

In order to measure the length, width and area of the dunes, the selected dunes were digitized to form definite polygons, as the classifications are pixel based and difficult to use to measure the parameters of dunes. The dunes were digitized by placing a 30 m grid over the slope classification class and digitizing the dunes by “circling” the clusters of pixels classified as slope and crest (as the base can be delineated as the pixels immediately down slope and the crest as the pixels immediately upslope) (Figure 3.4). Those pixels within one grid square of the clusters were included in the polygon and those within and further than two grid squares were excluded from the polygons. The

final polygons were smoothed with the use of the “Smooth Polygon” function in ArcGIS with the Bezier-interpolation.

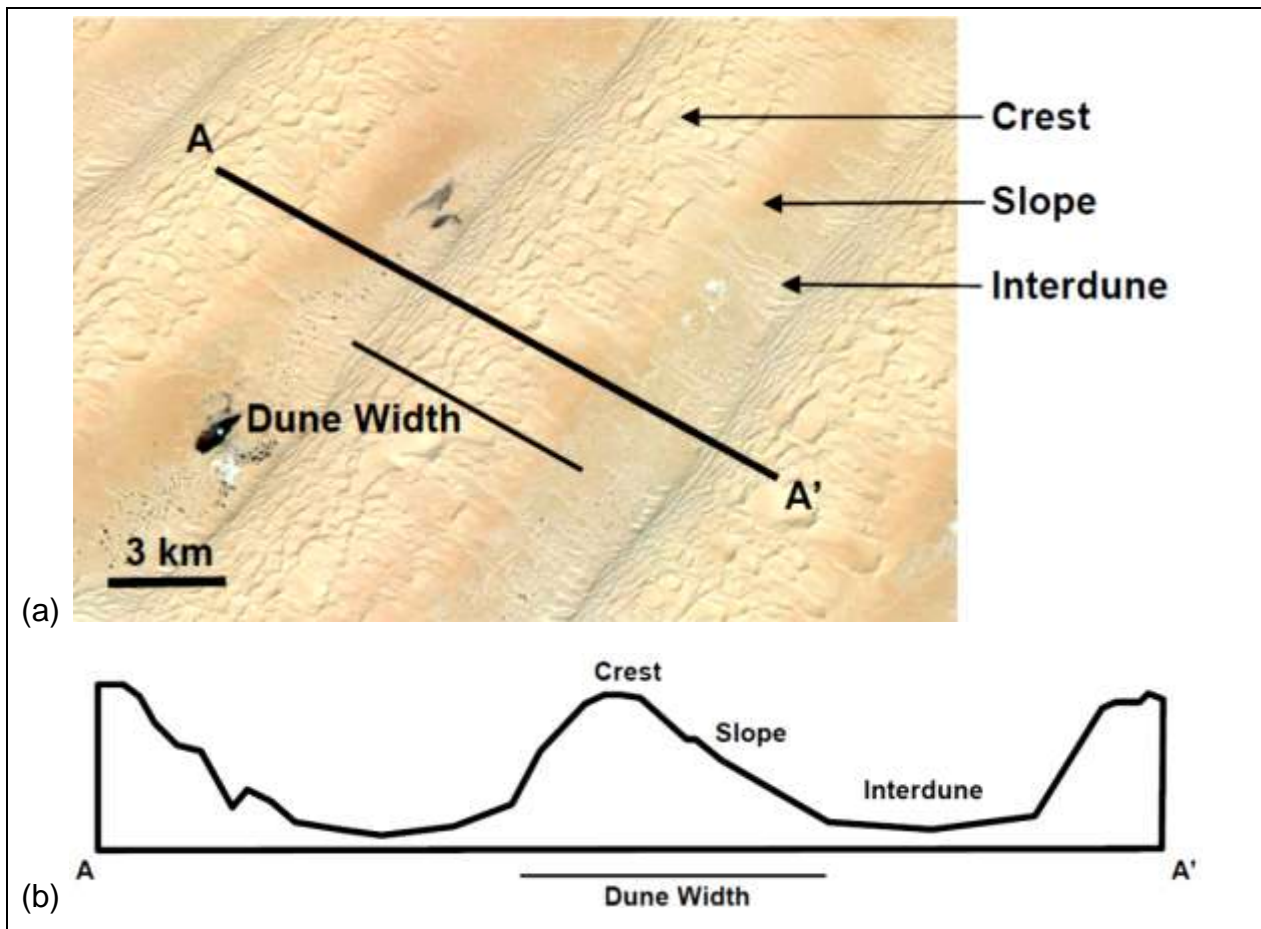


Figure 3.4: Google Earth image of a linear dune within the Ubārī Sand Sea showing the morphology of a dune as (a) a cross section and (b) view from above

This was done for the same 39 dunes digitized from the 2002 and 2015 imagery – thus two sets of 39 dunes were digitized (see section 4.2).

Dune Shape and Orientation

A visual comparison of the dune shape and orientation was made by placing the digitized dune base layer from 2015 over the digitized dune base layer from 2002 (Figure 4.12). The change in the orientation of the dunes was determined by visually comparing the crest lines of the two sets of digitized dunes (Figure 4.6).

Dune area, length and width

The dune crest was delineated and used as a measure of dune length and change in dune orientation as well as dune migration in relation to the dune base (Fig. 3.5). For each dune, transect lines (Fig. 3.5) were inserted perpendicular to the orientation of the dune at 300 m intervals in order to measure the width of each dune – an average of dune width was used. The dune area was also calculated within ArcGIS and compared.

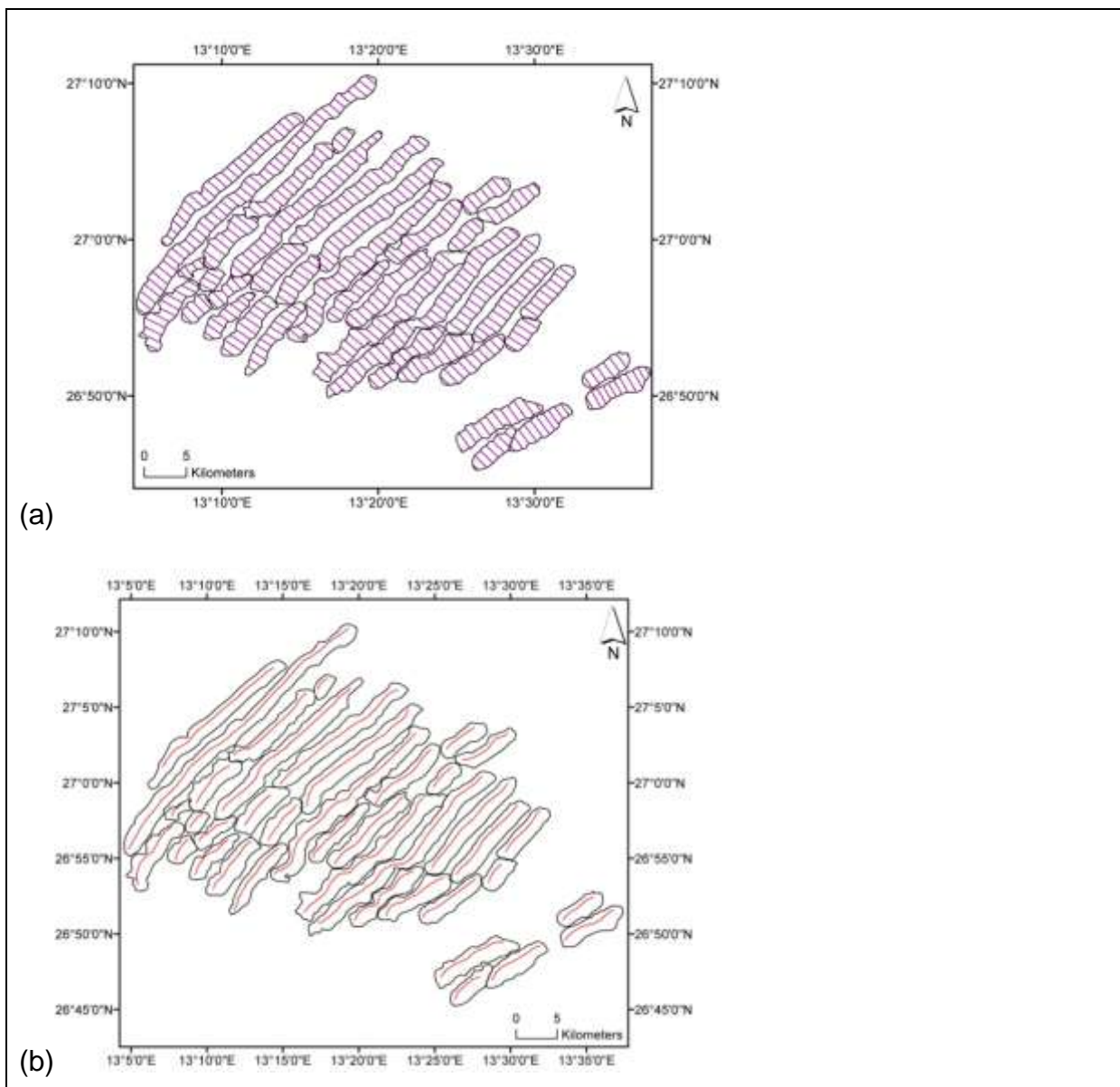


Figure 3.5: (a) The transect lines (purple lines) used in the measurements of the width of the dunes (outlined in black); (b) Crest lines (red) used in the measurement of the length of the dunes (outlined in black).

Dune Location

In order to quantify the “migration” that occurred between 2002 and 2015, the vectors of the digitized dunes and from 2015 was subtracted from the vectors of the digitized dunes of 2002 in order to determine the change in location of the windward slopes base. The polygons resulting from the subtraction were measured at 300 m intervals, perpendicular to the orientation of the dunes (Fig 3.6). These values were used to calculate the average migration rate of each individual dune and also to calculate an overall migration rate of the linear dunes within the subsection.

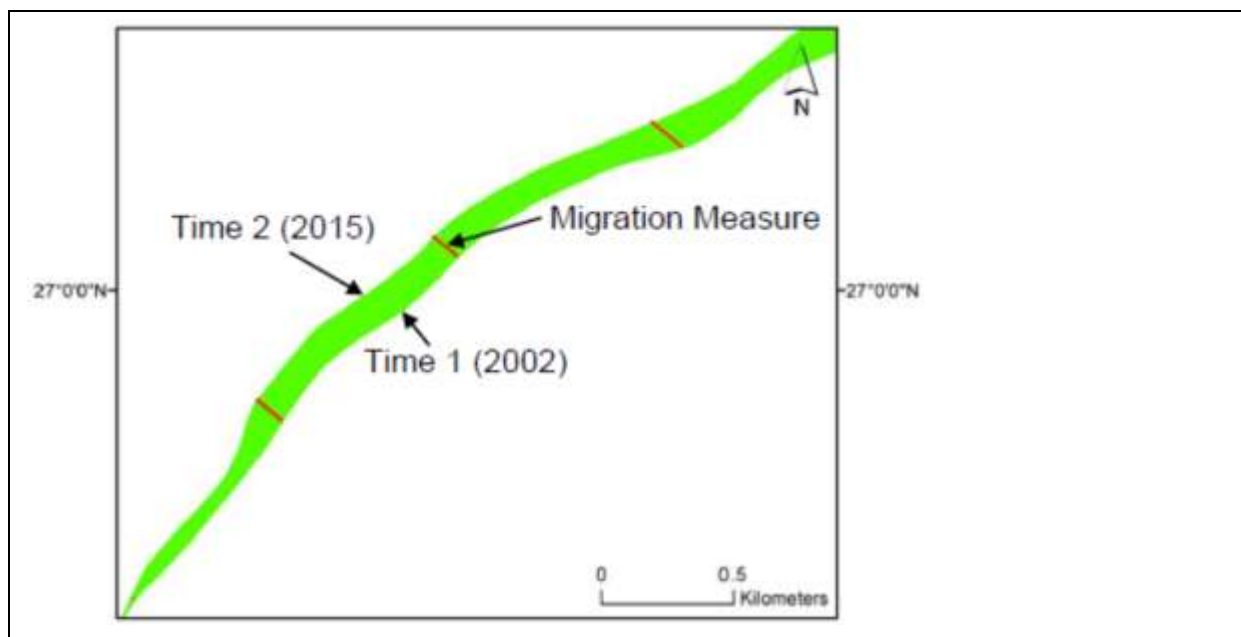


Figure 3.6: Migration measurement transect lines (red lines) at 300 m intervals perpendicular to the orientation of the dune.

Chapter 4: Results

4.1 Introduction

This results section comprises of two sections: Phase 1: a comparison of the coarse (Landsat 8) and fine (Worldview 2) spatial resolution imagery and a comparison of the two supervised classification methods (minimum distance and maximum likelihood) and the band combinations that were used to perform these. Phase 2: An analysis of dune migration within a subset of the Ubārī Sand Sea with the use of Landsat imagery. These analyses (of both phase 1 and 2) were conducted on atmospherically corrected imagery (both fine and coarse spatial resolution imagery as defined previously). The images acquired from the Landsat and Worldview sensors were pre-processed as described in section 3.3, the resulting images can be seen in Figure 4.1. Figure 4.1 A1 (Landsat 8, coarse spatial resolution) and A2 (Worldview 2, fine spatial resolution) show the atmospherically corrected imagery for the study area of phase 1. On these images the linear dunes are clearly visible. Figure 4.1 B1 (Landsat 7, image from 2002) and B2 (Landsat 8, image from 2015) show the atmospherically corrected images depicting the entire Ubārī sand sea, with a zoomed in section on the study area for time series analyses of phase 2.

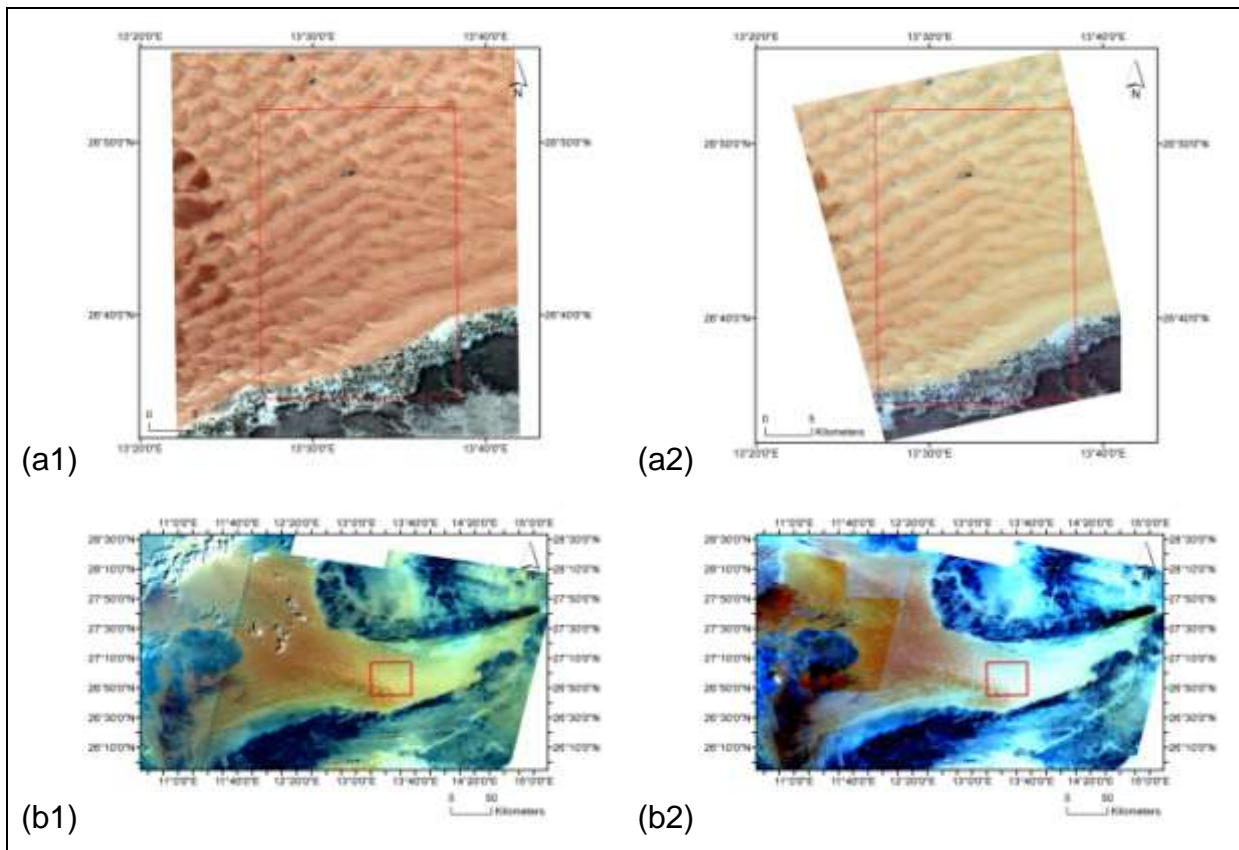


Figure 4.1: Atmospherically corrected images for Phase 1 (the comparison of the spatial resolutions and classification methods): Landsat 8 (a1), Worldview 2 (a2), and Phase 2 (the time series analysis): Landsat 7 (b1) and Landsat 8 (b2), with the study areas boxed in red.

Phase 1:

The results from Phase 1 address Aim 1 of the project (Refer to section 1.2)

4.1.1 Unsupervised Classification

Visual Results:

The analysis was initiated with an unsupervised classification (K-Means, with 9 classes, refer to section 3.4.1) - on both the Landsat 8 and Worldview 2 images; with two band combinations (see section 3.4.1) - to determine if dune features can be distinguished based on spectral signatures alone. Since an unsupervised classification classifies pixels into classes based on their spectral signature alone, the resulting classes were assigned to predefined dune features as can be seen in Table 4.1). The classes that did not represent dune features were not assigned to predefined features

as the goal of the unsupervised classification was to determine if dune features can be identified based on spectral signature alone. From Figure 4.2 it can be seen that some of dune features are distinguished – e.g. the interdune areas. The crests and slopes however are less defined and some overlap occurs between these two feature classes. Within the Landsat images (Figure 4.2 A1 and A2) the crest is represented by class 9, the slope by classes 6-8 and the interdune by classes 3-5 – there are thus several combined classes that represent a feature whereas on the Worldview 2 images the three dune features are more defined and represented by only one class each (in two out of the three features); the crest is represented by class 9, the slopes by class 8 and the interdunes by class 6 and class 7. The use of Worldview 2 resulted in a “cleaner” classified image (fewer classes per feature, see Table 4.1) – the features being better defined/ classified when compared to the result from the Landsat imagery.

Table 4.1: The classes resulting from the unsupervised K-Means classification were assigned to predefined features as follows:

Landsat 8		Worldview 2	
K-Means Class	Assigned Feature	K-Means Class	Assigned Feature
Unclassified	Not Applicable	Unclassified	Not Applicable
1	Not Applicable	1	Not Applicable
2	Not Applicable	2	Not Applicable
3	Interdune	3	Not Applicable
4	Interdune	4	Not Applicable
5	Interdune	5	Not Applicable
6	Dune Slopes	6	Interdunes
7	Dune Slopes	7	Interdunes
8	Dune Slopes	8	Dune Slopes
9	Dune Crest	9	Dune Crest

The band combinations does not seem to have a big effect on the classification as both combinations resulted in a similarly classified image both with the Landsat and Worldview 2 imagery (Figure 4.2).

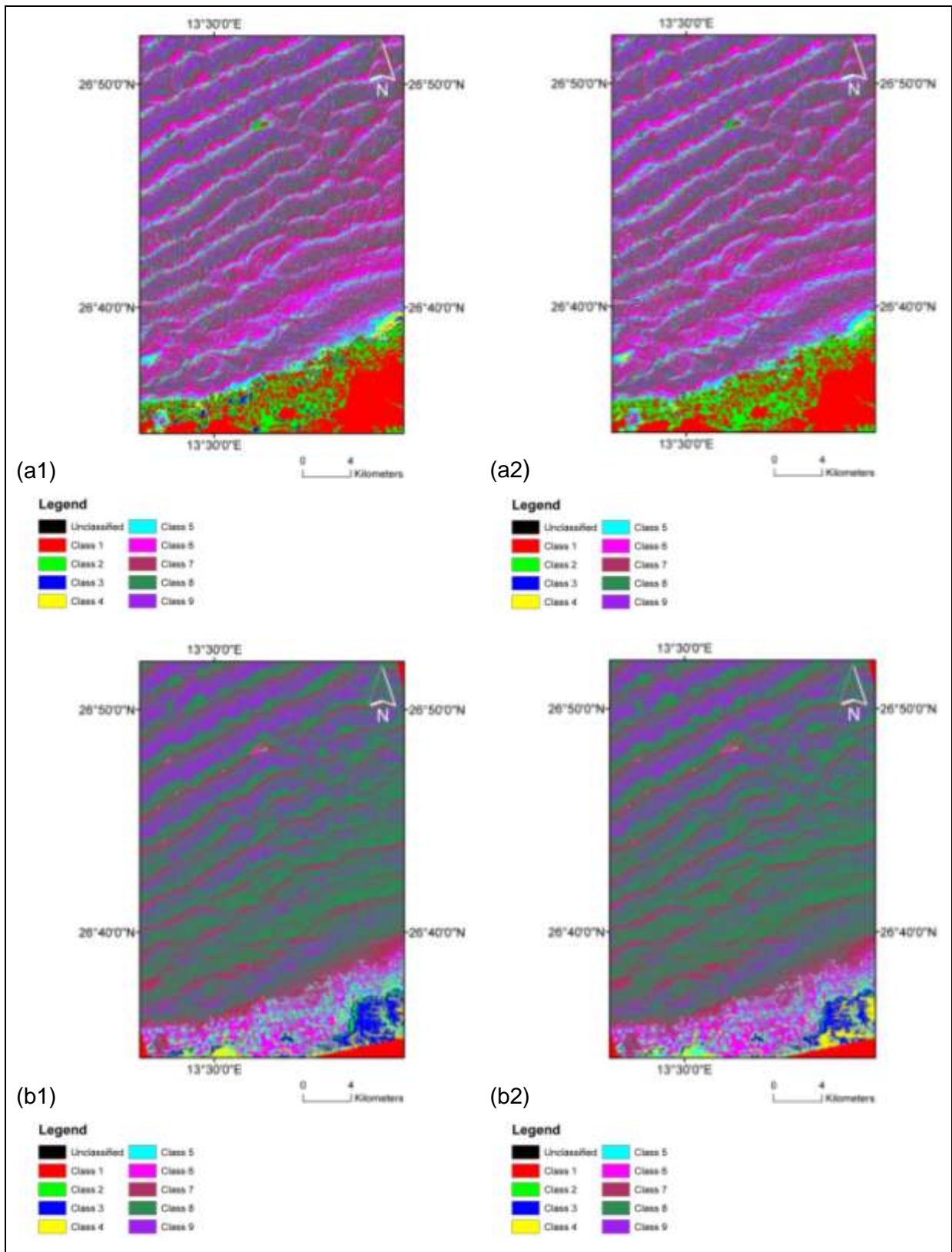


Figure 4.2: The resulting images from the unsupervised classification module (K-Means) for Landsat 8 (for band combinations: (a1): R+NIR; (a2): RGB+NIR) and Worldview 2 (for band combinations: (b1): R+NIR; (b2): RGB+NIR).

From the change detection map (Figure 4.3) and change detection statistics (Table 4.2) it can be seen that there is some variation between the classifications resulting from the two band combinations. The variations in the Landsat images are located mainly on the dune features, with small variations in the boundary areas. The area changes ranged from increases of 7.37 km² (for class 6 - slope) and decreases of 5.68 km² (for class 8 - slope). The crest (class 9) showed a decrease in area of 2.34 km², which is smaller than the difference in the crest class for the Worldview classifications (with a decrease in area of 12.34 km²). The variations in the Worldview images are mainly located in the boundary areas, and the changes in the dune features were more concentrated (than the changes in the Landsat classifications which were spread out) but the amount of change was more (with respect to the area of change). The changes in area ranged from increasing areas of 13.6 km² (for class 8 -slope) and decreasing areas of 12.34 km² (for class 9 - crest). Thus there is less variability between the two band combinations for the Landsat classified Landsat images compared to the Worldview classified images.

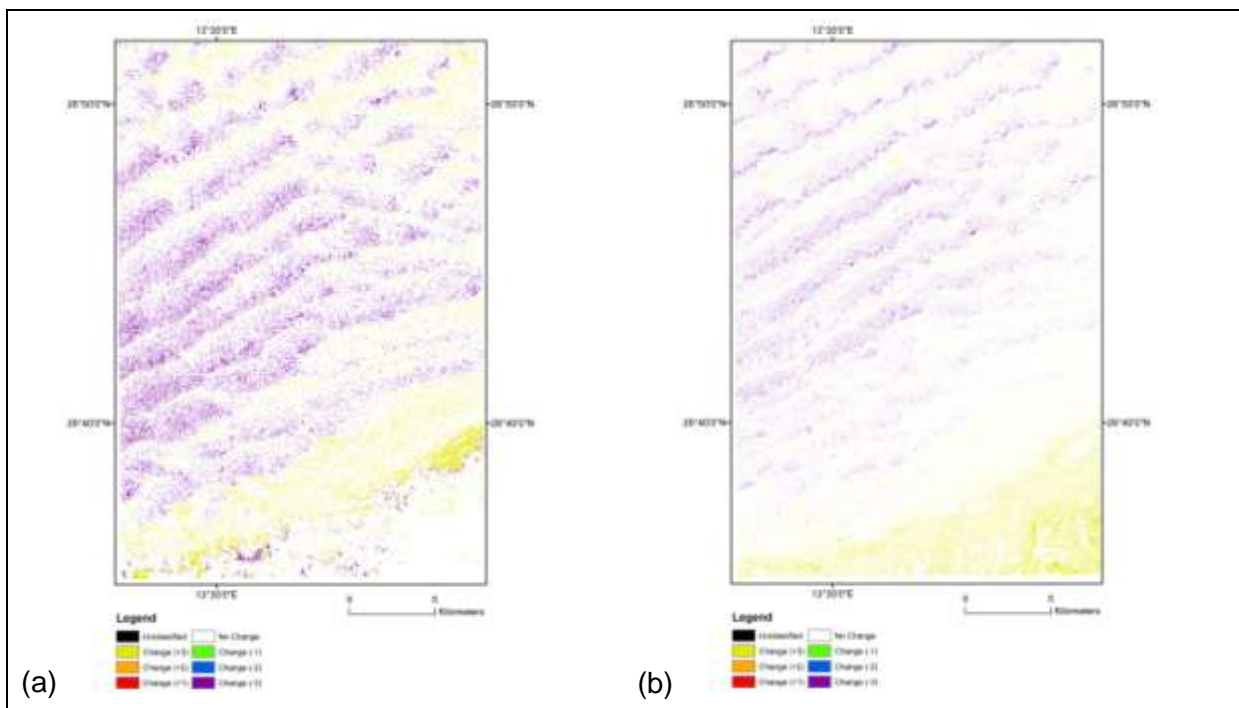


Figure 4.3: The resulting change maps of the comparison of the two band combinations used in the unsupervised classification module (K-Means) for (a) Landsat 8 and (b) Worldview 2.

Table 4.2: The change in area (km²) per class from the (R+NIR) band combination to the (RGB+NIR) band combination – of the K-Means (unsupervised classification) images for Landsat 8 and Worldview 2, respectively.

		Landsat 8 - Bands R+NIR (Initial State)								
		Class 1	Class 2	Class 3	Class 4	Class 5	Class 6	Class 7	Class 8	Class 9
Landsat 8 - Bands RGB+NIR (Final State)	Class 1	37.31	0.25	0	0	0	0	0	0	0
	Class 2	1.22	24.47	1.69	0	0	0	0	0	0
	Class 3	0	1.13	8.88	0.29	0	0	0	0	0
	Class 4	0	0	1.81	20.36	1.7	0	0	0	0
	Class 5	0	0	0	4	52.97	4.68	0	0	0
	Class 6	0	0	0	0	3.63	114.83	13.51	0	0
	Class 7	0	0	0	0	0	5.1	135.1	12.99	0
	Class 8	0	0	0	0	0	0	4.97	96.06	4.46
	Class 9	0	0	0	0	0	0	0	2.12	35.52
	Class Total	38.53	25.85	12.38	24.65	58.31	124.61	153.58	111.18	39.98
Class Changes	1.22	1.38	3.51	4.29	5.33	9.78	18.48	15.12	4.46	
Image Difference	-0.97	+1.54	-2.08	-0.77	+3.34	+7.37	-0.39	-5.68	-2.34	

Table 4.2 continued

		Worldview 2- Bands R+NIR (Initial State)								
		Class 1	Class 2	Class 3	Class 4	Class 5	Class 6	Class 7	Class 8	Class 9
Worldview 2 - Bands RGB+NIR (Final State)	Class 1	0.02	0	0	0	0	0	0	0	0
	Class 2	0	1.37	0	0	0	0	0	0	0
	Class 3	0	1.44	8.38	0.01	0	0	0	0	0
	Class 4	0	0	3.61	9.18	0.04	0	0	0	0
	Class 5	0	0	0	2.32	11.6	0	0	0	0
	Class 6	0	0	0	0	4.12	34.3	0	0	0
	Class 7	0	0	0	0	0	5.44	96.42	2.06	0
	Class 8	0	0	0	0	0	0	3.32	314.61	13.57
	Class 9	0	0	0	0	0	0	0	1.23	75.84
Class Total		0.03	2.81	11.98	11.51	15.76	39.74	99.74	317.9	89.42
Class Changes		0	1.44	3.61	2.33	4.17	5.44	3.32	3.29	13.57
Image Difference		0	-1.44	-2.15	+1.32	-1.85	-1.31	+4.18	+13.6	-12.34

4.1.2 Supervised Classification

The results from the supervised classifications, performed on both the Landsat 8 and Worldview 2 (refer to section 3.4.1) can be seen in Figures 4.4 and 4.5. From these images it can be seen that the dunes at the edge of the sand sea (lower part of the images) are less defined than the dunes located in the centre (this could be due to less sand availability and or the presence of bedrock), irrespective of the platform and or the band combination used. Similar to the unsupervised classifications' results the dune features can be identified – in particular the crest and interdunal areas. The dune features appears to be better defined in the images obtained from the RGB and NIR band combination than those from the R and NIR combination, this may be an artefact from the classification but the accuracy assessment supports a higher accuracy of the RGB and NIR bands, therefore it will be used for further analysis (no additional ground truthing could be conducted to confirm this).

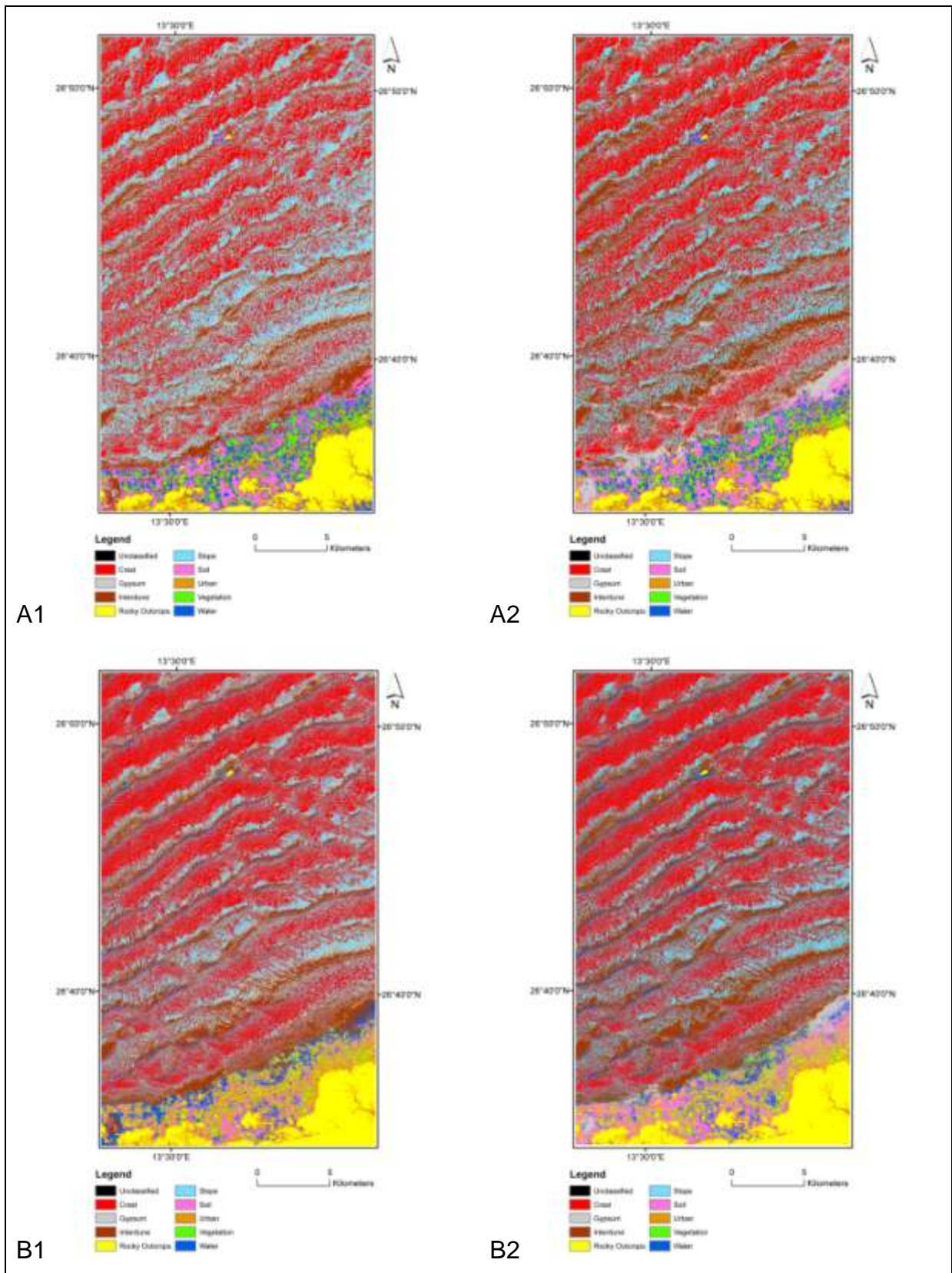


Figure 4.4: Minimum Distance Supervised Classification Images: Landsat 8 (A1: R+NIR; A2: RGB+NIR) and Worldview 2 (A3: R+NIR; A4: RGB+NIR).

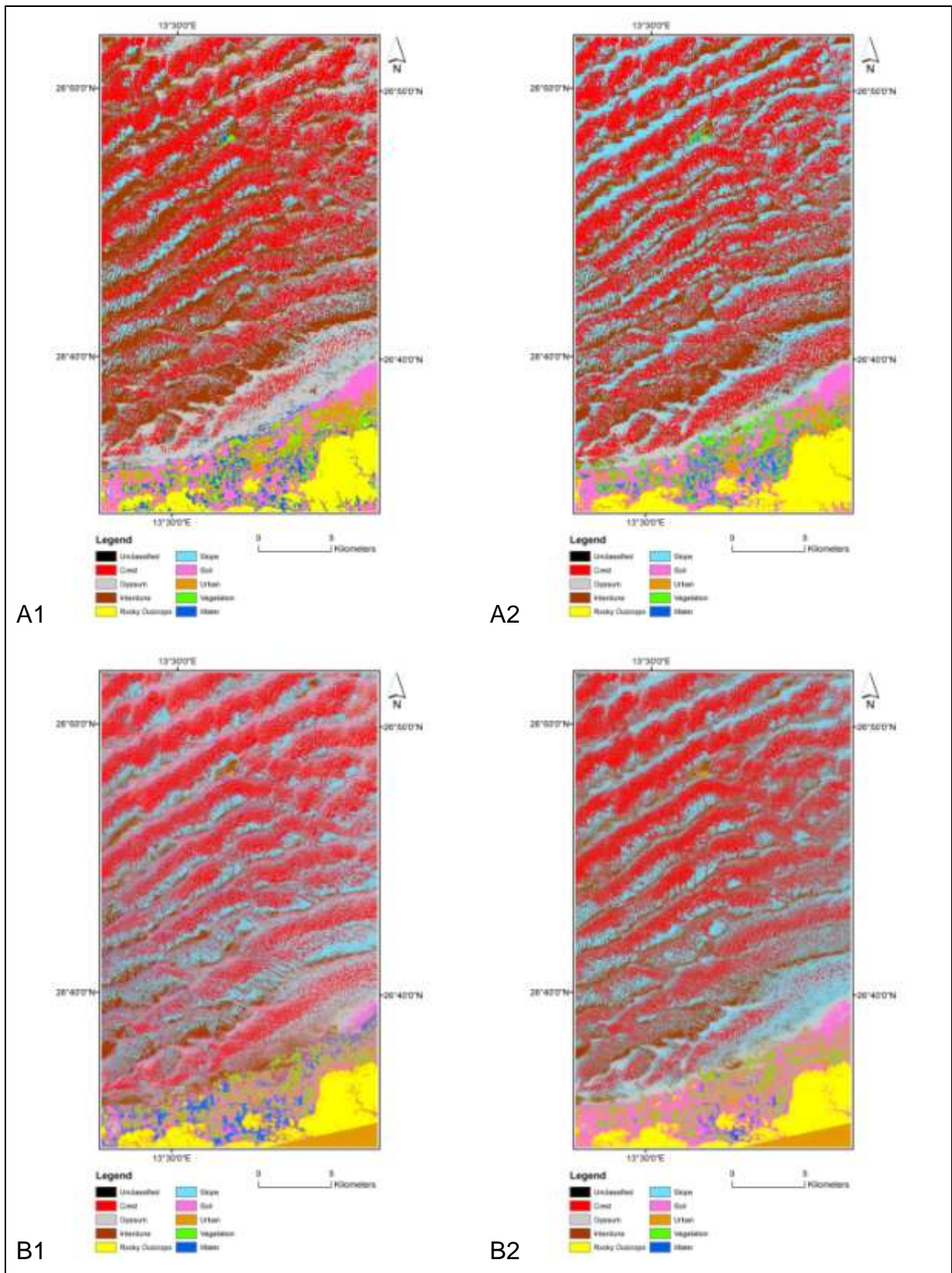


Figure 4.5: Maximum Likelihood Supervised Classification Images: Landsat 8: (A1: R+NIR; A2: RGB+NIR); Worldview 2 (A3: R+NIR; A4: RGB+NIR).

4.1.3 Accuracy Assessment

In order to compare the two classification methods and band combinations the amount of error associated with each classification module was calculated with the use of a confusion matrix performed on the two sets of imagery (Table 4.4). The results of the confusion matrices (kappa, overall accuracy and user accuracy) are shown in Tables 4.3 and 4.4.

The maximum likelihood classifier (Landsat image) and the RGB and NIR band combination resulted in the highest overall accuracy – with a value of 64.667% - and the highest kappa coefficient – with a value of 0.5355, followed by the maximum likelihood with the red and NIR band combination (Landsat image) with an overall accuracy value of 57.42% (and a kappa of 0.4575); maximum likelihood classifier (Worldview image) with the RGB and NIR band combination with an overall accuracy of 60.83% (and a kappa of 0.4225) and minimum distance (Worldview image) with the RGB and NIR band combination with an overall accuracy of 59.42% (and a kappa of 0.3913). This indicates that the maximum likelihood classifier (with the RGB and NIR band combination) performed better than the other combinations on both the Worldview 2 and Landsat 8 imagery. These accuracy and Kappa values are, however, very low compared to the accuracies of classifications in vegetated environments (which are usually approximately 80% and higher) (Adelabu *et al.*, 2013), but these are acceptable for the arid desert (a relatively homogeneous environment; thus the different classes having similar spectral signatures/ behaviour). It is also important to note that the three dune feature classes are arbitrary classes, and if the error matrix is performed on only the arbitrary classes (thus excluding classes such as vegetation and urban) the accuracy and Kappa values are even lower (Table 4.5 and 4.6).

The user accuracy of the four classification combinations of the three dune feature classes for the Worldview image is as follows in descending order of accuracy:

1. Crest: maximum likelihood (RGB+NIR bands) (77.54%); maximum likelihood (R+NIR bands) (76.26%); minimum distance (RGB+NIR bands) (73.75%) and minimum distance (R+NIR bands) (72.59%);
2. Slope: maximum likelihood (R+NIR) (48.91%); minimum distance (R+NIR) (46.22%); minimum distance (RGB+NIR) (45.70%) and maximum likelihood (RGB+NIR) (45.48%); and

3. Interdune: maximum likelihood (R+NIR) (46.48%); minimum distance (R+NIR) (40.38%); minimum distance (RGB+NIR) (38.75%) and maximum likelihood (RGB+NIR) (33.76%)

The user accuracy of the four classification combinations of the three dune feature classes for the Landsat image is as follows in descending order of accuracy:

1. Crest: maximum likelihood (R+NIR bands) (76.26%); maximum likelihood (RGB+NIR bands) (74.52%); minimum distance (RGB+NIR bands) (70.83%) and minimum distance (R+NIR bands) (69.37%);
2. Slope: maximum likelihood (R+NIR) (48.91%); maximum likelihood (RGB+NIR) (48.26%); minimum distance (R+NIR) (40.79%) and minimum distance (RGB+NIR) (38.41%); and
3. Interdune: maximum likelihood (R+NIR) (46.48%); maximum likelihood (RGB+NIR) (46.02%); minimum distance (R+NIR) (45.24%) and minimum distance (RGB+NIR) (44.53%)

There is some confusion between the classes. On both the Landsat and Worldview images the least confusion between classes occurs with the maximum likelihood classification on the RGB and NIR band combination. The confusion occurs between the crest, interdune and slope classes and then there are small amounts of confusion between the gypsum and slope classes, the soil and water classes, urban and soil classes and the water and gypsum classes. The least amount of confusion occurs in the vegetation class (this class is thus well defined and spectrally unique compared to the other classes) as is to be expected. There is a high value of confusion between the crest and slope classes – this may be due to poor training samples resulting from the difficulty of identifying the crest of the dunes on the imagery.

Based on these results further analyses were performed with the use of the maximum likelihood classification and the RGB and NIR band combination.

Table 4.3: The error matrix for the Minimum Distance and Maximum Likelihood classifications across the two spatial resolutions (Landsat & Worldview) and band combinations (red & near infrared; and red, green, blue & near infrared) .

Landsat - Minimum Distance - Red & Near Infrared												
Test Data												
Class	Crest	Gypsum	Interdune	Rocky Outcrop	Slope	Soil	Urban	Vegetation	Water	Total	User's Accuracy (%)	
Classification Image	Crest	351	1	0	0	154	0	0	0	0	506	69.37
	Gypsum	71	7	29	0	46	0	0	0	0	153	4.58
	Interdune	63	2	95	0	28	21	0	1	0	210	45.24
	Rocky Outcrop	0	0	0	75	0	5	11	1	0	92	81.52
	Slope	171	5	4	0	124	0	0	0	0	304	40.79
	Soil	1	0	3	3	4	62	7	1	3	84	73.81
	Urban	0	0	0	30	0	17	41	3	1	92	44.57
	Vegetation	0	0	0	0	0	0	4	35	0	39	89.74
	Water	0	0	0	3	0	19	13	2	0	37	0.00
	Total	657	15	131	111	356	124	76	43	4	1517	
Producer's Accuracy (%)	53.42	46.67	72.52	67.57	34.83	50	53.95	81.4	0			
Overall Accuracy = 52.08%												

Table 4.3 continued

Landsat - Minimum Distance - Red, Green, Blue & Near Infrared												
Test Data												
Classification Image	Class	Crest	Gypsum	Interdune	Rocky Outcrop	Slope	Soil	Urban	Vegetation	Water	Total	User's Accuracy (%)
		Crest	369	1	0	0	151	0	0	0	0	521
	Gypsum	8	11	5	0	25	22	0	0	0	71	15.49
	Interdune	89	1	114	0	51	0	0	1	0	256	44.53
	Rocky Outcrop	0	0	0	75	0	8	10	0	0	93	80.65
	Slope	191	2	9	0	126	0	0	0	0	328	38.41
	Soil	0	0	3	4	3	58	13	1	1	83	69.88
	Urban	0	0	0	31	0	8	45	3	1	88	51.14
	Vegetation	0	0	0	0	0	4	5	36	0	45	80
	Water	0	0	0	1	0	24	3	2	2	32	6.25
	Total	657	15	131	111	356	124	76	43	4	1517	
	Producer's Accuracy (%)	56.16	73.33	87.02	67.57	35.39	46.77	59.21	83.72	50		
	Overall Accuracy = 55.11%											

Table 4.3 continued

Landsat - Maximum Likelihood - Red & Near Infrared												
	Class	Test Data								Total	User's Accuracy (%)	
		Crest	Gypsum	Interdune	Rocky Outcrop	Slope	Soil	Urban	Vegetation			Water
Classification Image	Crest	426	0	0	0	167	0	0	0	0	593	71.84
	Gypsum	121	13	27	0	78	2	0	0	0	241	5.39
	Interdune	63	1	100	0	34	0	0	0	0	198	50.51
	Rocky Outcrop	0	0	0	91	0	1	5	0	0	97	93.81
	Slope	47	1	1	0	74	2	0	0	0	125	59.2
	Soil	0	0	3	4	3	75	8	2	0	95	78.95
	Urban	0	0	0	16	0	19	53	1	0	89	59.55
	Vegetation	0	0	0	0	0	2	4	35	0	41	85.37
	Water	0	0	0	0	0	23	6	5	4	38	10.53
	Total		657	15	131	111	356	124	76	43	4	1517
Producer's Accuracy (%)		64.84	86.67	76.34	81.98	20.79	60.48	69.74	81.4	100		
Overall Accuracy= 57.42%												

Table 4.3 continued

Landsat - Maximum Likelihood - Red, Green, Blue & Near Infrared												
	Test Data									Total	User's Accuracy (%)	
	Class	Crest	Gypsum	Interdune	Rocky Outcrop	Slope	Soil	Urban	Vegetation			Water
Classification Image	Crest	427	1	0	0	145	0	0	0	0	573	74.52
	Gypsum	4	12	11	0	15	4	0	1	0	47	25.53
	Interdune	79	0	104	0	43	0	0	0	0	226	46.02
	Rocky Outcrop	0	0	0	94	0	0	1	0	0	95	98.95
	Slope	147	1	16	0	153	0	0	0	0	317	48.26
	Soil	0	1	0	6	0	86	5	2	0	100	86
	Urban	0	0	0	10	0	4	64	1	0	79	81.01
	Vegetation	0	0	0	1	0	2	4	37	0	44	84.09
	Water	0	0	0	0	0	28	2	2	4	36	11.11
Total	657	15	131	111	356	124	76	43	4	1517		
Producer's Accuracy (%)	64.99	80	79.39	84.68	42.98	69.35	84.21	86.05	100			
Overall Accuracy = 64.67%												

Table 4.3 continued

Worldview - Minimum Distance - Red & Near Infrared												
Test Data												
	Class	Crest	Gypsum	Interdune	Rocky Outcrop	Slope	Soil	Urban	Vegetation	Water	Total	User's Accuracy (%)
Classification Image	Crest	70640	157	403	0	25994	0	125	0	0	97319	72.59
	Gypsum	8151	124	2039	0	5875	0	42	0	0	16231	0.76
	Interdune	11362	53	12118	0	5077	809	586	0	7	30012	40.38
	Rocky Outcrop	0	0	31	7885	0	392	946	248	0	9502	82.98
	Slope	17150	145	1519	0	16178	0	7	0	0	34999	46.22
	Soil	920	0	136	51	341	3103	199	1	38	4789	64.79
	Urban	4	0	72	590	0	1210	583	6	0	2465	23.65
	Vegetation	0	0	2	0	0	0	2	3671	0	3675	99.89
	Water	3663	0	683	1	820	1660	448	3	74	7352	1.01
	Total	111890	479	17003	8527	54285	7174	2938	3929	119	206344	
Producer's Accuracy (%)	63.13	25.89	71.27	92.47	29.8	43.25	19.84	93.43	62.18			
Overall Accuracy = 55.43%												

Table 4.3 continued

Worldview - Minimum Distance - Red, Green, Blue & Near Infrared												
Test Data												
Class	Crest	Gypsum	Interdune	Rocky Outcrop	Slope	Soil	Urban	Vegetation	Water	Total	User's Accuracy (%)	
Classification Image	Crest	71673	23	478	0	25008	0	3	0	0	97185	73.75
	Gypsum	120	392	106	0	210	595	845	0	0	2268	17.28
	Interdune	13307	30	13041	0	7021	236	1	0	6	33642	38.76
	Rocky Outcrop	0	0	47	7971	0	459	937	228	0	9642	82.67
	Slope	22307	34	2489	0	20896	0	0	0	0	45726	45.7
	Soil	0	0	7	60	0	3684	367	1	0	4119	89.44
	Urban	0	0	23	496	0	808	769	1	0	2097	36.67
	Vegetation	0	0	4	0	0	0	4	3692	0	3700	99.78
	Water	4483	0	808	0	1150	1392	12	7	113	7965	1.42
Total	111890	479	17003	8527	54285	7174	2938	3929	119	206344		
Producer's Accuracy (%)	64.06	81.84	76.7	93.48	38.49	51.35	26.17	93.97	94.96			
Overall Accuracy = 59.24%												

Table 4.3 continued

Worldview - Maximum Likelihood - Red & Near Infrared												
Test Data												
Classification Image	Class	Crest	Gypsum	Interdune	Rocky Outcrop	Slope	Soil	Urban	Vegetation	Water	Total	User's Accuracy (%)
	Crest	66076	24	311	0	20231	0	3	0	0	86645	76.26
	Gypsum	17074	413	2789	0	8846	187	106	0	0	29415	1.4
	Interdune	6659	10	10410	0	5089	211	3	0	17	22399	46.48
	Rocky Outcrop	0	0	5	7925	0	5	330	1	0	8266	95.87
	Slope	17056	22	2553	0	18795	0	1	0	0	38427	48.91
	Soil	3064	1	591	135	989	3634	700	8	22	9144	39.74
	Urban	11	9	135	452	11	436	1744	33	0	2831	61.6
	Vegetation	0	0	14	0	0	1	30	3886	0	3931	98.86
	Water	1950	0	195	15	324	2700	21	1	80	5286	1.51
Total	111890	479	17003	8527	54285	7174	2938	3929	119	206344		
Producer's Accuracy (%)	59.05	86.22	61.22	92.94	34.62	50.66	59.36	98.91	67.23			
Overall Accuracy = 54.75%												

Table 4.3 continued

Worldview - Maximum Likelihood - Red, Green, Blue & Infrared												
Test Data												
Classification Image	Class	Crest	Gypsum	Interdune	Rocky Outcrop	Slope	Soil	Urban	Vegetation	Water	Total	User's Accuracy (%)
	Crest	66857	2	263	0	19106	0	0	0	0	86228	77.54
	Gypsum	605	385	505	0	949	272	4	0	22	2742	14.04
	Interdune	15580	3	11030	0	6054	0	1	2	0	32670	33.76
	Rocky Outcrop	0	0	4	7761	0	2	53	0	0	7820	99.25
	Slope	28686	54	4937	0	28094	0	0	0	0	61771	45.48
	Soil	2	3	70	172	3	5072	526	7	2	5857	86.6
	Urban	159	32	176	594	77	366	2313	18	0	3735	61.93
	Vegetation	0	0	17	0	0	3	35	3902	0	3957	98.61
	Water	1	0	1	0	2	1459	6	0	95	1564	6.07
Total	111890	479	17003	8527	54285	7174	2938	3929	119	206344		
Producer's Accuracy (%)	59.75	80.38	64.87	91.02	51.75	70.7	78.73	99.31	79.83			
Overall Accuracy = 60.83%												

Table 4.4: The Kappa Coefficient Statistic values for the minimum distance and maximum likelihood classifications of the two platforms and two sets of band combinations, resulting from the Confusion (Error) Matrix.

Imagery	Classification Module	Band Combination	Kappa Coefficient
Landsat 8	Minimum Distance	Red, Near-Infrared	0.3878
		Red, Green, Blue, Near-Infrared	0.4191
	Maximum Likelihood	Red, Near-Infrared	0.4575
		Red, Green, Blue, Near-Infrared	0.5355
Worldview 2	Minimum Distance	Red, Near-Infrared	0.3486
		Red, Green, Blue, Near-Infrared	0.3913
	Maximum Likelihood	Red, Near-Infrared	0.3628
		Red, Green, Blue, Near-Infrared	0.4225

Table 4.5: The error matrix for the Minimum Distance and Maximum Likelihood classifications across the two spatial resolutions (Landsat & Worldview) and band combinations (red & near infrared; and red, green, blue & near infrared), based only on the three dune feature classes that were identified (i.e. crest, slope and interdune).

Landsat - Minimum Distance - Red & Near Infrared						
	Class	Test Data			Total	User's Accuracy (%)
		Crest	Interdune	Slope		
Classification Image	Crest	351	0	154	505	69.50
	Interdune	63	95	28	186	51.08
	Slope	171	4	124	299	41.47
Total		585	99	306	990	
Producer's Accuracy (%)		60.00	95.96	40.52		
Overall Accuracy = 57.58%						

Table 4.5 continued

Landsat - Minimum Distance - Red, Green, Blue & Near Infrared						
Test Data						
	Class	Crest	Interdune	Slope	Total	User's Accuracy (%)
Classification Image	Crest	369	0	151	520	70.96
	Interdune	89	114	51	254	44.88
	Slope	191	9	126	326	38.65
Total		649	123	328	1100	
Producer's Accuracy (%)		56.86	92.68	38.41		
Overall Accuracy = 55.36%						
Landsat - Maximum Likelihood - Red & Near Infrared						
Test Data						
	Class	Crest	Interdune	Slope	Total	User's Accuracy (%)
Classification Image	Crest	889	2	312	1203	73.90
	Interdune	121	220	48	389	56.56
	Slope	102	6	171	279	61.29
Total		1112	228	531	1871	
Producer's Accuracy (%)		79.95	96.49	32.2		
Overall Accuracy = 68.41%						
Landsat - Maximum Likelihood - Red, Green, Blue & Near Infrared						
Test Data						
	Class	Crest	Interdune	Slope	Total	User's Accuracy (%)
Classification Image	Crest	427	0	145	572	74.65
	Interdune	79	104	43	226	46.02
	Slope	147	16	153	316	48.42
Total		653	120	341	1114	
Producer's Accuracy (%)		65.39	86.67	44.87		
Overall Accuracy = 61.40%						
Worldview - Minimum Distance - Red & Near Infrared						
Test Data						
	Class	Crest	Interdune	Slope	Total	User's Accuracy (%)
Classification Image	Crest	70640	403	25994	97037	72.80
	Interdune	11362	12118	5077	28557	42.43
	Slope	17150	1519	16178	34847	46.43
Total		99152	14040	47249	160441	
Producer's Accuracy (%)		71.24	86.31	34.24		
Overall Accuracy = 61.67%						

Table 4.5 continued

Worldview - Minimum Distance - Red, Green, Blue & Near Infrared						
	Class	Crest	Test Data Interdune	Slope	Total	User's Accuracy (%)
Classification Image	Crest	71673	478	25008	97159	73.77
	Interdune	13307	13041	7021	33369	39.08
	Slope	22307	2489	20896	45692	45.73
Total		107287	16008	52925	176220	
Producer's Accuracy (%)		66.8	81.47	39.48		
Overall Accuracy = 59.93%						
Worldview - Maximum Likelihood - Red & Near Infrared						
	Class	Crest	Test Data Interdune	Slope	Total	User's Accuracy (%)
Classification Image	Crest	66076	311	20231	86618	76.28
	Interdune	6659	10410	5089	22158	46.98
	Slope	17056	2553	18795	38404	48.94
Total		89791	13274	44115	147180	
Producer's Accuracy (%)		73.59	78.42	42.6		
Overall Accuracy = 64.74%						
Worldview - Maximum Likelihood - Red, Green, Blue & Near Infrared						
	Class	Crest	Test Data Interdune	Slope	Total	User's Accuracy (%)
Classification Image	Crest	66857	263	19106	86226	77.54
	Interdune	15580	11030	6054	32664	33.77
	Slope	28686	4937	28094	61717	45.52
Total		111123	16230	53254	180607	
Producer's Accuracy (%)		60.16	67.96	52.75		
Overall Accuracy = 58.68%						

Table 4.6: The Kappa Coefficient Statistic resulting from the Confusion (Error) Matrix module, based on only the three dune feature classes (crest, slope and interdune).

Imagery	Classification		Kappa Coefficient
	Module	Band Combination	
Landsat 8	Maximum Likelihood	Red, Green, Blue, Near-Infrared	0.3461
		Red, Near-Infrared	0.4259
	Minimum Distance	Red, Green, Blue, Near-Infrared	0.2645
		Red, Near-Infrared	0.2766
Worldview 2	Maximum Likelihood	Red, Green, Blue, Near-Infrared	0.2988
		Red, Near-Infrared	0.3579
	Minimum Distance	Red, Green, Blue, Near-Infrared	0.2961
		Red, Near-Infrared	0.2988

4.1.4 Comparison of Mapped Dunes Based on the Spatial Resolution of Imagery

The maximum likelihood classification was used in the comparison of the spatial resolution of Landsat 8 and Worldview 2 in the use in arid desert environments. In Table 4.6 and Figure 4.5 the differences and/ or changes that are present between the two images can be seen.

Firstly in Figure 4.5 (a change detection map) indicates the areas where differences between the two images are present, these differences fall within the “Change (+1)” class that range from 0-7.5 %. These changes/ differences between the images are mostly located at the dune crest and slope areas (Figure 4.6) and thus relate to the width and roundness of the dunes. Visually, the dune orientation, appear to be similar for both 2002 and 2015 (Figure 4.8). There are limited changes in the classification classes bordering the sand sea (those classes not located within the sand sea, including the urban, soil and vegetation classes) (Figure 4.6).

Table 4.7a and b gives a more quantifiable image of the differences between the two classified images. There has been a 20% or more change in the area per class in all classes from the Worldview 2 to Landsat 8 image, this change is most likely related to the coarser resolution of the Landsat 8 image. These changes vary from 0.77 km² (for the water class) to 112.05 km² change in area for the crest class. Thus even although the percentages appear high in most classes the actual area that has changed is not as high in all instances. For example a 25.43% increase in area for the water class equates to 0.77 km², and a 55.53% increase in area for the interdune class equates to an increase in area of 55.69 km². It can also be seen that 25% of the area that was classified as crest on the Worldview 2 image was classified as slope on the Landsat 8 image, as well as 8.9% as interdunal area. Similarly of the area classified as slope on the Worldview 2 images 22.92% was classified as crest on the Landsat 8 image and 22.62% as interdune. The areas classified as interdune on the Worldview 2 image was also classified slightly different on the Landsat 8 image, 14.31% was classified as crest and 27.14% as slope (Figure 4.7).

The increase in area from the Worldview 2 to the Landsat 8 classifications may be an indication that the Worldview 2 imagery may be more accurate in terms of mensuration – however without ground truthing this cannot be proven or disproven. Therefore, even although this indicates that the Wordlview 2 imagery may be “better” than the Landsat 8 imagery the accuracy assessment indicated that the classification of the Landsat 8 image was “better” than that of the Wordlview 2 image (refer to section 3.4.1) and thus these differences may also be attributable to the decreased accuracy of the classification of the Worldview image compared to the Landsat 8 classification.

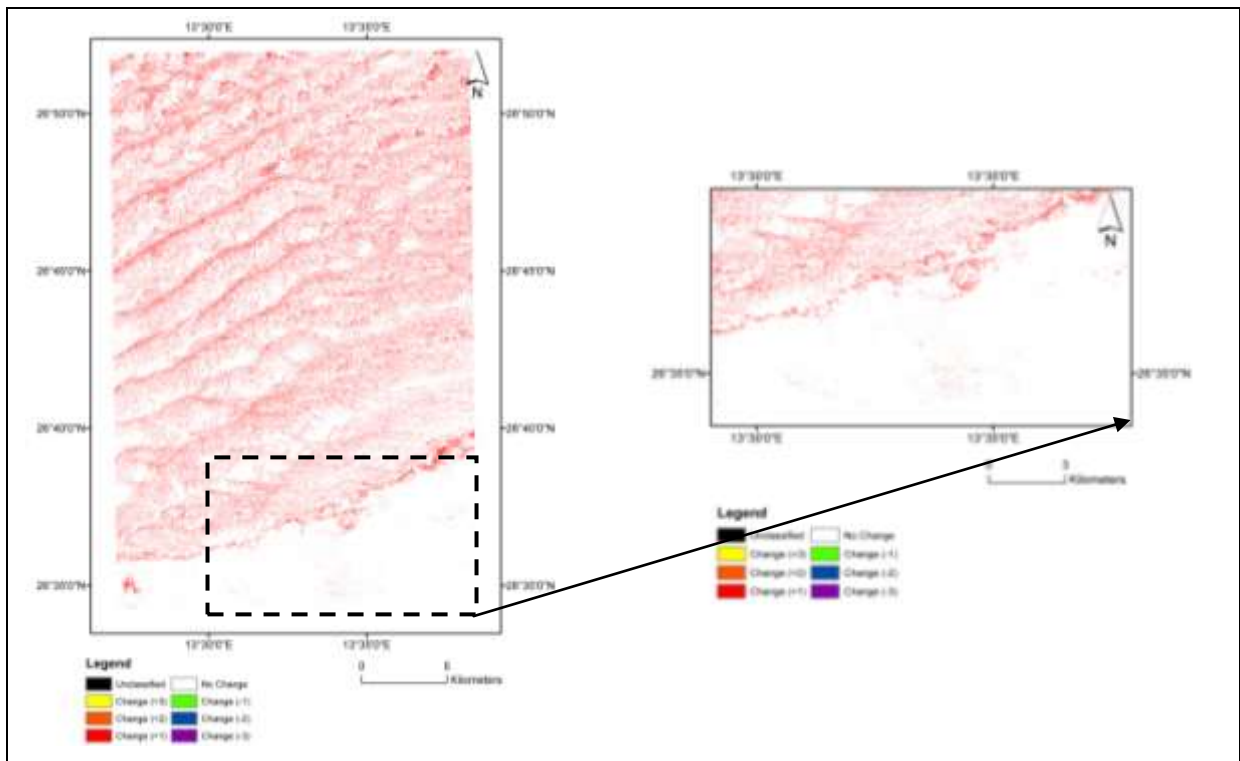


Figure 4.6: Change detection map indicating the areas of difference between the Worldview 2 and Landsat 8 Maximum Likelihood classifications; zoomed in section on the edges of the sand sea – showing the smaller amount of change that occurred.

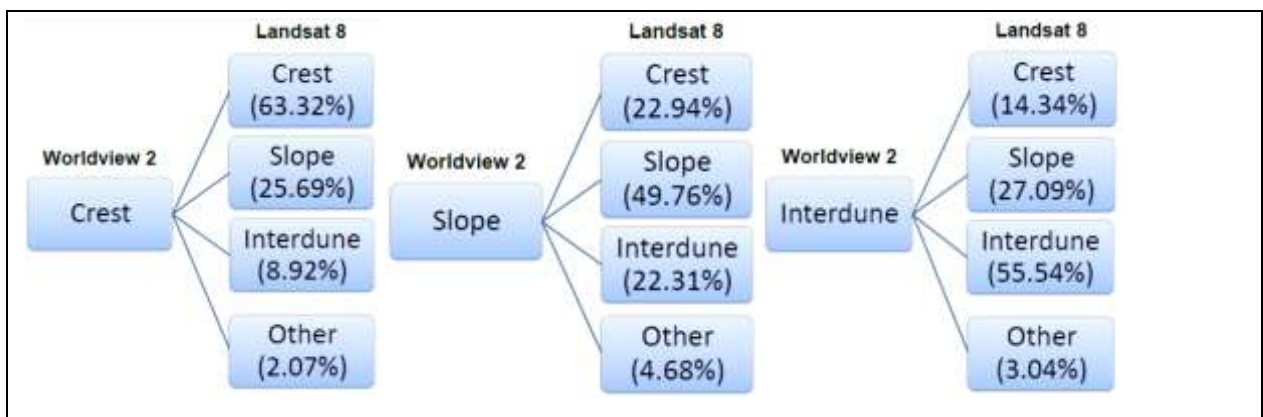


Figure 4.7: Flow diagrams of the changes that occurred in the dune feature classes from the Worldview 2 image to the Landsat 8 Image.

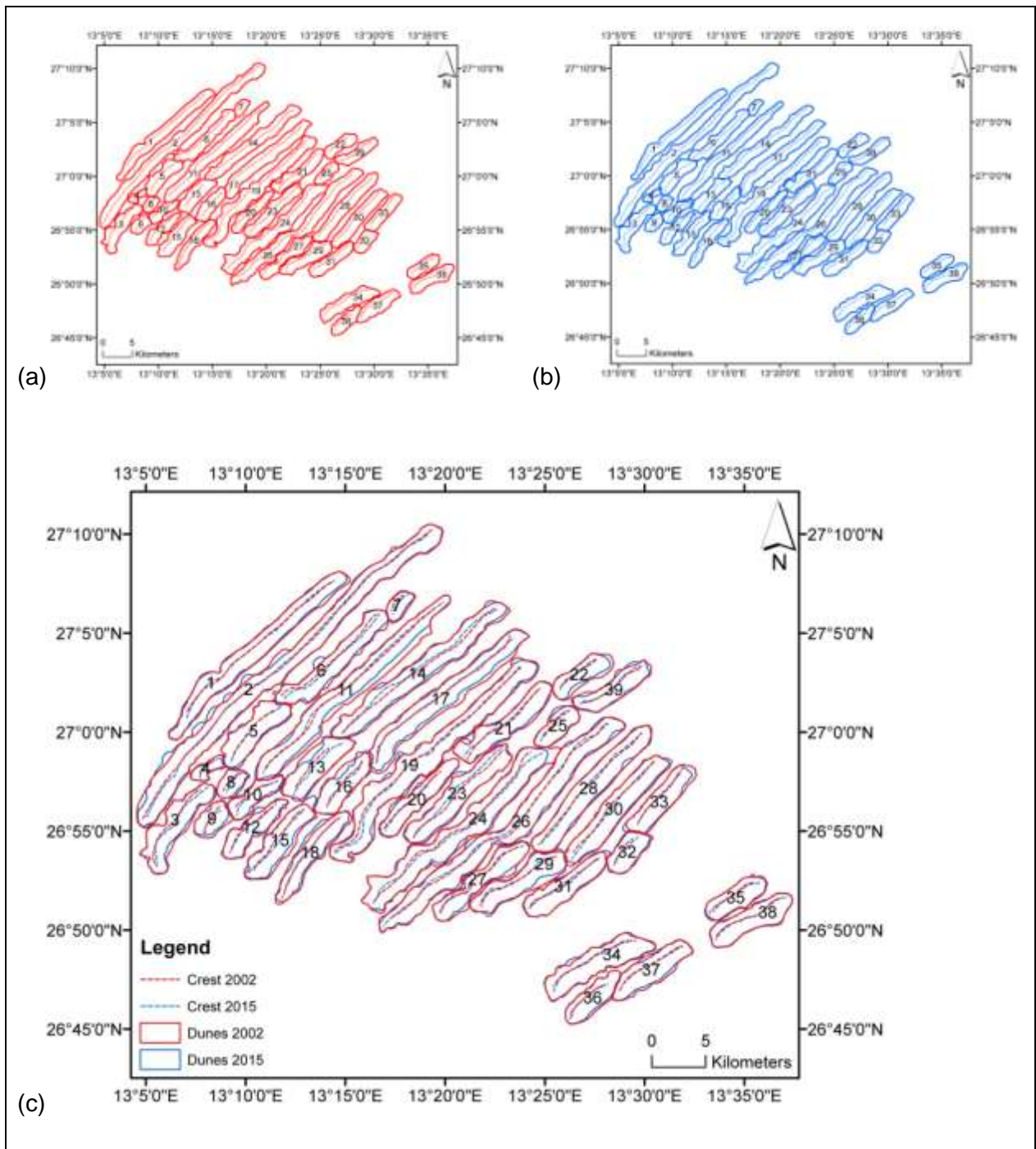


Figure 4.8: The dune outlines and crest lines for (a) 2002 (dune outline: solid and crest: dashed red lines); (b) 2015 (dune outline: solid and crest: dashed blue lines) and (c) the crest lines from 2002 over laid over those from 2015

Table 4.7a: The change in area (km²) per class from the Wordlview 2 to Landsat 8 Maximum Likelihood Classification Images

		Worldview 2 (Initial State)								
		Crest	Gypsum	Interdune	Rocky Outcrop	Slope	Soil	Urban	Vegetation	Water
Landsat 8 (Final State)	Crest	111.83	2.86	14.36	0	48.36	0.01	0.09	0	0.01
	Gypsum	3.52	11.14	2.2	0.01	9.33	0.39	0.43	0.14	0.21
	Interdune	15.75	0.75	55.65	0	47.67	0.08	0.64	0.11	0.01
	Rocky Outcrop	0	0.01	0	26.05	0	1.63	6.62	0.02	0.07
	Slope	45.36	5.9	27.14	0	104.95	0.14	0.74	0.01	0.08
	Soil	0.05	2.04	0.05	0.39	0.13	23.88	3.32	1.02	1.67
	Urban	0	0.03	0.01	1.06	0	6.61	4.56	1.69	0.11
	Vegetation	0.09	0.79	0.71	0.09	0.39	2.98	3.31	6.99	0.1
	Water	0	0.23	0.08	0.13	0.01	5.69	1.38	1.18	0.77
	Class Total	100.00	176.6	23.76	100.19	27.96	210.84	41.47	21.29	11.15
Class Changes	36.62	64.77	12.62	44.54	1.92	105.89	17.59	16.73	4.16	
Image Difference	+0.56	+0.93	+3.60	+20.49	+6.42	-26.52	-8.91	-7.22	+4.29	

Table 4.7b: The percentage change per class from the Worldview 2 to Landsat 8 Maximum Likelihood Classification Images

		Worldview 2 (Initial State)								
		Crest	Gypsum	Interdune	Rocky Outcrop	Slope	Soil	Urban	Vegetation	Water
Landsat 8 (Final State)	Crest	63.32	12.05	14.34	0.00	22.94	0.03	0.43	0.04	0.23
	Gypsum	1.99	46.89	2.19	0.02	4.43	0.94	2.00	1.23	6.78
	Interdune	8.92	3.17	55.54	0.01	22.61	0.21	3.02	1.01	0.44
	Rocky Outcrop	0.00	0.03	0.00	93.14	0.00	3.92	31.09	0.14	2.26
	Slope	25.69	24.85	27.09	0.00	49.78	0.33	3.46	0.06	2.63
	Soil	0.03	8.59	0.05	1.41	0.06	57.59	15.59	9.11	55.22
	Urban	0.00	0.12	0.01	3.78	0.00	15.95	21.44	15.14	3.74
	Vegetation	0.05	3.34	0.71	0.34	0.18	7.18	15.54	62.71	3.17
	Water	0.00	0.96	0.08	0.47	0.00	13.72	6.48	10.57	25.51
	Class Total	100.00	100.00	100.00	100.00	100.00	100.00	100.00	100.00	100.00
Class Changes	36.62	36.68	53.11	44.46	6.86	50.22	42.41	78.56	37.29	
Image Difference	+0.56	+0.52	+15.14	+20.45	+22.95	-12.58	-21.48	-33.92	+38.50	

Phase 2:

The results from Phase 2 address Aim 2 of the project (Refer to section 1.2).

4.2 Dune Migration

Landsat 7 (September 2002) and Landsat 8 (September 2015) Imagery was used to do a preliminary analysis on the migration, within a subsection (Figure 4.9) of the Ubārī Sand Sea, by quantifying the changes in the dune boundaries – specifically the base boundary of the windward slope and the orientation of the dune (refer to section 3.5).

4.2.1 Supervised Classification

The resulting maximum likelihood classification images (refer to section 3.4) can be seen in Figure 4.8. The Kappa coefficient (Table 4.8) for the Landsat 7 and Landsat 8 classified images are 0.5032 and 0.5937 respectively indicating an acceptable accuracy level of the overall classification. The user accuracy of the three dune feature classes for the Landsat 7 image (2002) were as follows: Crest (71.12%); Slope (51.22%) and Interdune (48.04%). Of these classes the crest was sometimes confused with the slope and interdune classes, the interdune was mostly only confused with the slope and gypsum classes. The slope class however was often confused with the crest, gypsum and interdune classes. The user accuracy for the Landsat 8 (2015) image was as follows: Crest (75.78%); Slope (55.16%) and Interdune (54.57%). On the Landsat 8 image there were also confusion of classes, the crest and interdune classes showed some confusion as well as the interdune and slope classes – this confusion is most likely due to the similar spectral behaviour of the three dune feature classes as mentioned before.

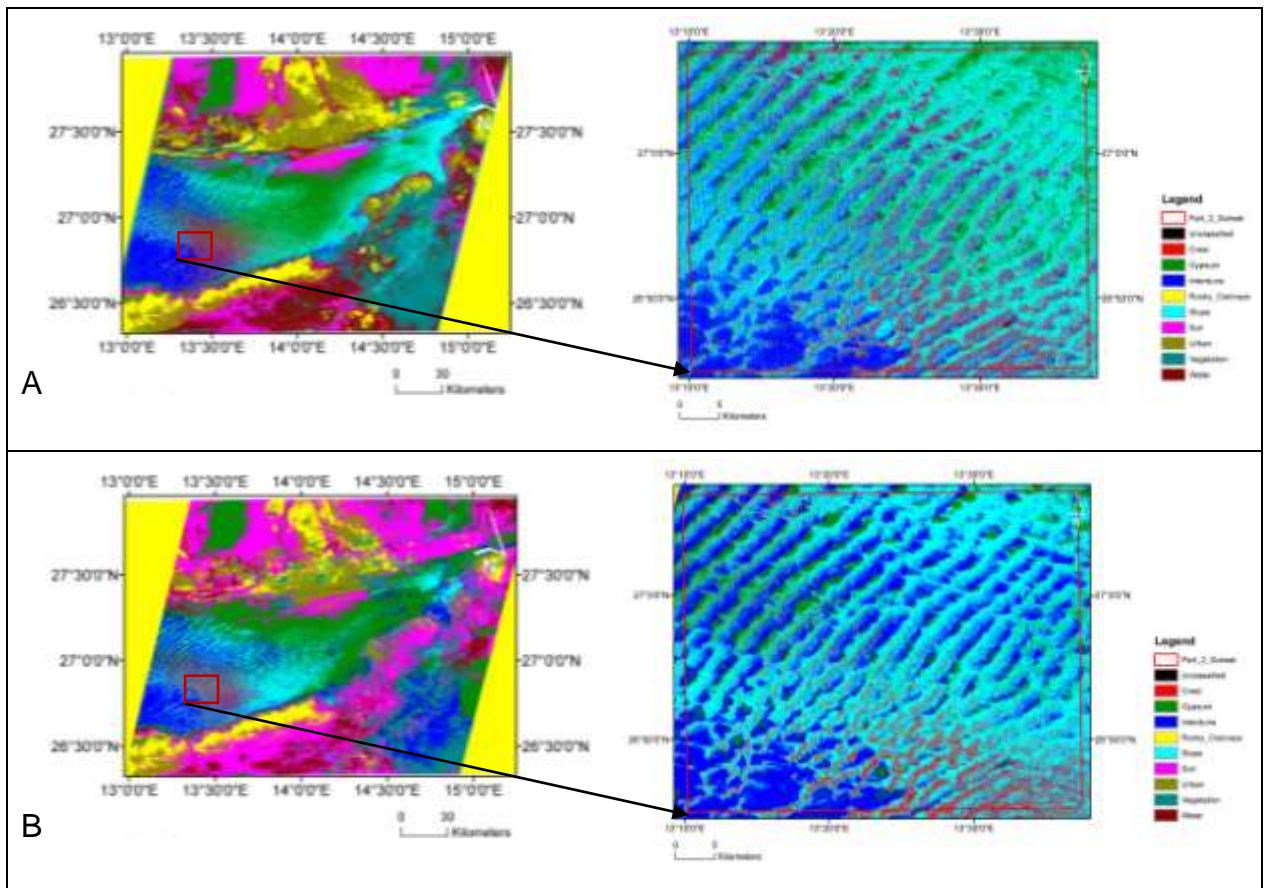


Figure 4.9: The resulting maximum likelihood classified images for A: 2002 (Landsat 7) and B: 2015 (Landsat 8) (zoomed in on study area - right)

Table 4.8: Error Matrix for the Maximum Likelihood Classification for; (a) Landsat 7 (2002) and (b) Landsat 8 (2015) imagery.

(a)		Test Data										
Classified Image	Class	Crest	Gypsum	Interdune	Rocky Outcrop	Slope	Soil	Urban	Vegetation	Water	Total	User Accuracy (%)
	Crest	953	2	0	0	385	0	0	0	0	1340	71.12
	Gypsum	25	80	18	0	111	3	0	2	0	239	33.47
	Interdune	164	9	245	0	91	0	0	1	0	510	48.04
	Rocky Outcrop	0	0	0	252	0	1	5	1	0	259	97.30
	Slope	136	3	21	0	168	0	0	0	0	328	51.22
	Soil	0	1	0	1	0	70	7	32	0	111	63.06
	Urban	0	0	0	18	0	24	60	14	1	117	51.28
	Vegetation	0	0	5	0	0	18	7	49	3	82	59.76
	Water	0	0	0	1	0	44	3	20	40	108	37.04
Total	1278	95	289	272	755	160	82	119	44	3094		
Producer Accuracy (%)	74.57	84.21	84.78	92.65	22.25	43.75	73.17	41.18	90.91			

Overall Accuracy = 61.96%

Kappa Coefficient = 0.50

Table 4.8 continued

(b)		Test Data										
Classified Image	Class	Crest	Gypsum	Interdune	Rocky Outcrop	Slope	Soil	Urban	Vegetation	Water	Total	User Accuracy (%)
	Crest	881	0	2	0	280	0	0	0	0	1163	75.75
	Gypsum	8	85	2	0	20	8	0	6	0	129	65.89
	Interdune	123	6	233	0	65	0	0	0	0	427	54.57
	Rocky Outcrop	0	0	0	253	0	1	3	0	0	257	98.44
	Slope	266	1	50	0	390	0	0	0	0	707	55.16
	Soil	0	3	0	4	0	112	4	7	0	130	86.15
	Urban	0	0	0	15	0	16	68	22	0	121	56.2
	Vegetation	0	0	2	0	0	11	5	70	1	89	78.65
	Water	0	0	0	0	0	12	2	14	43	71	60.56
Total	1278	95	289	272	755	160	82	119	44	3094		
Producer Accuracy (%)	68.94	89.47	80.62	93.01	51.66	70.00	82.93	58.82	97.73			
Overall Classification = 69.01%												
Kappa Coefficient = 0.59												

4.2.2 Change Analysis

With the use of a change detection map the area used to estimate the migration rate was identified (Figure 4.10). The changes from 2002 to 2015 were mostly located within the central areas of the sand sea, where the dunes are most likely more active. The changes appear to be localized along the dunes. The least amount of change occurred at the boundaries of the sand sea, changes at the boundaries may also be related to anthropogenic activity (Figure 4.10).

The results from the change detection statistics module (Table 4.9) gives a more quantifiably image of the amount of change that occurred per feature class. There was an overall decrease of 41.90 % (1704.42 km²) in the slope areas, and an increase of 22.95 % (73.57 km²) in the crest area, and 48.12 % (119.33 km²) in the interdune area in the subset over the time period of 2002-2015. This is indicative that dune migration occurred in that time period.

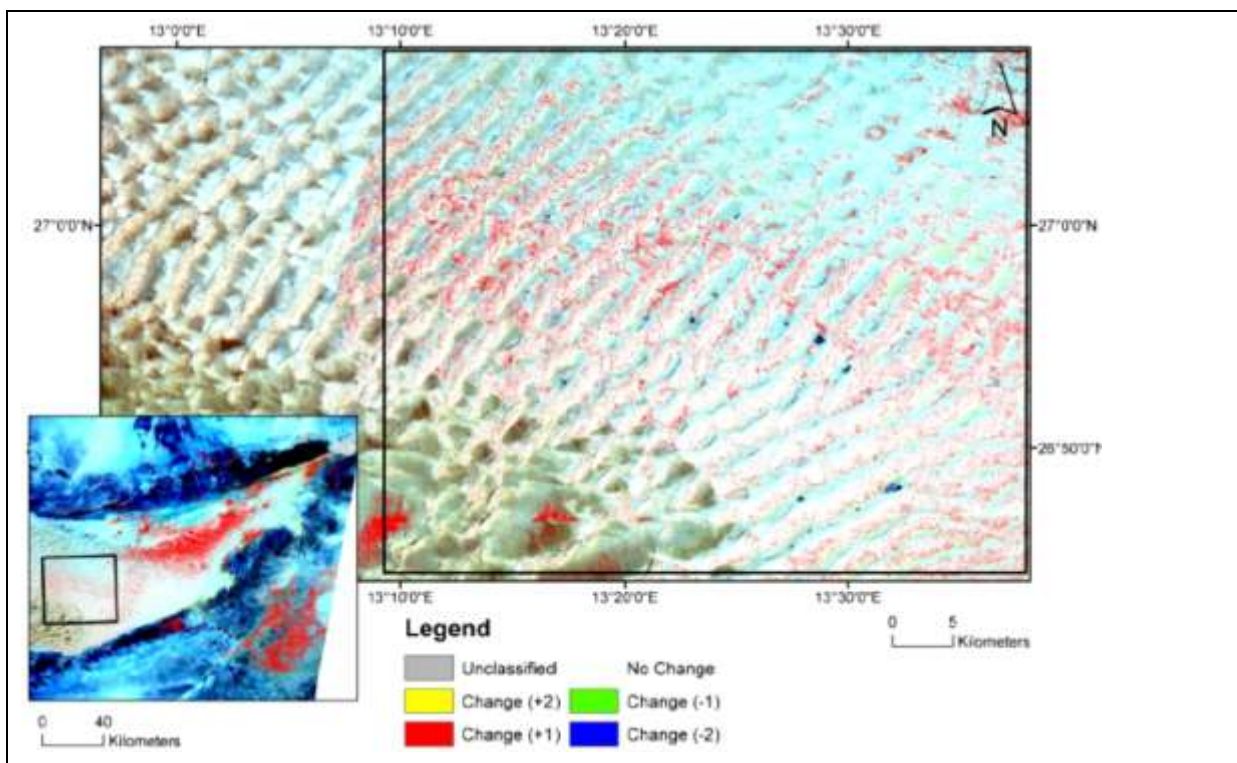


Figure 4.10: A change detection map superimposed on the atmospherically corrected image from 2015 – indicating the areas where change occurred and finally the subsection (boxed) that was used in the analyses (where no change occurred there is no colour - it is transparent).

Table 4.9a: The overall change in area (km²) per class for the time period of 2002-2015.

		Initial State (2002)							
		Crest	Gypsum	Interdune	Slope	Soil	Urban	Vegetation	Water
Final State (2015)	Crest	73.57	105.52	30.61	110.63	0.01	0.09	1.44	0.56
	Gypsum	12.83	7165.3	22.21	1693.77	5.46	0.01	809.57	887.55
	Interdune	110.51	695.23	119.33	530.57	0.03	0.67	3.61	14.06
	Slope	120.75	1217.09	72.19	1704.42	0	0.58	3.35	22.6
	Soil	0	176.08	0.01	0.1	5.04	0	210.34	33.16
	Urban	0	0.06	0	0	0	0	0.57	0.02
	Vegetation	2.93	408.02	3.53	25.84	5.62	0	532.25	164.9
	Water	0.02	139.65	0.13	2.94	0.03	0	26.38	101.01
Class Total		320.61	9907.46	248.01	4068.27	16.38	2.6	1590.61	1224.2
Class Changes		247.04	2742.16	128.68	2363.85	11.34	2.6	1058.37	1123.19
Image Difference		1.83	689.24	1226	-927.29	408.36	-1.95	-447.52	-954.02

Table 4.9b: The overall percentage change per class for the time period of 2002-2015

		Initial State (2002)							
		Crest	Gypsum	Interdune	Slope	Soil	Urban	Vegetation	Water
Final State (2015)	Crest	22.95	1.07	12.34	2.72	0.06	3.57	0.09	0.05
	Gypsum	4.00	72.32	8.95	41.63	33.30	0.56	50.90	72.50
	Interdune	34.47	7.02	48.12	13.04	0.16	25.86	0.23	1.15
	Slope	37.66	12.29	29.11	41.90	0.01	22.15	0.21	1.85
	Soil	0.00	1.78	0.01	0.00	30.77	0.00	13.22	2.71
	Urban	0.00	0.00	0.00	0.00	0.01	0.00	0.04	0.00
	Vegetation	0.92	4.12	1.42	0.64	34.28	0.00	33.46	13.47
	Water	0.01	1.41	0.05	0.07	0.20	0.00	1.66	8.25
Class Total		100.00	100.00	100.00	100.00	100.00	100.00	100.00	100.00
Class Changes		77.05	27.68	51.89	58.11	69.23	100.00	66.54	91.75
Image Difference		0.57	6.96	48.12	-22.79	2492.47	-75.08	-28.14	-77.93

4.2.3 Changes in Dune Morphology (Shape, Size, Length, Width)

The overall morphological changes in the selected dunes over the period of 2002-2015 can be seen in Figures 4.11 – 4.13 and Table 4.10 (refer to section 3.6 to review how this was done). The general shape of the dunes remained the same during this period, but there were some changes in the crest length, dune width and area of the dunes in question. The crest lengths for 2002 ranged from 1.90 km – 36.50 km; for 2015 the crest lengths ranged from 2.40 km – 36.10 km and from 2002 to 2015 varied from decreasing lengths of 13.70 km and increases in length of 16.40 km. The width of the dunes also showed small variations from decreasing widths of 0.35 km and increasing widths of 0.02 km. The changes in the total area of the dunes were more pronounced, ranging from decreases in the area of 8.05 km² to increases in the dune area of .15 km². Of the 39 dunes in question, 17 dunes showed a decrease in crest length and 37 of the dunes showed a decrease in width and/ or area respectively (Table 4.10).

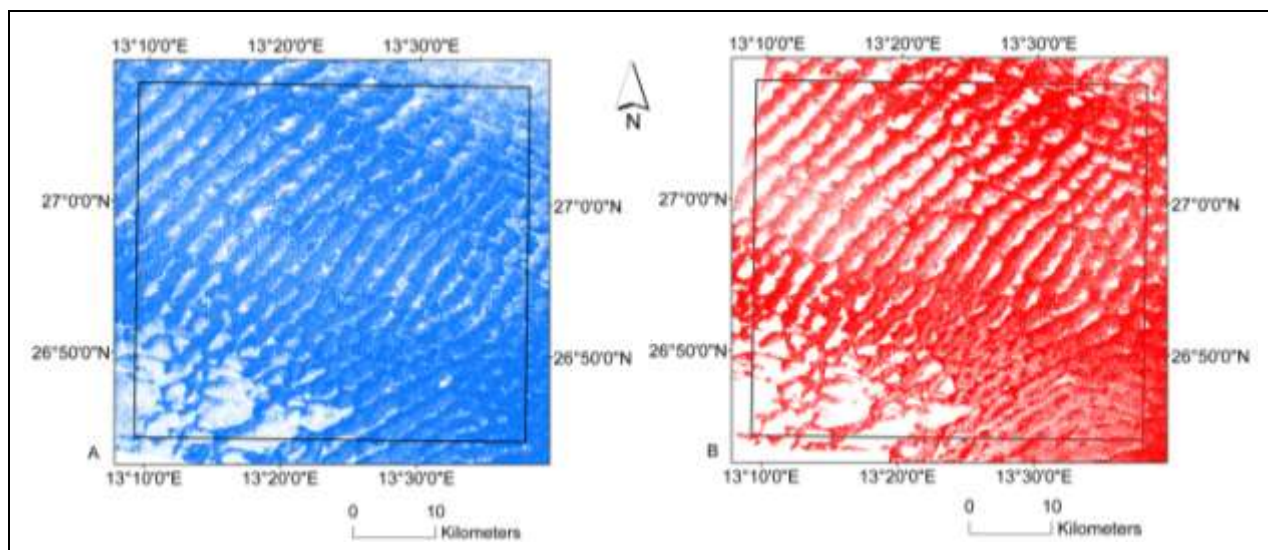


Figure 4.11: The isolated dune classes extracted from the maximum likelihood classification images for A: 2002 and B: 2015.

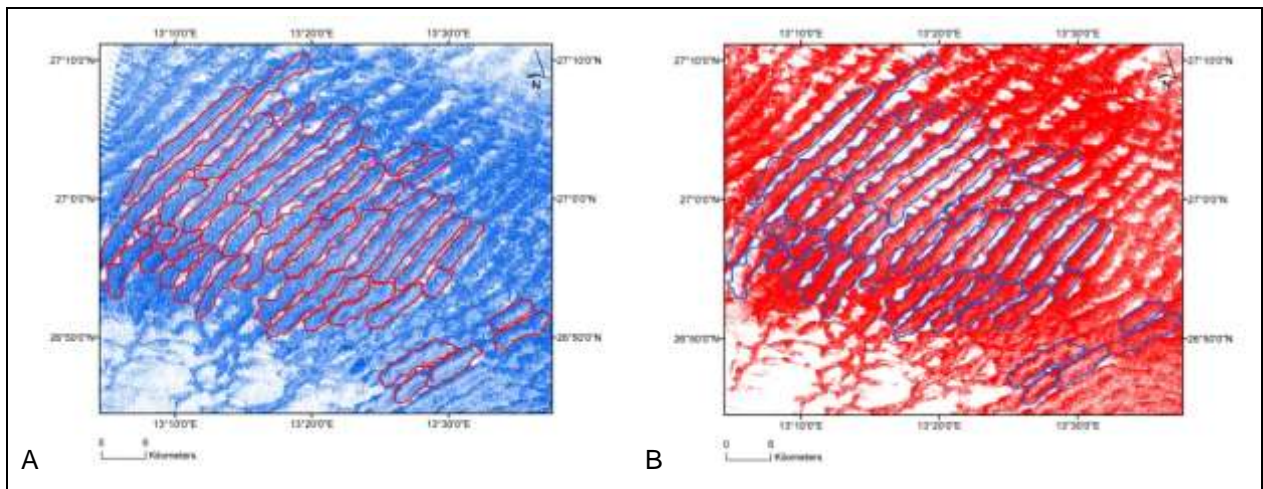


Figure 4.12: The isolated dune classes extracted from the maximum likelihood classification images for A: 2002 and B: 2015 with the overlay of the digitized dunes (outlined in red (A) and blue (B))

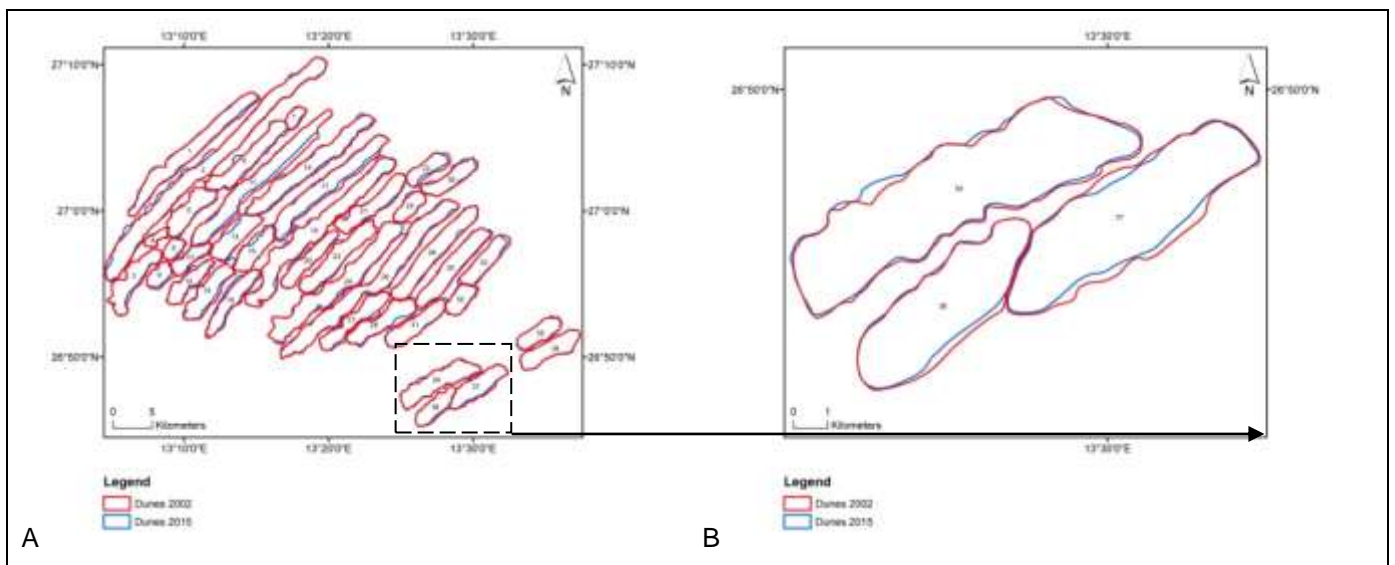


Figure 4.13: Digitized dunes from 2002 (blue) superimposed on top of the digitized dunes from 2015 (red); A: the 39 dunes that were used for the migration analysis and B: zoomed in section

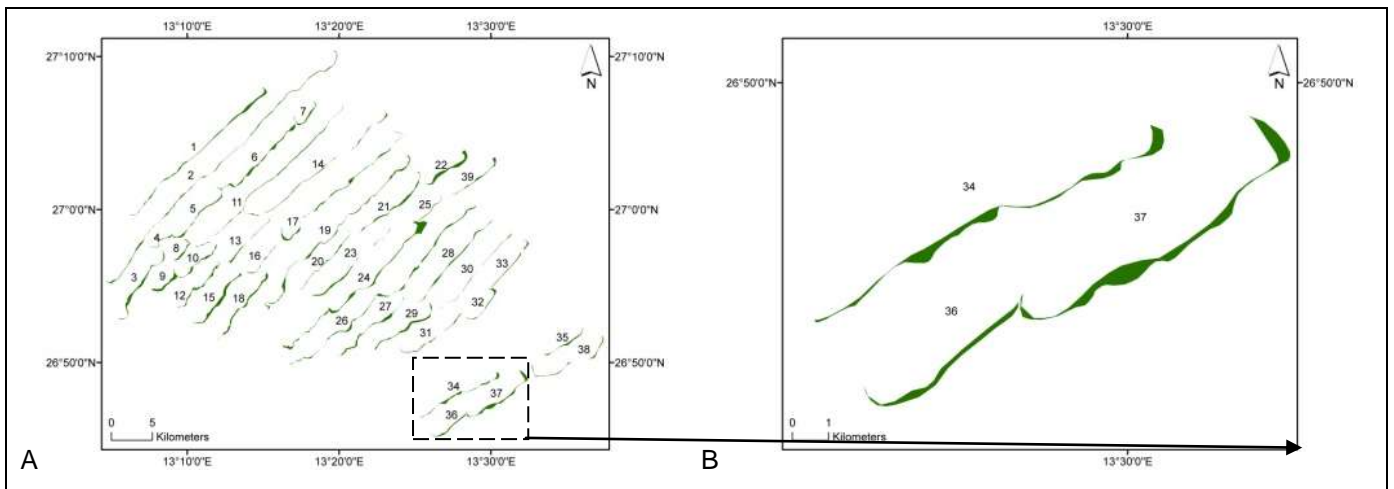


Figure 4.14: Sand dune movement map - resulting areas of change (green polygons) from the subtraction of the digitized dunes of 2015 from the digitized dunes of 2002; A: the dunes used in the analysis of the dune migration and B: zoomed in section

4.2.4 Changes in Location

Figure 4.14 and Table 4.11 gives an estimate of the changes in the physical location (refer to section 3.6 to review how this was accomplished) of the dunes in question, based on the position of the windward slope boundary. For the 39 dunes migration distances from 2002 to 2015 ranged from 29.79 (± 17.25) m to 316.65 (± 146.76) m. Overall the dunes migrated an average total of 112.33 (± 60.64) m in the time period and resulting in an average yearly migration rate of 8.64 (± 4.65) m.

Table 4.10: Changes in dune crest length, dune width and area from 2002-2015.

Dune # (See Fig 4.13)	Crest Length (km)			Average Width (km)			Area (km ²)		
	2002	2015	Difference (2015-02)	2002	2015	Difference (2015-02)	2002	2015	Difference (2015-02)
1	17.40	18.10	0.70	1.60	1.48	-0.12	33.77	31.12	-2.65
2	36.50	36.10	-0.40	1.75	1.72	-0.03	65.01	63.94	-1.07
3	8.50	9.20	0.70	1.99	1.84	-0.15	18.39	17.02	-1.37
4	3.10	2.60	-0.50	1.23	1.10	-0.12	3.48	3.18	-0.30
5	2.10	2.40	0.30	2.06	1.95	-0.12	15.98	14.81	-1.17
6	2.30	5.10	2.80	1.81	1.71	-0.10	21.64	19.94	-1.69
7	4.10	5.90	1.80	1.36	1.16	-0.20	4.33	3.70	-0.63
8	5.90	2.80	-3.10	1.78	1.61	-0.16	4.80	4.53	-0.27
9	20.70	7.00	-13.70	1.97	1.73	-0.24	6.80	5.97	-0.83
10	11.30	11.60	0.30	1.41	1.38	-0.03	8.08	7.85	-0.23
11	1.90	2.40	0.50	1.75	1.41	-0.34	41.53	33.48	-8.05
12	5.90	22.30	16.40	1.49	1.42	-0.07	11.06	10.81	-0.25
13	7.20	6.70	-0.50	2.23	1.97	-0.26	15.69	14.28	-1.42
14	9.20	7.70	-1.50	1.89	1.69	-0.21	34.41	31.06	-3.35
15	4.70	8.40	3.70	2.04	1.80	-0.24	16.47	15.19	-1.29
16	5.40	5.20	-0.20	1.91	1.72	-0.19	12.72	11.55	-1.17
17	17.50	17.30	-0.20	1.98	1.63	-0.35	35.23	28.92	-6.31
18	16.80	16.90	0.10	1.56	1.54	-0.03	15.41	14.82	-0.59
19	23.80	23.90	0.10	1.93	1.83	-0.11	47.54	44.78	-2.76
20	7.40	7.10	-0.30	1.32	1.23	-0.09	13.74	12.92	-0.83
21	9.20	11.10	1.90	1.76	1.70	-0.06	18.16	17.30	-0.86
22	4.10	20.40	16.30	1.79	1.43	-0.35	10.30	8.32	-1.99
23	6.10	9.00	2.90	1.78	1.80	0.01	22.07	21.76	-0.31
24	3.20	4.00	0.80	2.09	1.99	-0.10	43.42	39.81	-3.61

Table 4.10 Continued

Dune # (See Fig 4.13)	Crest Length (km)			Average Width (km)			Area (km ²)		
	2002	2015	Difference (2015-02)	2002	2015	Difference (2015-02)	2002	2015	Difference (2015-02)
25	11.30	4.40	-6.90	1.76	1.78	0.02	7.71	7.68	-0.02
26	19.90	6.60	-13.30	1.86	1.73	-0.12	50.98	47.68	-3.31
27	26.10	27.30	1.20	1.69	1.53	-0.16	17.13	15.52	-1.61
28	9.40	9.80	0.40	1.90	1.83	-0.08	27.15	26.10	-1.05
29	8.20	7.90	-0.30	2.12	1.93	-0.19	18.58	16.83	-1.74
30	13.40	7.70	-5.70	1.92	1.81	-0.12	23.44	22.49	-0.94
31	10.90	3.40	-7.50	1.86	1.84	-0.01	15.43	15.59	0.15
32	7.50	13.70	6.20	1.99	1.88	-0.12	8.68	8.05	-0.63
33	2.80	11.30	8.50	1.87	1.72	-0.15	13.84	12.65	-1.19
34	6.30	6.10	-0.20	2.05	2.03	-0.02	20.92	21.03	0.11
35	8.40	8.20	-0.20	1.80	1.74	-0.06	10.70	10.42	-0.28
36	4.20	4.80	0.60	1.68	1.58	-0.09	10.41	9.83	-0.58
37	6.90	6.70	-0.20	2.00	1.79	-0.21	15.94	14.17	-1.77
38	4.50	5.20	0.70	1.96	1.92	-0.04	15.25	15.02	-0.23
39	6.70	7.50	0.80	1.73	1.57	-0.16	12.38	11.54	-0.83
SD*	7.55	7.54	5.61	0.23	0.23	0.09	14.03	13.10	1.66

*SD = Standard Deviation

Table 4.11: The average distance each of the sample dunes migrated (m) for the time series (13 years), as well as the average migration rate per dune per year (m/yr) and the overall migration distance (m) and migration rate (m/yr) for the dunes in question

Dune # (See Fig 4.13)	Average Migration per Dune (m)	Standard Deviation	Average Migration Rate per Dune per Year (m/yr)
1	111.81	80.98	8.60
2	65.94	47.03	5.07
3	143.66	88.06	11.05
4	79.32	41.50	6.10
5	103.20	50.69	7.94
6	129.03	83.66	9.93
7	134.37	57.50	10.34
8	159.34	73.43	12.26
9	316.65	146.76	24.36
10	118.87	77.18	9.14
11	59.30	25.67	4.56
12	135.17	72.41	10.40
13	76.50	62.74	5.88
14	47.00	15.95	3.62
15	212.86	91.41	16.37
16	42.89	50.07	3.30
17	77.21	40.29	5.94
18	146.40	70.32	11.26
19	92.90	82.93	7.15
20	57.48	28.66	4.42
21	117.20	80.76	9.02
22	293.80	109.89	22.60
23	100.02	63.66	7.69
24	109.69	78.96	8.44

Table 4.11 Continued

Dune # (See Fig 4.13)	Average Migration per Dune (m)	Standard Deviation	Average Migration Rate per Dune per Year (m/yr)
25	56.58	17.12	4.35
26	101.84	65.70	7.83
27	115.55	94.86	8.89
28	88.87	53.22	6.84
29	196.29	71.52	15.10
30	29.79	17.32	2.29
31	79.40	37.66	6.11
32	71.95	38.81	5.53
33	67.20	23.38	5.17
34	118.38	89.11	9.11
35	112.08	76.05	8.62
36	116.24	15.37	8.94
37	151.15	123.99	11.63
38	71.25	40.89	5.48
39	73.64	50.41	5.66
Overall Average Dune Migration (m)			112.33 (± 60.46)
Overall Average Dune Migration Rate per Year (m/yr)			8.64 (± 4.65)

4.3 Key Findings

In general the dune features can be identified/ discriminated based on the spectral signature alone (Figure 4.2). The dune features, namely the crest, slope and interdunal areas were successfully classified based on both the coarse and fine resolution imagery, but the accuracy with which it can be classified are different between the two resolutions (Figure 4.3). The classifications based on the Worldview 2 imagery had overall accuracies ranging from 55.43 - 60.83% with kappa values of 0.3486 – 0.4225 compared to the overall accuracies and kappa values of the classifications based on the Landsat 8 imagery ranging from 52.11 – 64.67% and 0.3878 – 0.4927 respectively.

From the resulting images and measurements it can be argued that similar dune patterns and crest orientations can be identified from the different spatial resolution data sources (refer to section 4.2.4). However, it can be suggested that the accuracy, precision and ease with which the dune features can be defined increases with the use of a finer spatial resolution. The smaller pixel size of higher resolution imagery may result in increased precision as the features can be more closely defined.

Landsat is sufficient in mapping the general dune patterns, orientation and size, however other features (such as ripples and superimposed dunes) that are clearly visible on the Worldview 2 imagery is less defined if at all visible on the Landsat 8 image (see Figure 5.1). For the purposes of this study, the Landsat imagery was sufficient in determining the overall migration rate and direction of the dunes present in the Ubārī Sea.

There is dune migration present within the Ubārī Sand Sea, with regards to the linear dunes. As mentioned previously the star dunes were not included in the scope of this project but it could be interesting to “play around” with those dunes as well. An average migration rate of 8.64 (\pm 4.65) m/yr was measured for the dunes within the subsection of the Ubārī that was analysed.

Chapter 5: Discussion

5.1 Introduction

Sand dune migration has been identified as one of the greatest threats to anthropogenic developments, agricultural activities and the preservation of historical sites in arid areas (such as Egypt and Libya) (Hermas *et al.*, 2012; El-Magd *et al.*, 2013; Sparavinga, 2013). In order to limit and/ or prevent this threat, dune dynamics and dune migration rates and direction need to be studied (Sparavinga, 2013). Previous studies have been limited to extensive and expensive field surveys that are spatially and temporally (frequency of successive measurements) limited and time consuming (Paisley *et al.*, 1991; Levin *et al.*, 2004; Yao *et al.*, 2007; Hermas *et al.*, 2012; Mohamed & Verstraeten, 2012; El-Magd *et al.*, 2013). Recently, remote sensing and GIS has been suggested and used as a solution to overcome these limitations (White *et al.*, 1997; Al-Dabi *et al.*, 1998; Janke, 2002; Levin *et al.*, 2004, 2006; Yao *et al.*, 2007; Hermas *et al.*, 2012; Mohamed & Verstraten *et al.*, 2012; El-Magd *et al.*, 2013). Several different remote sensing platforms exist, with different specifications; purposes and availability (see Table 1.1), but not all of these platforms are useful for studies in arid environments (Hermas *et al.*, 2012; El-Magd *et al.*, 2013).

This dissertation aimed at: 1. determining if Landsat 7 and 8 (a coarser spatial resolution) was sufficient to study arid dune environments (compared to a finer spatial resolution, Worldview 2 in this case) – in particular the study of dune migration. 2. To determine if dune migration occurred within the Ubārī Sand Sea during the time period of 2002-2015, and if so what the rate and direction of said migration was. Previous studies in this area has been limited due to its remote location, the size of the dunes and the extent of the sand sea which would result in very expensive expeditions to study the dunes and to determine the migration rates in an area that is not widely populated, and the sand sea is located within a basin which constricts the movement of the sand to a degree and lowering the immediate threat of this particular sand sea.

This study is original in the way that it considers the identification and monitoring of sand dunes and sand dune migration by way of classification methods within the Ubārī Sand Sea. Limited sand dune studies have been conducted in this area due to its location and size. Results from this study contribute to our knowledge of the usability and effectiveness of using remote sensing platforms and automated classification

methods to study dunes and their migration. The results also contribute to the knowledge of the dynamics of linear dunes located within the Ubārī Sand Sea.

5.2 Phase 1: The Comparison of Two Spatial Resolutions (Worldview 2 and Landsat 8 Images)

Within this section of the research two band combinations were used to classify the Landsat 8 and Worldview 2 imagery with the use of the minimum distance and maximum likelihood classification modules. In order to compare these classifications an accuracy assessment was applied to each of the combinations in order to determine the “best” combination to study sand dunes in arid environments (refer to section 3.4).

5.2.1 Band Combinations & Classification Module

It was found that the classifications classified with the maximum likelihood classification algorithm on the visible (red, green, blue) and near infrared bands resulted in the highest overall accuracy and kappa value (Worldview 2: 60.83% & 0.4225 and Landsat 8: 64.67% & 0.5355), respectively. The highest class accuracy for the crest class was achieved with the combination of the visible and near infrared bands and the maximum likelihood classification, and the highest class accuracy for the slope and interdune classes were achieved with the combination of the red and near infrared bands and the maximum likelihood classification.

These resulting “best” bands combination coincides with the comment Collado *et al.* (2002) made; that most authors rely on the visible spectral range (red, green and blue bands) to study sand dunes, as a high reflectance of bare soil is seen in the visible band range. Additional analysis into the use of the panchromatic, thermal, blue and deep-blue (violet) bands in arid dune environments can also be considered, as some authors have found these bands to be useful in discriminating the different dune features (Pease *et al.*, 1999; Mohamed & Verstraten, 2012; Telfer *et al.*, 2015) (these bands were excluded in this research because the spatial resolution was the parameter being questioned not the spectral resolution, and not all of the previously mentioned bands are included in the Worldview 2 platform).

The use of automated classification methods in arid environments (particularly dune environments) has been very limited – it is more commonly used in vegetated and/ or areas with urban development. In the research of vegetated environments the maximum likelihood classification has also been found to be the better classifier (compared to minimum distance) by Maselli *et al.* (1990); Keuchel *et al.* (2003); Adelabu *et al.*, 2013). Other research (Conese & Maselli, 1992; de Souza *et al.*, 2013) has identified some limitations associated with the maximum likelihood classifier including bias in area estimates and errors in the area estimation. Bias and errors in the estimation of the area within this study cannot be commented on as no ground truthing could be done – and thus the accuracy in relation to reality cannot be definitively defined. De Souza *et al.* (2013) also noted that the ideal classification method will be different in each study depending on the question that needs answering, therefore this result of maximum likelihood being the better classifier in arid dune environments can be considered a pilot to further research which can consider other classification methods compared to the maximum likelihood classifier to better define dune features more efficiently and more accurately (as the accuracy of the maximum likelihood classifier even although it was the “best”, the accuracy was still very low with a kappa value of 0.5355).

5.2.2 Spatial Resolution Comparison: Landsat 8 vs Worldview 2

There was an average difference of 20% per class between the Worldview and Landsat classifications. This difference is assumed to be as a result of the difference in the spatial resolution, because the spectral resolution was constant for the two images. It was found that the Worldview classifications are more accurate in terms of measurements than the Landsat classification but the Landsat classification is sufficient for delineating the basic dune morphology.

From the resulting images (Figures 4.4, 4.5, 4.6) and measurements (Tables 4.7a and b) it can be argued that similar dune patterns and crest orientations can be identified from the different spatial resolution data sources. However, it can also be suggested that the accuracy and ease with which the dune features can be defined increases with a finer spatial resolution – as the dune features are more easily defined in all their components.

Bryantt (2014) compared classifications of Landsat 8 and Worldview 2 imagery in an agricultural context, and found that the classifications of Landsat 8 imagery yielded in a higher accuracy than those of the Worldview 2 imagery. It is interesting to note that within the current research similar results were found (to what Bryantt, 2014 found) with reference to the accuracy of resulting classifications maps of Landsat 8 (at 64.67% overall accuracy and kappa of 0.4927) being higher than that of Worldview 2 (with an overall accuracy of 60.83% and kappa value of 0.4225) (refer to Tables 4.5 and 4.6). It would be expected that the higher spatial resolution data would yield higher accuracies in classifications (as the features are better defined). However, Bryantt (2014) noted this “better defined features” as the cause of the lower accuracy – gaps in the crop cover are more defined with a higher spatial resolution thus the training classes are less homogeneous on the Worldview 2 image than on the Landsat 8 image (where small differences in ground cover is lost due to the coarser spatial resolution). Also the area that resulted in this low accuracy value was relatively homogeneous in terms of spectral signature or behaviour – thus it is difficult to discriminate different features based on the spectral signature alone – which is similar to the limitations of this study due to the homogeneity of arid dune environments. Bryantt (2014) noted that the Worldview 2 platform resulted in classifications with higher accuracies than those based on Landsat 8 imagery in the more heterogeneous areas that were studied; and that this was most likely due to the mixed pixel effect that was exacerbated by the coarser pixel resolution of Landsat 8.

The identification of dune crests (and slope boundaries) based solely on multispectral imagery (containing no data on the altitude of the features) is very difficult in some cases depending on the shape of the dune. Some dunes have a sharp, well defined crest whereas others have a more rounded, broad crest. The sharp well defined crests are more easily identified from multispectral imagery than the broad rounded crests. This could result in the misinterpretation of the data and ultimately influence the resulting classified images. Because of the finer spatial resolution of the Worldview 2 imagery it may be easier to define the crests of both sharp and round crested dunes, but it may also result in confusion of the classes when training data based on a finer spatial resolution is used to classify an image with a coarser spatial resolution.

Landsat is sufficient in mapping the general dune patterns (crest and interdunal areas), orientation and size independent of the classification method, but is not sufficient in the detection of the ripples or smaller and/or superimposed dunes that are present within the study site (which is visible on the Worldview imagery, Figure 5.1). This finding coincides with the findings of Al-Dabi *et al.* (1998) and Yao *et al.* (2007) that Landsat is a useful tool for dune pattern identification and tracking dune migration. For the purposes of this study Landsat imagery is deemed sufficient in determining the overall migration rate and direction of the dunes present in the Ubārī Sand Sea. Studies concerned with the specific dynamics and dimensions of dunes and superimposed dunes (especially) should consider using higher resolution imagery.

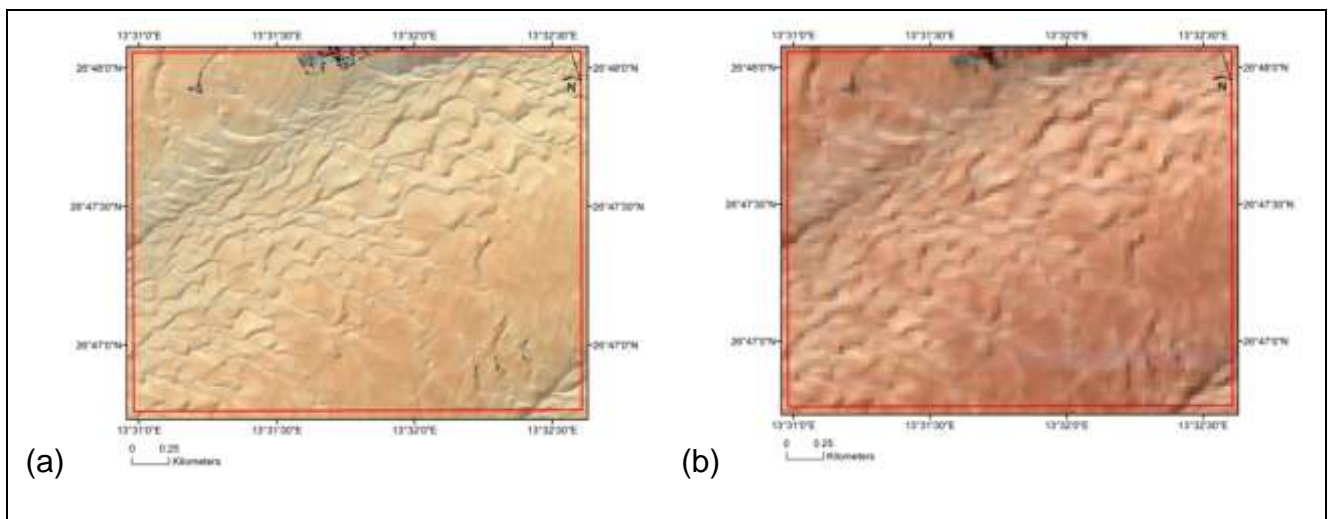


Figure 5.1: Zoomed in area (boxed in red) of the (a) Worldview 2 image showing the better visibility of the superimposed dunes compared to the same zoomed in area of the (b) Landsat 8 image. On the Worldview 2 image (left) ripples on top of the dune can be seen as well as better defined urban structures (top centre) which are not identifiable as urban structures on the Landsat 8 image (right)

5.3 Phase 2: Dune Migration within the Ubārī Sand Sea

Dune morphology (shape and size) and the migration (location and orientation) were studied by digitizing dunes from the classified images of two Landsat images for the time period of 2002-2015 (refer to section 3.6).

5.3.1 Morphology

Linear dunes within the Ubārī Sand Sea retained their general shape and crest orientation (SW-NE) between 2002 and 2015 (Figure 4.8 and 4.13), but there was some variations in the length, width and area of the dunes (Table 4.10). The length of the dune crests varied from 1.9 km (minimum recorded) to 36.10 km (maximum recorded) in 2002 and from 2.40 km to 36.10 km in 2015 respectively. Changes in the dune crest length varied from lengths decreasing up to 13.70 km and increasing up to 16.40 km (increasing dune lengths were observed in 22 out of the 39 dunes).

The average width varied from a minimum of 1.23 km and a maximum recorded average width of 2.23 km in 2002 and ranging from 1.10 km to 2.03 km in 2015 (Table 4.10). Thus there was also some variation in the average width of the dunes between 2002 and 2015, this variation ranged from average widths decreasing up to 0.35 km to increasing up to 0.02 km (a decrease in average width was observed in 37 of the 39 dunes). Bolghoubra (2016) found that the barchans dunes from Erg Sidi Moussa ranged in widths of 50 to 335 m – these are much smaller than that of the linear dunes of the Ubārī, but this is expected since barchan dunes are usually smaller than linear dunes.

Due to these changes in length and width there were also variations in the area (and most likely the height – which is beyond the scope of this research) of the dunes, the area of the dunes varied from 3.48 km² to 65.01 km² in 2002 and from 3.18 km² to 63.94 km² in 2015. The variation in the area of the dunes ranged from decreases of 8.05 km² to increases of 0.15 km² (Table 4.10).

5.3.2 Location

An overall average lateral migration of 112.33 (\pm 60.46) m and an average yearly lateral migration rate of 8.64 (\pm 4.65) m/yr in a general north-western direction was observed for the 13 year time period. The lateral migration rates per dune ranged from 2.29 m/yr to 11.63 m/yr (Table 4.11). The lateral migration rates of these dunes are considerably faster than the lateral migration rates of 0.7 – 2 m/yr for two linear dunes in North West Sinai, Egypt, measured with conventional field measurements (Phillip *et al.*, 2004). Phillip *et al.* (2004) also identified that the linear dunes in NW Sinai elongated at a much faster rate of 2.25 - 13 m/yr. This was attributed to the wind velocity that differs in the two main wind directions (when the wind flows parallel to the

dunes the wind velocity increases and when the wind is angled to the dune the velocity and thus the migration rate decreases) (Phillip *et al.*, 2004), this is unlikely to be the case within the Ubārī as the main wind direction is East (sometimes deviating northeast) with a small seasonal variation in of wind velocity throughout the year (refer to section 1.4.5; WeatherOnline, 2014a; 2014b; Weatherbase, 2015a; 2015b). Bolghoubra (2016) measured the migration rates of barchans dunes in the Erg Sidi Moussa (Central Algeria) with the use of Google Earth imagery (Digital Globe and Pleiades) and found that the barchans migrate at an astonishing average rate of 12 m/yr (range 7 – 18 m/yr).

Traditionally, linear dunes mainly elongate parallel to the dominant wind regime (Fitzsimmons *et al.*, 2007; Telfer *et al.*, 2015), with small amounts of displacement occurring laterally as a result of the bimodal wind regime. The direction of the migration (either lateral displacement or elongation) may have an effect on the rate at which linear dunes migrate. Several studies found that the elongation of linear dunes occurs at a faster rate than lateral migration. Hermas *et al.* (2012) noted the average lateral migration rates (as determined by several different authors) ranging from 0.7 – 10.6 m/yr; whilst the elongation in the same areas ranged from 2.3 – 27 m/yr – thus the elongation occurred at a faster rate than the lateral migration. Phillip *et al.* (2004) found that linear dunes elongates at a faster rate than the lateral migration that can occur. Lateral migration rate of 2.8-10 m/yr were measured for the complex dunes (barchan section and transverse section) in Jockey's Ridge, North California (Mitasova *et al.*, 2005). These migration rates are similar to the rates identified in the Ubārī sand sea, but these are from different dune types. Bailey & Bristow (2004) measured an average dune migration rate of 1.3 m/yr for the barchans dunes located at Aberffraw (Anglesey, north Wales).

Other migration rates of linear dunes range from 0.7-2 m/yr (North West Sinai, Phillip *et al.*, 2004); 1.3 m/yr (north west China, Livingstone *et al.*, 2007); and average rate of 0.5-1.5 m/yr for a combination of linear, transverse and barchans dunes were calculated for the Great Kobuk Sand Dunes of Alaska (Necsiou *et al.*, 2009). These migration rates are much lower than those measured in this research, this could occur for several reasons; an overestimation could have occurred due to the spatial resolution of the Landsat imagery; stronger wind velocities could be present in the Ubārī region, as well as the difference in the climate of Libya compared to Alaska and/

or the difference in the topography of the study areas. Other possible factors that could be considered are the methods that were used to study the migration rates (which ranged from field studies to point analysis compared to the windward boundary base that was used in this research).

It was found that the larger dunes (for example dunes 2, 11, 14 and 17; Figure 4.14) had a slower migration rate; ranging from 3.62 – 5.07 m/yr (Table 4.11; Figure 5.2) than the smaller dunes (dunes 7 – 10 and 22; Figure 4.14); with migration rates ranging from 9.14 – 24.35 m/yr (Table 4.10; Figure 5.2). These results supports the conclusion made by Gay (1999) and Boulghobra (2016) which stated that the migration rate is inversely proportional to the size of the dune – thus the larger the dune the slower the migration rate. This occurs because large dunes have large volumes of sand that is transported (compared to small dunes), or is required to be transported for displacement to show.

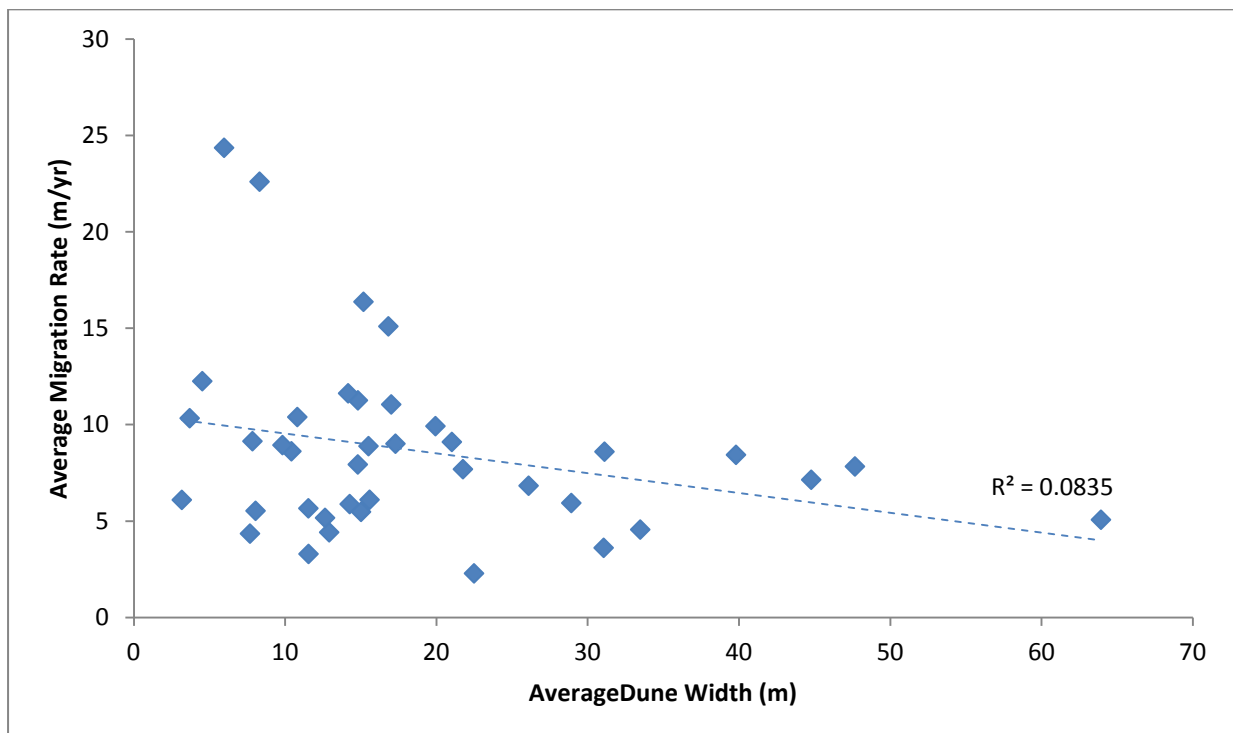


Figure 5.2: The average migration rate (m/yr) in relation to the dune width (m) with a trend line (dashed blue line)

However, there was an anomaly: dune 30 (a moderate sized dune) had a migration rate of 2.29 m/yr. This dune is smaller than the other dunes so it would be expected that it would have a faster migration rate, as found by Gay (1999) and Boulghobra (2016), but instead it has a slower migration rate. A possible reason for dune 30 to have a slower migration rate than the other smaller dunes is the presence of an oasis located at its windward side (Figure 5.3). This may influence the moisture content in the windward side of the dune restricting sand movement (Gay, 1999) and “slowing down” the dune’s migration.

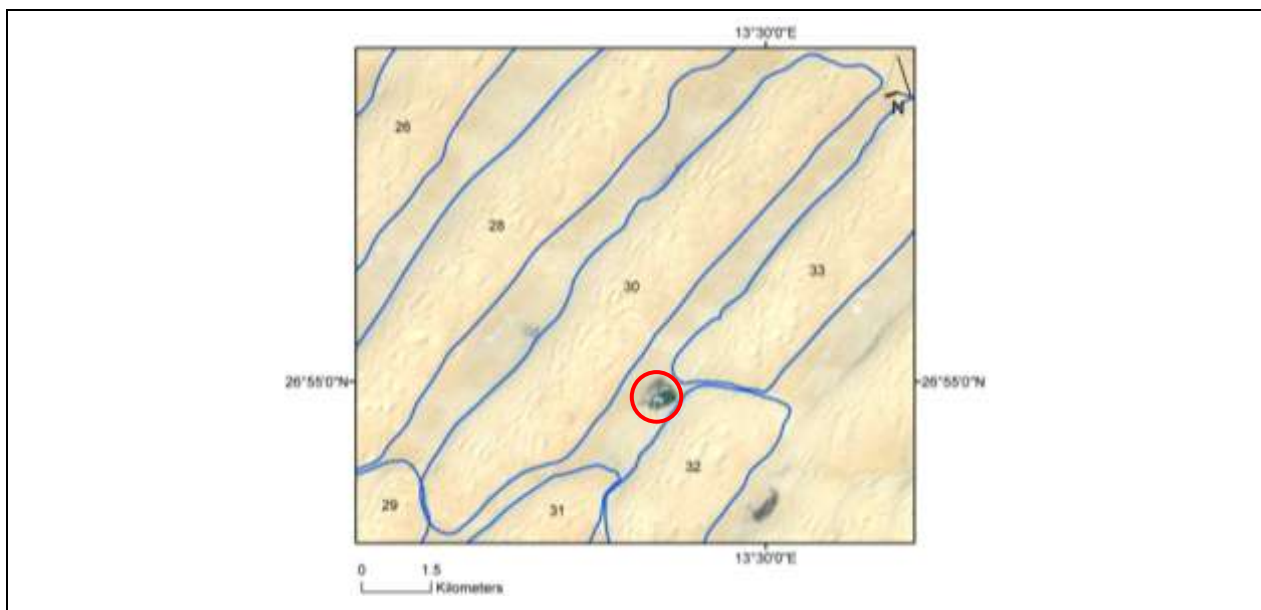


Figure 5.3: Zoomed in image on dune 30 showing the oasis (circled in red) on its windward side.

The dominant wind regime in the Ubārī sand sea area is east/ north east (WeatherOnline, 2014a; 2014b; Weatherbase, 2015a; 2015b). The general orientation of the dunes does not match the current wind regime, and are thus most likely representations of past wind regimes. Bubbenzer and Bolten (2008) also noted that linear dunes are sensitive to changes in the climate and record the wind regimes that result in their formation. Several research has considered the use of linear dunes (similar to those of the Ubārī Sand Sea) as proxies for quaternary climate reconstructions, especially of arid periods (when, where and how long it occurred; Thomas *et al.*, 2000; Livingstone, 2003; Bristow *et al.*, 2007). This is mainly because

linear dunes are less mobile than other dune types (such as barchans dunes) and thus would most likely still be present in the same areas even if they are no longer considered active dunes (Thomas *et al.*, 2000). A possible explanation then for the dune migration direction within the Ubārī could be that the (current) incoming north eastern winds are deflected by the Messak Plateau carrying the sand grains in a north western direction (the “ancient” linear megadunes now forming the erodible bedforms).

Due to the coarse spatial resolution there may have been an over estimation of the changes in the size (width, length and area) as well as the amount of migration that occurred over the 13 years in question. This became apparent in the high migration rates obtained in this study compared to the previous research of linear dunes in arid environments. However, even although an over estimation may have resulted from the coarse spatial resolution, the occurrence of migration in the area is still apparent (the magnitude may just be less).

Further analyses and ground truthing would be beneficial in order to validate these results. Landsat imagery is definitely beneficial in establishing areas where movement has occurred (refer to section 4.2.4) and can in future form a preliminary analyses to larger studies in order to identify areas of interest – thus narrowing down the area and assisting in cost saving and more efficient use of other resources (e.g. time, funding, high resolution imagery etc.). It is however, important to note that the use of Landsat imagery should be done with caution. Assessing the co-registration of the imagery is very important (can be done by examining hard, anthropogenic features as was done in this study) to ensure that the change that is observed is not artefacts resulting from a mis-alignment between the images.

Several studies utilized the COSI-Corr (co-registration of optically sensed images and correlation) method (Necsoiu *et al.*, 2009; Hermas *et al.*, 2012). The COSI-Corr method identifies changes in the ground surface (including sand dune migration) based on multi-temporal imagery (Necsoiu *et al.*, 2009; Hermas *et al.*, 2012). It would be interesting apply this method to the Ubārī sand sea using the COSI-Corr method to see if similar results are found.

5.4 Limitations

The main limitation to this research was the inability to conduct ground truthing to not only collect training data but also to verify the classification results that were obtained (especially with regards to the crests of the dunes that are difficult to identify on a two dimensional aerial view of the dunes). The homogeneity of the area was also a limitation but was managed by comparing different band combinations in order to determine the best combination to delineate the different dune features that were in question.

The methods used also proved to be a limitation. It is very difficult to classify natural features based on the spectral signature as it was found that they are rarely homogeneous throughout an entire area. Also opting to distinguish between the crest and slope of the dune proved troublesome as the most confusion of classes were between these two.

Chapter 6: Conclusions

The aims of this research were to 1. compare the spatial resolution of Landsat and Worldview imagery and 2. to determine the net migration rate and direction of the dunes within a subsection of the Ubārī sand sea from 2002-2015.

It was found that the advantage of the higher spatial resolution of the Worldview imagery was beneficial for identifying training samples for the supervised classification and ultimately it would most likely result in more accurate and precise measurements of the dune morphology and migration. However, the classifications based on the Landsat imagery had a higher overall accuracy and kappa value – thus in this case for this area the Landsat imagery yielded better results than the Worldview imagery. It is important to note that the algorithms that were used for the classifications were designed for use on non-arid landscapes, and the uniformity of the spectral signatures of the land surface represent a special case, contributing to the low accuracy values that were obtained. Research concerned with the specific dynamics and dimensions of dunes (especially in the cases with superimposed dunes) should consider using higher resolution imagery and or active sensors (such as ASTER or SRTM or possibly even drone imagery).

With the use of bi-temporal Landsat imagery it was determined that the linear dunes of the Ubārī sand sea migrate at an average rate of 6.32 m/yr in a north-north west direction. This is much faster than the average migration rates of other linear dunes that were previously studied - for example Phillip *et al.* (2004) noted a lateral migration rate of 0.7 – 2.0 m/yr.

At this stage no comment can be made to the accuracy of the classifications as no field data could be collected to verify the classification. The future of this study might consider using SRTM or another DEM to verify some of the resulting classifications.

Recommendations for Future Research

Future research may consider the following:

- Testing this method in an area with known migration rates in order to compare the results.
- Other classification methods including object based classifications, Support Vector Machine (SVM) and Random Forest (RF) methods can also be considered, and may even result in a higher accuracy.
- Focussing on the dune as a whole (one feature) instead of attempting to classify the different features (crest, slope and interdune) may yield more tangible results from a supervised classification.
- A different study area with ample historical wind climate records would also prove useful in the study of past and present dune migrations. Considering an area with more than one dune type would also prove useful especially in developing a method/s with global applicability.
- The use of active remote sensing platforms (e.g. SRTM and ASTER) to study dune migration may yield more tangible results as both the changes in location and the volume of the dunes can be studied with the use of DEM data.
- Usually sand dunes are studied with remotely sensed data by the use of on-screen digitizing of the RGB image (Al-Dabi *et al.*, 1998; Hugenholtz *et al.*, 2012; El-Magd *et al.*, 2013). The use of a classified image proves helpful in identifying the general dune pattern and determining the areas where the most and least migration occurred – the analyses can then be focused on these areas. The digitization process was also quicker with the use of the classified image, and the repeatability is higher as it is not as reliant on the previous knowledge of the digitizer – thus a knowledgeable person can assist in the identification of the training samples in order to run the classifications with the highest possible accuracy but thereafter the digitization can then probably be done by several people with similar resulting accuracies (as long as the digitization rule of thumb is adhered to). This could be useful in research concerned with very large areas that have thousands of dunes, where several hours of digitization by one or two persons can be reduced by using more people for the digitization.

References

- Adelabu, S., Mutanga, O., Adam, E., and Cho, M.A., 2013: Exploiting machine learning algorithms for tree species classification in semiarid woodland using RapidEye image, *Journal of Applied Remote Sensing*, 7, 1-13.
- Al-Dabi, H., Koch, M., El-Baz, F. and Al-Sawari, M., 1998: Mapping and monitoring sand dune patterns in northwest Kuwait using Landsat TM images. In: S. A.S. Omar, R. Misak and D. Al-Ajmi (eds.), *Sustainable Development in Arid Zones: Assessment and Monitoring of Desert Ecosystems*, A.A. Balkema, Rotterdam, Netherlands, 273-279.
- Aldossary, A., 2012: Analysis of urban change detection techniques in desert cities using remote sensing, unpublished paper, California State University, Northridge, <http://hdl.handle.net/10211.2/1043>.
- Al-Masrahy, M.A. and Mountney, N.P., 2013: Remote sensing of spatial variability in Aeolian dune and interdune morphology in the Rub' Al-Khali, Saudi Arabia, *Aeolian Research*, 11, 155-170.
- Asha Rani, K.P, Asha, K.N., Manjunath, M., 2013: Image mosaicing and registration, *International Journal of Computer Science Issues*, 10, 534-540.
- Badescu, V., Cathcart, R.B., Bolonkin, A.A., 2008: Sand dune fixation: A solar-powered Sahara seawater pipeline macroproject, *Land Degradation & Development*, 19, 676-691.
- Bailey, S.D., and Bristow, C.S., 2004: Migration of parabolic dunes at Abberffraw, Anglesey, north Wales, *Geomorphology*, 59, 165-174.
- Biagetti, S. and di Lernia, S., 2014: Holocene deposits of Saharan rock shelters: The case of Takarkori and other sites from the Tadrart Acacus Mountains (Southwest Libya), *African Archaeological Review*, 30, 305-338.
- Birnie, R.W., Parr, J.T., Naslund, H.R., Nichols, J.D. and Turner, P.A., 1989: Applications of Landsat Thematic Mapper and ground based spectrometer data to a study of the Skaergaard and other mafic intrusions of east Greenland. *Remote Sensing of Environment*, 28, 297-304.

- Bishop, M.A., 2010: Nearest neighbour analysis of mega-barchanoid dunes, Ar Rub' al Khali, sand sea: The application of geographical indices to the understanding of dune field self-organization, maturity and environmental change, *Geomorphology*, 120, 186-194.
- Blumberg, D.G., 1998: Remote Sensing of Desert Dune Forms Polarimetric Synthetic Aperture Radar (SAR), *Remote Sensing of Environment*, 65, 204-216.
- Blumberg, D.G., 2006: Analysis of large Aeolian (wind-blown) bedforms using Shuttle Radar Topography Mission (SRTM) digital elevation data, *Remote Sensing of Environment*, 100, 179-189.
- Boulghobra, N., 2016: Climatic data and satellite imagery for assessing the Aeolian sand deposit and barchans migration, as a major risk sources in the region of In-Salah (Central Algerian Sahara), *Arab Journal of Geoscience*, 9, 450, DOI [10.1007/s12517-016-2491-x](https://doi.org/10.1007/s12517-016-2491-x).
- Bristow, C.S., Duller, G.A.T., Lancaster, N., 2007: Age and dynamics of linear dunes in the Namib Desert, *Geology*, 35, 555-558
- Bryantt, C., 2014: Comparison of two satellite imaging platforms for use in land use/land cover classification in agricultural regions, unpublished paper, Texas Tech University, USA.
- Bubenzer, O. and Bolten, A., 2008: The use of new elevation data (SRTM/ASTER) for the detection and morphometric quantification of Pleistocene megadunes (draa) in the eastern Sahara and the southern Namib, *Geomorphology*, 102, 221-231.
- Bullard, J.E., White, K. and Livingstone, I., 2011: Morphometric analysis of Aeolian bedforms in the Namib Sand Sea using ASTER data. *Earth Surface Processes and Landforms*, 36, 1534-1549.
- Canty, M.J., 2010: *Image Analysis, Classification, and Change Detection in Remote Sensing. With Algorithms for ENVI/IDL*, 2nd Edition. CRC Press, Taylor and Francis Group, USA.

- Collado, A.D., Chuvieco, E., and Camarasa, A., 2002: Satellite remote sensing analysis to monitor desertification processes in the crop-rangeland boundary of Argentina, *Journal of Arid Environments*, 52, 121-133.
- Congalton, R.G., and Green, K., 2009: *Assessing the Accuracy of Remotely Sensed Data: Principles and Practices (2nd edition)*, CRC Press (Taylor & Francis Group), USA.
- Cremschi, M. and Zerboni, A., 2009: Early to middle Holocene landscape exploitation in a drying environment: Two case studies compared from the central Sahara (SW Fezzān, Libya). *C. R. Geoscience*, 341, 689-702.
- Cremschi, M., Pelfini, M., Santilli, M., 2006: *Cupressus dupreziana*: a dendroclimatic record for the middle-late Holocene in the central Sahara, *The Holocene*, 16, 293-303.
- De Souza, C.H.W., Mercante, E., Prudente, V.H.R., and Justina, D.D.D., 2013: Methods of performance evaluation for the supervised classification of satellite imagery in determining land cover classes, *Ciencia e Investigación Agraria*, 40, 419-428.
- Devi, M.R. and Baboo, S.S., 2011: Land use and land cover classification using RGB&L based supervised classification algorithm, *International Journal of Computer Science and Engineering Technology*, 2, 167-180.
- Du Pont, S.C., 2015: Dune Morphodynamics, *Comptes Rendus Physique*, 16, 118-138.
- Du Pont, S.C., Narteau, C., Gao, X., 2014: Two modes of dune orientation, *Geology*, 42, 743-746.
- Edmunds, W.M. and Wright, E.P., 1979: Groundwater recharge and paleoclimate in the Sirte and Kufra basins, Libya. *Journal of Hydrology*, 40, 215-241.
- Effat, H.A., Hegazy, M. and Behr, F.J., 2012: Cartographic modelling of potential sand dunes movement risk using remote sensing and geographic information systems in Sinai, Egypt, unpublished paper, National Authority for Remote Sensing and Space Sciences,

<https://www.researchgate.net/publication/231345711> Cartographic Modeling of Potential Sand Dunes Movement Risk Using Remote Sensing and Geographic Information System in Sinai Egypt.

- El-Baz, 2000: Satellite observations of the interplay between wind and water processes in the Great Sahara, *Photogrammetric Engineering & Remote Sensing*, 66, 777-782.
- El-Magd, I.A., Hassan, O. and Arafat, S., 2013: Quantification of sand dune movements in the south western part of Egypt, Using remotely sensed data and GIS, *Journal of Geographic Information Systems*, 5, 498-508.
- Fitzsimmons, K.E., Bowler, J.M., Rhodes, E.J., and Magee, J.M., 2007: Relationships between desert dunes during the late Quaternary in the Lake Frome region, Strzelecki Desert, Australia, *Journal of Quaternary Science*, 22, 549-558.
- Flagg, C.B., Neff, J.C., Reynolds, R.L., and Belnap, J., 2014: Spatial and temporal patterns of dust emissions (2004-2012) in semi-arid landscapes, southeastern Utah, USA, *Aeolian Research*, 15, 31-43.
- Fontes, J.Ch. and Gasse, F., 1991: PALHYDAF (Paleohydrology in Africa) program: objectives, methods and major results. *Palaeogeography, Palaeoclimatology, Palaeoecology*, 84, 191-215.
- Foody, G.M., 2002: Status of land cover classification accuracy assessment, *Remote Sensing of Environment*, 80, 185-201.
- Gay Jr, S.P., 1999: Observations regarding the movement of barchan sand dunes in the Nazca to Tanaca area of southern Peru, *Geomorphology*, 27, 279–293.
- Ghadiry, M., Shalaby, A. and Koch, B., 2012: A new GIS-based model for automated extraction of sand dune encroachment case study: Dakhla Oases, western desert of Egypt. *The Egyptian Journal of Remote Sensing and Space Sciences*, 15, 53-65.
- Giraudi, C., 2005: Eolian sand in peridesert northwestern Libya and implications for Late Pleistocene and Holocene Sahara expansions, *Palaeogeography, Palaeoclimatology, Palaeoecology*, 218, 161-173.

- Giraudi, C., Mercuri, A.M., Esu, D., 2012: Holocene palaeoclimate in the northern Sahara margin (Jefara Plain, northwestern Libya), *The Holocene*, 23, 339-352.
- Goudarzi, G.H., 1970. *Geology and Mineral Resources of Libya – A Reconnaissance*. United States Government Printing Office, Washington, pp. 13-18.
- Goudarzi, G.H., 1980: Structure-Libya, in M.J. Salem and M.T. Busrewil (eds), *The Geology of Libya* Vol. 3, Academic Press Inc., London, 879-892.
- Grove, A.T., 1980: Geomorphic evolution of the Sahara, in M.A.J. Williams and H. Faure (eds.), *The Sahara and The Nile*, Balkema, Netherlands, 7-16.
- Hadjimitsis, D.G., Papadavid, G., Agapiou, A., Themistocleous, K., Hadjimitsis, M.G., Retails, A., Michaelides, S., Chrysoulakis, N., Toullos, L., and Clayton, C.R.I., 2010: Atmospheric correction for satellite remotely sensed data intended for agricultural applications: impact on vegetation indices. *Natural Hazards and Earth System Sciences*, 10, 89-95.
- Hallett, D., 2002: *Petroleum Geology of Libya*, Elsevier Science, Amsterdam.
- Hermas, E., Leprince, S., and El-Magd, I.A., 2012: Retrieving sand dune movements using sub-pixel correlation of multi-temporal optical remote sensing imagery, northwest Sinai Peninsula, Egypt, *Remote Sensing of Environment*, 121, 51-60.
- Hesse, R., 2009: Using remote sensing to quantify Aeolian transport and estimate the age of the terminal dune fields Dunas Pampa Blanca in southern Peru. *Quaternary Research*, 71, 426-436.
- Howari, F.M., Baghdady, A. and Goodell, P.C., 2007: Mineralogical and geomorphological characterization of sand dunes in the eastern part of United Arab Emirates using orbital remote sensing integrated with field investigations. *Geomorphology*, 83, 67-81.
- Hugenholtz, C.H. and Barchyn, T.E., 2010: Spatial analysis of sand dunes with a new global topographic dataset: new approaches and opportunities. *Earth Surface Processes and Landforms*, 35, 986-992.

- Hugenholtz, C.H., Levin, N., Barchyn, T.E., Baddock, M.C., 2012: Remote sensing and spatial analysis of Aeolian sand dunes: A review and outlook, *Earth-Science Reviews*, 111, 318-334.
- Huggett, R.J., 2007: *Fundamentals of Geomorphology Second Edition*, Routledge, USA & Canada.
- Hussain, M., Chen, D., Cheng, A. and Stanley, D., 2013: Change detection from remotely sensed images: From pixel-based to object-based approaches, *ISPRS Journal of Photogrammetry and Remote Sensing*, 80, 91-106.
- Janke, J.R., 2002: An analysis of current stability of the dune fields at Great Sand Dunes National Monument using temporal TM imagery (1984-1998). *Remote Sensing of Environment*, 83, 488-497.
- Kennedy, R.E., Townsend, P.A., Gross, J.E., Cohen, W.B., Bolstad, P., Wang, Y.Q., Adams, P., 2009: Remote sensing change detection tools for natural resource managers: Understanding concepts and tradeoffs in the design of landscape monitoring projects, *Remote Sensing of Environment*, 113, 1382-1396.
- Keuchel, J., Naumann, S., Heiler, M., and Sigmund, A., 2003: Automatic land cover analysis for Tenerife by supervised classification using remote sensed data, *Remote Sensing of Environment*, 86, 530-541.
- Laity, J., 2008: *Deserts and Desert Environments*, Wiley-Blackwell, Singapore.
- Lam, D.K., Rimmel, T.K. and Drenzer, T.D., 2011: Tracking desertification in California using remote sensing: A sand dune encroachment approach. *Remote Sensing*, 3, 1-13.
- Levin, N., Ben-Dor, E. and Karnieli, A., 2004: Topographic information of sand dunes as extracted from shading effects using Landsat images. *Remote Sensing of Environment*, 90, 190-209.
- Levin, N., Kidron, G.J. and Ben-Dor, E., 2006: The spatial and temporal variability of sand erosion across a stabilizing coastal dune field. *Sedimentology*, 53, 697-715.

- Levin, N., Levental, S. and Morag, H., 2012: The effect of wildfires on vegetation cover and dune activity in Australia's desert dunes; a multisensory analysis. *International Journal of Wildland Fire*, 21, 459-475.
- Livingstone, I., 2003: A twenty-one year record of surface change on a Namib linear dune, *Earth Surface Processes and Landforms*, 28, 1025-1031.
- Livingstone, I., Wiggs, G.F.S. and Weaver, C.M., 2007: Geomorphology of desert sand dunes: A review of recent progress, *Earth-Science Reviews*, 80, 239-257.
- Manguet, M.M., El-Baz, F., 1986: Deciphering wind directions from dune orientations in space images of deserts and semiarid lands, unpublished paper, Twentieth International Symposium on Remote Sensing of Environment, Nairobi, Kenya., https://www.researchgate.net/publication/223036303_Dune_morphology_sand_transport_pathways_and_possible_source_areas_in_east_Thaumasia_Region_Mars.
- Mamtimin, B., Et-Tantawi, A.M.M., Schaefer, D., Meixner, F.X. and Domroes, M., 2011: Recent trends of temperature change under hot and cold desert climates: Comparing the Sahara (Libya) and Central Asia (Xinjiang, China). *Journal of Arid Environments*, 75, 1105-1113.
- Maselli, F., Conese, C., Zipoli, G., and Pittau, M.A., 1990: Use of error probabilities to improve area estimates based on maximum likelihood classifications, *Remote Sensing of Environment*, 31, 155-160.
- Masselink, G., Hughes, M.G. and Knight, J., 2011: *Introduction to Coastal Processes & Geomorphology*, Hodder Education, London.
- McKee, E.D., 1979: *A Study of Global Sand Sea*, United States Government Printing Office, Washington.
- Mercuri, A. M., 2008: Human influence, plant landscape evolution and climate inferences from the archaeobotanical records of the Wadi Teshuinat area (Libyan Sahara). *Journal of Arid Environments*, 72, 1950-1967.
- Minu, S., Shetty, A., and Gopal, B., 2016: Review of preprocessing techniques used in soil property prediction from hyperspectral data, *Cogent Geoscience*, 2, 1-7.

- Mitasova, H., Overton, M., and Harmon, R.S., 2005: Geospatial analysis of a coastal sand dune field evolution: Jockey's Ridge, North California, *Geomorphology*, 72, 204-221.
- Mohamed, I.N.L. and Verstraeten, G., 2012: Analyzing dune dynamics at the dune field scale assessed on multi-temporal analysis of Landsat TM images. *Remote Sensing of Environment*, 119, 105-117.
- Necsoiu, M., Leprince, S., Hooper, D.M., Dinwiddie, C.L., McGinnis, R.N. and Walter, G.R., 2009: Monitoring migration rates of an active subarctic dune field using optical imagery. *Remote Sensing of Environment*, 113, 2441-2447.
- Paisley, E.C.I., Lancaster, N., Gaddis, L.R. and Greeley, R., 1991: Discrimination of active and inactive sand from remote sensing: Kelso Dunes, Mojave Desert, California, *Remote Sensing of Environment*, 37, 153-166.
- Pease, P.P., Bierly, G.D., Tchakerian, V.P. and Tindale, N.W., 1999: mineralogical characterization and transport pathways of dune sand using Landsat TM data, Wahiba Sand Sea, Sultanate of Oman, *Geomorphology*, 29, 235-249.
- Perumal, K. and Bhaskaran, R., 2010: Supervised classification performance of multispectral images, *Journal of Computing*, 2, 2151-9617.
- Phillip, G., Attia, O.E.A., and El-Banna, M.S., 2004: Dynamics of sand dunes movement and their environmental impacts on the reclamation area in NW Sinai, Egypt, unpublished paper, Proceeding of the 7th Conference: Geology of Sinai for Development, Ismailia, https://www.google.co.za/url?sa=t&rct=j&q=&esrc=s&source=web&cd=1&cad=rja&uact=8&ved=0ahUKEwj1seO9icvOAhXrIMAKHf4vCU0QFggcMAA&url=http%3A%2F%2Ffaculty.ksu.edu.sa%2FDr.%2520Osama%2520E.A.%2520Attia%2FPublications%2FDynamics%2520of%2520sand%2520dunes%2520movement.pdf&usq=AFQjCNEVU-6jx4IEQAv_KE3iwfp7i-TrPA.
- Qong, M., 2000: Sand Dune Attributes Estimated from SAR Images, *Remote Sensing of Environment*, 74, 217-228.

- Ramsey, M.S., Christensen, P.R., Lancaster, N. and Howard, D.A., 1999: Identification of sand sources and transport pathways at the Kelso Dunes, California, using thermal infrared remote sensing. *GSA Bulletin*, 111, 646-662.
- Rubin, D.M., Tsoar, H. and Blumberg, D.G., 2008: A second look at western Sinai seif dunes and their lateral migration, *Geomorphology*, 93, 335-342.
- Sinha, S.C. and Pandey, S.M., 1980: Hydrogeological studies in a part of the Murzuq Basin using geophysical logs, in M.J. Salem and M.T. Busrewil (eds), *The Geology of Libya* Vol. 2, Academic Press Inc., London, 629-634.
- Sparavinga, A.C., 2013: A study of moving sand dunes by means of satellite images, *International Journal of Sciences*, 2, 32-42.
- Swezey, C., 2001: Eolian sediment responses to late Quaternary climate changes: temporal and spatial patterns in the Sahara, *Palaeogeography, Palaeoclimatology, Palaeoecology*, 167, 119-155.
- Swezey, C.S., 2009: Cenozoic stratigraphy of the Sahara, Northern Africa, *Journal of African Earth Sciences*, 53, 89-121.
- Tawardos, E.E., 2001: *Geology of Egypt and Libya*, A.A.Balkema, Netherlands.
- Telfer, M.W., Fyfe, R.M., and Lewin, S., 2015: Automated mapping of linear dunefield morphometric parameters from remotely-sensed data, *Aeolian Research*, 19, 215-224.
- Thomas, D.S.G., 1997: *Arid Zone Geomorphology: Process, form and change in drylands*, John Wiley & Sons, England.
- Thomas, D.S.G., O'Connor, P.W., Bateman, M.D., Shaw, P.A., Stokes, S., Nash, D.J., 2000: Dune activity as a record of late Quaternary aridity in the Northern Kalahari: new evidence from northern Namibia interpreted in the context of regional arid and humid chronologies, *Palaeogeography, Palaeoclimatology, Palaeoecology*, 156, 243-259.
- Tsoar, H., 2001: Types of Aeolian sand dunes and their formation, in N.J. Balmforth and A. Provenzale (eds.), *Geomorphological Fluid Mechanics*. Lecture Notes in Physics Series, vol. 582. Springer-Verlag, Berlin, 403-429.

- Tsoar, H., Blumberg, D.G. and Stoler, Y., 2004: Elongation and migration of sand dunes, *Geomorphology*, 57, 293-302.
- Varma, S., Shah, V., Banerjee, B., Buddhiraju, K.M., 2014: Change detection of desert sand dunes: A remote sensing approach, *Advances in Remote Sensing*, 3, 10-22.
- Walsh, S.J., Butler, R., Malanson, G.P., 1998: An overview of scale, pattern, process relationships in geomorphology: a remote sensing and GIS perspective, *Geomorphology*, 21, 183-205.
- WeatherBase, 2015a. Sabhā, Libya
<http://www.weatherbase.com/weather/weatherall.php3?s=42126&cityname=Sabhā%2C+Sabhā%2C+Libya&units=> (accessed 16 March, 2015).
- WeatherBase, 2015b. Ubārī, Libya
<http://www.weatherbase.com/weather/weatherall.php3?s=603246&cityname=Ubārī%2C+Sha%27biyat+Wadi+al+Hayat%2C+Libya&units=> (accessed 16 March, 2015).
- WeatherOnline, 2014a. Weather, Ubārī
<http://www.weatheronline.in/weather/maps/city?FMM=1&FYY=2005&LMM=12&L YY=2014&WMO=62200&CONT=afri®ION=0011&LAND=LY&ART=TEM&R =0&NOREGION=0&LEVEL=162&LANG=in&MOD=tab> (accessed 16 March 2015).
- WeatherOnline, 2014b. Weather, Sabhā
<http://www.weatheronline.in/weather/maps/city?FMM=1&FYY=2005&LMM=12&L YY=2014&WMO=62124&CONT=afri®ION=0011&LAND=LY&ART=TMX&R =0&NOREGION=1&LEVEL=162&LANG=in&MOD=tab> (accessed 16 March 2015).
- White, K., Charlton, M., Drake, N., McLaren, S., Mattingly, D., Brooks, N., 2006: Lakes of the Edeyen Ubārī and the Wadi al-Hayat, in D. Mattingly, S. McLaren, E. Savage, Y. al-Fasatwi and K. Gadgood (eds.), *The Libyan Desert: Natural Resources and Cultural Heritage*, The Society for Libyan Studies, 123-130.
- White, K., Walde, J., Drake, N., Eckardt, F. and Settle, J., 1997: Mapping the iron oxide content of dune sands, Namib Sand Seas, Namibia, using Landsat Thematic Mapper data, *Remote Sensing of Environment*, 62, 30-39.

Yao, Z.Y., Wang, T., Han, Z.W., Zhang, W.M. and Zhao, A.G., 2007: Migration of sand dunes on the northern Alxa Plateau, Inner Mongolia, China, *Journal of Arid Environments*, 70, 80-93.